Fall 2021

Preparation, Characterization and Evaluation of Rationally Designed Catalysts by Electroless Deposition

Wen Xiong

PREPARATION, CHARACTERIZATION AND EVALUATION OF RATIONALLY DESIGNED CATALYSTS BY ELECTROLESS DEPOSITION

by

Wen Xiong

Bachelor of Engineering
Nanjing University of Science and Technology, 2012

Master of Engineering
Nanjing University of Science and Technology, 2015

Submitted in Partial Fulfillment of the Requirements

For the Degree of Doctor of Philosophy in

Chemical Engineering

College of Engineering and Computing

University of South Carolina

2021

Accepted by:

John R. Monnier, Major Professor

John R. Regalbuto, Committee Member

Donna A. Chen, Committee Member

William E. Mustain, Committee Member

Tracey L. Weldon, Interim Vice Provost and Dean of the Graduate School

Dedication

To my dear husband, my parents, my sister and brother and my little boy, Leo.

Acknowledgements

I want to thank my advisor, Prof. John R. Monnier, the big moon, who is the greatest advisor I have ever been working with. He knows how to advise a graduate student and how to make things go to the right direction when it is not going well. From him, I have learned so much about designing, improving, and repairing equipment. Most importantly, his passion on science, work ethics, hard-working spirit, profound knowledge and critical thinking set a great example of a good scientist. I have learned so many things I didn't expect. Moon, I appreciate everything you have taught me, particularly, my pronunciation. Thank you very much for guiding me as a published Mom.

I also want to show my sincerely thanks to my committee members: Dr. John R. Regalbuto, Dr. Dona A. Chen, Dr. William E. Mustain, for their comments on my work and their time to review my work.

I would also like to acknowledge my group members and colleagues, Dr. weijian Diao, Dr. John Tengco, Abolfazl Shakouri, Jeremiah Lipp, Leandro Castro, Fahim Rahman, Masudur Rahman, haiying Zhou and Dr. Yanjiao Yi. I really enjoy working with them. I want to express my sincere gratitude to Dr. Bahareh Tavakoli, Benjamin Egelske, my best co-worker, Gregory Tate, who taught me and helped me a lot on experiments, and Mozhdeh Parizad, thank you for sharing your amazing reactors for CO_2 reduction.

Great thanks to the Chemical Engineering Department staffs, Marcia Rowen, Loretta Hardcastle, Vernon Dorrell and Shawn Hagan, for their technical and administrative help.

for their assistance and excellent work on providing a friendly and nice working environment. I also want to give the special thanks to Carol Stork for her generous help on experimental work.

Lastly, I would like to thank my dear husband Wenqiang Yang who is the greatest support behind me, and without whom I cannot overcome all the difficulties and hard times that I have met during my study here. Specially, I want to thank my little boy Leo, thank you for letting me as a graduated Mom, love you.

Abstract

In heterogeneous catalysis, it is a proven factor that the surface-specific activity and the catalyst selectivity strongly depends on the active sites which are determined by the composition, size, and shape of the particle. For structure-sensitive reactions favored by specific surface sites, such as corners, steps, or edges, TOF and selectivity can be greatly changed by the size of catalyst particles since the active site distribution will change with the size of the catalysts. Usually, metal particles are synthesized by two methods in industry, namely precipitation and impregnation, which often exhibit a broad size distribution. The grand challenge of colloidal chemistry, on the other side, is that the surfactants need to be thermally removed without losing original particle size distribution. Therefore, a precise composition and size control catalyst synthesis method needs to be developed to get a catalyst that have high activity and selectivity towards the desired product.

In this thesis, we therefore studied the electroless deposition (ED) in metal particles synthesis with precise control on the catalyst particle size and composition. Firstly, continuous ED is introduced to grow Pt particle on carbon support, and Pt particle average size and size distribution was found to be a function of the deposition time. Alumina supported silver (Ag) particles with different size are then generated using percolating ED bed with different deposition time. The catalyst performance on ethylene epoxidation under real conditions shows that the rate of ethylene oxide formation is a function of Ag particle

size and the intrinsic EO selectivity increases with Ag size. Lastly, the composition of the particles is tuned by depositing two or more metals through the ED method. In this case, a Pt-Ru bimetallic catalysts are prepared on oxygen groups functionalized carbon nanotubes support and its electro-catalytic activity toward methanol oxidation have been studied. Cyclic voltammetry (CV) testing shows that the ED driven Pt-Ru catalysts with strong Pt-support interaction have higher mass activities than the commercial Pt-Ru catalysts in the direct methanol fuel cells (DMFC). Moreover, co-ED is developed to co-deposit Cu and Pd and Ag plasmon with controlled composition, and the catalyst performance have been tested on the CO_2 reduction reactions.

Based on the work in this thesis, we demonstrate that the ED method we proposed can be readily used in precise size and composition control metal catalyst synthesis at industry scale.

Table of Contents

List of Tables

List of Figures

List of Abbreviations

CV ..... Cyclic Voltammery

DI ..... Dry Impregnation

DMAB ..... Dimethylamine Borane

DP ..... Deposition Precipitation

Dv ..... volume average size

Ds ..... surface average size

ED ..... Electroless Deposition

EDTA ..... Ethylenediaminetetraacetic

EDX ..... Energy Disperive X-ray

EN ..... Ethylenediamine

EO ..... Ethylene Oxide

ESA ..... Electrochemical Surface Area

GDP ..... Gross Domestic Product

ICP ..... Inductively Coupled Plasma

MOR.....Methanol Oxidation Reaction

MWCNTs.....Multi Wall Carbon Nanotubes

ORR .....Oxygen Reduction Reaction

PZC .....Point of Zero Charge

RA ..... Reducing Agent

ROP.....Ring Open Product

SEA .....Strong Electrostatic Adsorption

SEM .....Scanning Electron Microscopy

STEM..... Scanning Transmission Electron Microscopy

TOF .....Turnover Frequency

TOS .....Time on Stream

TPO ..... Temperature Programmed Oxidation

TPR .....Temperature Programmed Reduction

UV/VIS ..... Ultraviolet-Visible

WI..... Wet Impregnation

XPS ..... X-ray Photoelectron Spectroscopy

XRD ..... X-ray Diffraction

CHAPTER 1

INTRODUCTION

1.1 Background

Heterogenous catalysis is a well-established filed with a long and illustrious history. In the chemical industry, it is quite prevalent that over 90% of the chemical production is based or relies heavily on catalytic processes. Considering the large fraction (about 35%) that the heterogenous catalysis based chemical production taking in the world's gross domestic product (GDP) [1], it is very important to conduct research on the design of novel, cheap, safe and clean catalytic process. The first catalytic reactions were identified more than a century ago[2], and the fundamental kinetics and thermodynamics that associated with the adsorption, desorption and surface reactions underlying the catalysis have been firstly studied by Langmuir, Hinshelwood, Bond, Ostwald and many others. [3] Nowadays, more and more experimental and theoretical tools, such as transmission electron microscopy and chemisorption of gases, have been developed for the characterization of catalysts and the understanding of the structure-activity correlations [4]. Recent studies show that turnover frequency (TOF) and selectivity of a catalytic reactions depends strongly on the structure of the catalyst. Especially, nanoparticles will form various surface structures under different particle size resulting in various active sites on the surface, such as steps, kinks, and terraces, which will cause a dramatical change in the catalyst activity and selectivity.

The importance of particle size on the catalytic properties of metals was firstly recognized from the early days study of catalysis when the concept of active sites was introduced in 1925 by Taylor. [5] Studies thereafter on the dependence of reaction rate on particle size by Boudart [6] Van Hardveld and Hartog led to the conclusions of structure-sensitive and -insensitive reactions and rationalized the dependence of the fraction and type

of surface atoms on the particle size. For structure sensitive reactions favored by specific surface sites, the rate per unit surface area of metal can be influenced strongly by the degree of dispersion of the metal. With demanding reactions, which typically require severe temperature and pressure conditions, significant variations in activity have been often reported as a function of catalyst dispersion, which is often correlated with average particle size. In 1982, Somorjai first directly and unambiguously probed the structure sensitivity of ammonia synthesis reaction over iron surface under industrial conditions.[7] It is found that Fe (111) with the highest C_7 concentration is the most active surface sites comparing to Fe (110) and (100) surface. The relative rates of ammonia synthesis were found to be 418: 25: 1, respectively, for (111), (110), (100) surface at 798 K and a total 20 atm pressure of a stoichiometric mixture of hydrogen and nitrogen. Size dependency of CO oxidation on gold (Au) catalyst is widely accepted, and the source of the size sensitivity is the interfacial perimeter around Au metal particles.[8, 9] Work by Hartuna [10] demonstrated that the TOFs based on surface gold atoms are independent of the metal oxide support whereas they are significantly dependent on the particle size of Au. Krijin P.de Jong[11] firstly reported the size effects of the Fishcer-Tropsch reaction over the cobalt (Co) particle supported on an inert carbon nanofiber in 2006. The catalytic performance was independent of the Co particle size when it is larger than 6 nm (1bar) or 8 nm (35 bar) at 220℃ with a H_2 / CO ration of 2, however, both the activity and the selectivity were strongly particle size dependent on smaller Co particles at 2% CO conversion.

It therefore would be highly desirable to have full control of the design and synthesis of specific catalytic sites with specific local geometries. Uniform catalysts of the appropriate size, structure and composition are needed. Recent progress in nanoparticle syntheses

attains a completeness of artistic achievement. Now, the size of nanoparticles can be controlled on an atomic scale, preserving high uniformity and extremely narrow size distribution. New synthetic methodology is being incorporated into the preparation of better-defined and more complex catalysts for many applications, which will be discussed in the following sections in this chapter.

1.2 Supported metal catalyst preparation.

Traditionally, heterogeneous catalysts have been made by simple synthetic routes with limited control over the morphology and nature of the solids. To obtain a catalyst with high activity, selectivity, and stability at an industrial scale is always the most important aim of the catalyst preparation. An ideal preparation of metallic catalyst should result in a homogenous distribution of metallic particles of controlled size. Hutchings and Vedrine [12] reviewed many commercialized methods for the preparation of various different supported catalyst types while Bartholomew and Farrauto [13] also reported some important methods of catalyst preparation. Two highly-useful and complementary books on catalyst preparation edited by Regalbuto [14] and de Jong, [15] respectively, contain review chapters that focus in detail on different aspects of the chemistry and physics of the important preparation methods, including examples of studies on the critical steps in preparation and pretreatment of supported metals.

Supported metal catalyst synthesis methods discussed in this dissertation focus on those methods that can be produce catalyst at an industrial scale. The biggest challenges during catalyst preparation are the particle sizes and shapes control and the prevention of the intrinsic propensity of nanoscale aggregation. In addition, the way how the supported catalysts prepared has a significantly effect on the catalyst activity, selectivity and lifetime.

The most popular standard for a high-performance catalyst is well dispersed particles with narrow size distribution on the support. Considering these criteria, several innovative and cost-effective preparation methods have been developed, and the performance of the produced catalyst can be optimized by controlling the synthetic procedures and conditions. The most common methods involve impregnation, deposition precipitation, colloidal, strong electrostatic adsorption and electroless deposition.

1.2.1 Impregnation

By far the most widely used catalyst preparation route is impregnation, which is often referred to impregnation and drying, due to its simple execution and low waste streams on both the laboratory and industry levels. [14] Many types of catalysts are produced by impregnation of porous supports with solution containing the precursor of the active components, followed by the drying and calcination and or reduction of the impregnated support. Two main impregnation methods are used, namely, wet impregnation (WI), whereby an excess amount of solution is used, and dry impregnation (DI), in which an amount to just fill the pore volume of the support is used. There are many advantages of using impregnation, such as high efficiency, simplicity as no filtration is necessary and known metal loading. However, it is difficult to maintain catalyst dispersion and narrow size distribution.

1.2.2 Deposition precipitation

The limit of impregnation often relates to poor reproducibility, a very broad distribution of particle size, and low to medium loadings of the active phase. To overcome the disadvantage of the impregnation method, homogeneous deposition precipitation (DP) has been developed and become an attractive alternative. The biggest advantages of DP is the

ability to achieve very high wt. loading of catalysts. [16] DP concerns deposition from a precursor solution through a change of pH, temperature, or evaporation and has long been used to produce supported catalysts. Controlled precipitation from a precursor solution follows the principles of nucleation and growth. An initial nucleation boom of tiny crystallites followed by its growth without the formation of new nuclei can result in small and quite monodisperse particles. This concept is known as “burst nucleation” and is not only important for precipitation but also key in the synthesis of colloids, which will discuss in the following.

1.2.3 Colloidal

Colloidal preparation methods may serve as another promising alternatives as the produced catalyst are usually with a narrow size distribution. Four components, metal precursor, surfactant, solvent, and reducing agent, are needed for the colloidal synthesis of metal nanoparticles. For a typical synthesis procedure, desired precursors are selected firstly and then dissolved into the solvent in the presence of surfactants. The reduction process then proceeds at an elevated temperature to generate metallic nanoparticles by introducing a reducing agent. The subtle combinations of these four general components make it possible to control the final size and shape of the metal nanoparticles. Usually, one of the major challenges in catalysis is the thermal removal of surface capping molecules. The surfactant for nanoparticle synthesis plays a key role in endowing colloidal stability and surface regulations which determines the particle morphology. However, organic capping agents usually require a high temperature which can lead to nanoparticle sintering.

1.2.4 Strong Electrostatic Adsorption

Another preparation method that has been developed for supported catalysts preparation is strong electrostatic adsorption (SEA) method. Compared to those simple impregnation methods, the prepared catalysts from SEA were shown to have better mixing and interaction between the metal components due to the strong interaction between the precursor and the support. SEA is a wet impregnation synthesis technique where metal precursors are adsorbed onto a charged surface. By carefully adjusting the pH of the solution, anionic or cationic metal precursors will show a coulombic attraction to the support. Anion precursors will adsorb over a protonated surface below the point of zero charge (PZC), and similarly, cations will adsorb over a deprotonated surface above the PZC. The key behind the SEA is to control the pH of the excess liquid to arrive at the optimal point where the metal complex-surface interaction is the strongest. With the strong interaction, the metal migration is limited to minimum extent during thermal treatment, resulting in small metal particles.

The SEA catalyst preparation process is shown in Fig. 1.1. [17] The PZC of the support is first determined, [18] Followed by the second step where an uptake-pH survey on support over a range of Ph is conducted to determine the optimal pH at the maximum electrostatic adsorption. Then adsorbed precursor on the support at the optimal pH is dried and reduced to obtain the metallic nanoparticles. SEA has been successfully applied to synthesize highly dispersed metal nanoparticles (1-2 nm) on a variety of oxides and carbon supports. [19-21] SEA can also be used to synthesize bimetallic catalysts through a simultaneous way (co-SEA), and previous work from Regalbuto group produced homogenously alloyed supported nanoparticles via co-SEA. [22]

Selecting a suitable metal precursor with the correct charge is a challenge of SEA method. In addition, due to the nature of the metal complex adsorbing in a monolayer, achieving more than a monolayer coverage of precursor at one time is impossible. What's more, although this method works well for low to medium weight loadings of metal on high surface area supports, low surface area supports limit the total weigh loadings of metals due to the low surface charge of the support. However, the weight loading of a catalyst can be increased by cycling SEA. After a completed cycle, the metal is reduced, and available surface is freed for the adsorption of the precursor. Mehrabadi [23] increased Pt weight loading on carbon support by 3 successive cycling SEA and obtained a Pt weight loading of 21 % which is almost the same as the commercial impregnated 20 % Pt sample.

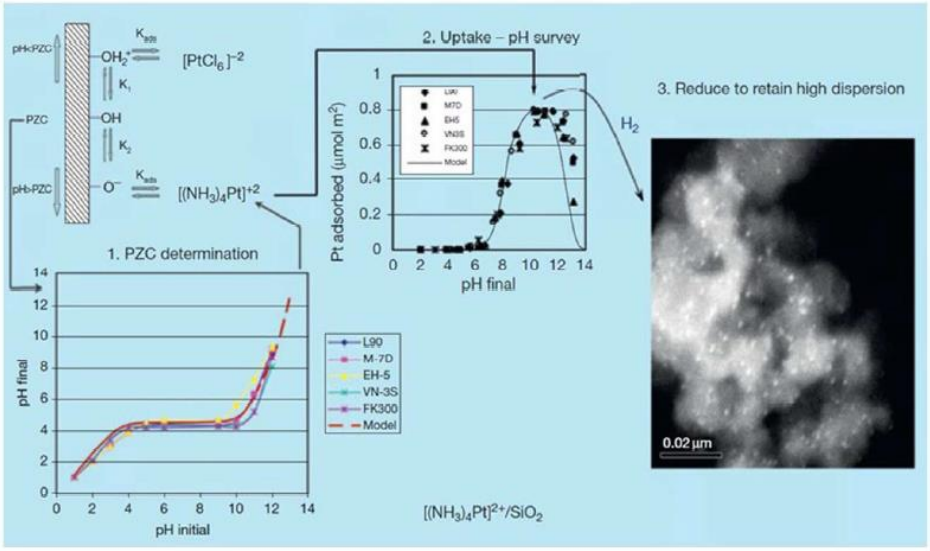

Figure 1.1 SEA procedure: 1, PZC determination, 2, uptake-pH survey, 3, reduction.

1.2.5 Electroless Deposition

Overview of electroless deposition

Electroless deposition (ED) is also one promising alternative to the conventional preparation methods. In this catalyst preparation method, a controlled chemical reaction is

used to deposit metal salt onto a pre-existing catalytic metal site that has been activated by a suitable reducing agent (RA). In 1835, for the first time, Von Liebig reduced a Ag (I) salt on Ag metal using aldehydes based on ED process.[24] In 1946, Brenner and Riddell successfully developed a liquid phase catalytic method for deposition of Ni metal on a variety of metal surfaces using $NiCl_2$ and NaH_2PO_2 as Ni metal source and RA, respectively, without using an external electrical current.[25] After that, Much attention has been attracted to develop systematic and reproducible electroless deposition baths for different metals, including the work of Ohno [26, 27]and Paunovic [28, 29]. A schematic representation of the ED process is shown in Fig. 1.2. The ED process may be either catalytic (deposition of metal salt [metal A^+] from solution onto a pre-existing metal surface [metal B^0] on a support) or autocatalytic deposition of metal salt [metal A^+] onto the just reduced and deposited metal [metal A^0]). Electroless deposition always begins with catalytic deposition, and at some points catalytic deposition and autocatalytic deposition occur simultaneously, or successively, depending on the selection of the RA and catalytic properties of the primary and secondary metals. If only catalytic deposition takes place, a mono-dispersed monolayer of the secondary metal will be deposited on the surface of the primary metal. On the other hand, three-dimensional deposition of the secondary metal can occur if autocatalytic deposition becomes dominant at some point during the reduction process. If autocatalytic deposition occurs only after the primary metal surface being covered, a core-shell bimetallic particle will then be formed. Most importantly, autocatalytic process will be optimized in this dissertation to deposit the same metal as the pre-existing metal to gradually grow the metal particle size forming monometallic catalysts. This will be discussed more in details in the chapter 2 and 3 of this dissertation.

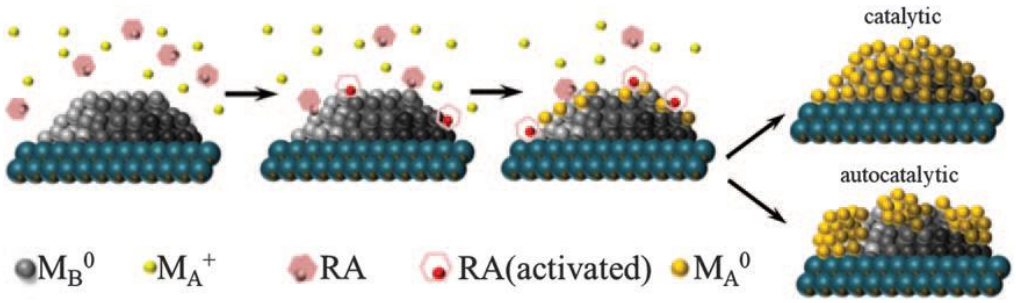

Figure 1.2 Electroless deposition method scheme

1.2.5.1 Parameters of electroless deposition

Prior to the ED process, important test on the precursor interactions with the support by SEA and unwanted thermal decomposition (which would hinder ED occurrence on the primary metal must be done.

Firstly, SEA test of the reducible salts needs to be considered. The charge of the reducible metal salt must be the same as the surface of the catalyst support to avoid the metal salt electrostatic adsorption on the support. For instance, the ED operating pH of reducible salt $PtCl_6^{2-}$ should be in the range of the negative charge of the catalyst support. Otherwise, $PtCl_6^{2-}$ will directly adsorb on the support instead of the pre-existing metal surface according to the ED mechanism. Thus, the reducible metal salt must be selected to be in a non-SEA situation. Because most reducing agents operate better in basic media (formic acid in acidic condition),[24] the surface of most supports must be negatively charged. Table 1.1 lists common metal precursor salts that are usually used in ED.

Secondly, the ED bath is formulated to be metastable, so the reaction is thermodynamically spontaneous but kinetically slow in solution. Thus, the developed ED bath must be stable for a period of time longer than the required deposition time. Therefore, the reducible metal salt, RA, and an optional stabilization must be carefully chosen to

ensure stability against spontaneous reduction to metal nanoparticles over some temperature and pH range.

Table 1.1 Common metal precursors and relative complexing agents for ED

Metal	Metal Precursor	Complexing agent
Pt	$H_2(PtCl_6)$, $Na_2(PtCl_6)$, $Pt(NH_3)_4(NO_3)_2$	Citrate, acetate, ammonium, ethylenediamine
Ag	$AgNO_3$, $NaAg(CN)_2$	Cyanide, ammonium
Pd	$Pd(NH_3)_4Cl_2$, $Na_2(PdCl_4)$, $PdCl_2$	Citrate, acetate, ammonium, ethylenediamine
Cu	$Cu(NO_3)_2$, $KCu(CN)_2$	Cyanide, triethyl amine, EDTA, glycolic acid
Ni	$Ni(NO_3)_2$, $NiSO_4$, $NiCl_2$	Propionate, succinate, citrate, EDTA, ethylenediamine
Co	$Co(NH_3)_6Cl_6$, $Co(NO_3)_2$, CoSO4	Propionate, succinate, citrate, EDTA, ethylenediamine
Ru	$Ru(NH_3)_6Cl_3$, K_2RuCl_5	Citrate, acetate, ammonium, ethylenediamine

RA dissociates on core metal and donates the electrons to reduce the metal salts in solution, so it is very important to find suitable RA. RA must have a favorable oxidation potential to thermodynamically reduce the metal ion, but not too strong that thermally reduction metal occurs in solution before activation on a primary metal surface. Common reducing agents being used in ED include dimethylamine borane (DMAB), hydrazine (N_2H_4), formaldehyde (HCHO), formic acid (HCOOH) and hypophosphite (NaH_2PO_2). A sufficient standard oxidation potential to reduce all Group VIII and Group IB metal salts is needed for RAs. Previous work by Ohno et al.[26] examined the anodic oxidation of various RAs (NaH_2PO_2, HCHO, $NaBH_4$, DMAB and N_2H_4) on noble metal electrodes (Au,

Pt, Pd, Ag, Cu, Ni, and Co) with special interest on the catalytic aspect of electroless plating. Fig. 1.3 shows comparison of the anodic oxidation potential of these reducing agents for different metal electrodes. Catalytic activity increases with decreasing anodic potentials. If the reducing agent is more active (more negative redox potential) on the secondary metal surface, autocatalytic deposition is favored. On the contrary, if reducing agent activity on the primary metal surface is more negative, catalytic deposition will be favored over autocatalytic deposition. The bath stability of the metal source and RA without the presence of primary metal should be investigated before ED experiment. If the bath is unstable, complexing agents, like ethylenediamine (EN) or ammonium (NH_4OH) could be added into the ED bath to increase the kinetic stability by preventing the thermal decomposition of metal salts with RAs. In addition, complexing can change the cationic metal source from cationic to anionic metal or vice versa. This would give another opportunity to select suitable meal salts and RA to avoid SEA for some typical supports. Some metal salts, like Ag $(CN)^-$ can function as a complexing agent by itself. A listing of common complexing agents for some metals is shown in Table 1.1. EN and is used in this dissertation to stablize Pt, Pd, Cu, Co and Ni metal ion while NH_4OH is used to stabilize Ag^+.

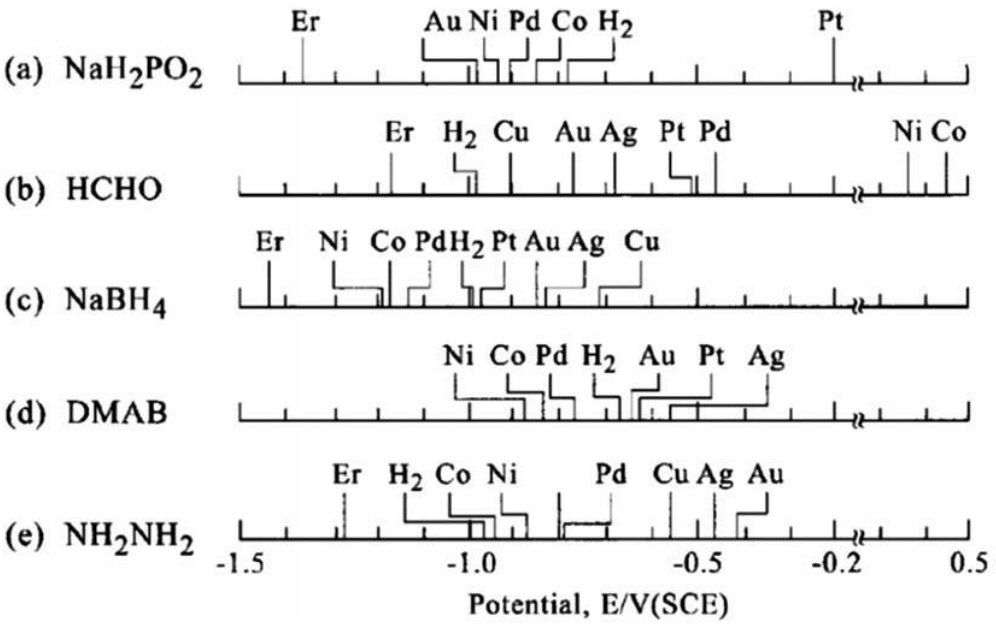

Figure 1.3 Catalytic activities of metals for anodic oxidation of different reductants

Besides, operating conditions such as agitation, pH and temperature also have significant effects on ED process. Increasing bath agitation may increase the rate of deposition by decreasing external mass transfer limitations. For external mass transfer limitations to be operative, the rate of diffusion must be slower than the rate of deposition. On the other hand, excessive agitation can attrite the base catalyst to fine powder which is difficult for filtration and may cause pressure drop in flow reactors during any subsequent evaluation process. Practically, powdered catalysts cannot be used in large volume commercial reactors, so ED conditions must be adapted to shaped and extruded supports. An example of formed sieved 20-40 mesh Al_2O_3 support will be discussed in chapter 3. Percolating ED bath is designed here to address this problem. Solution pH is another key aspect in ED method, because the stability of certain metal salts changes with pH. For instance, dissolved $AgNO_3$ in water precipitates (achieved by adding ammonia hydroxide and precipitation) disappears with more ammonia hydroxide.[30] As a result, a certain pH

range should be maintained during ED process. Also, the bath pH has a significant influence on the reducing agent's standard potential. For example, the standard potentials for oxidation of both formaldehyde and hydrazine can change ~1V with pH changes [24]. As a result, variations in pH can affect the rate of deposition. Finally, the impact of temperature on ED has also been investigated.[31] since temperature is exponentially related (Arrhenius factor) to the rate of deposition regardless of which reducing agent is used while ED baths can also become unstable at high temperatures. Therefore, choosing an appropriate temperature with the balance of bath stability and deposition rate is crucial in ED bath development.

1.2.5.2 Continuous electroless deposition

Batch ED method has been used in our laboratories to deposit a wide variety of metals including Pt [32], Cu [33], Ag[34], Au[35], Ru[36]. As shown in Fig. 1.4, the concentration of metal salts and RA are front-loaded into the bath, meaning bath instabilities are highest even before ED begins. This standard batch ED is not feasible in depositing large amount of Pt on high weight loading Pd/C catalyst. $(PtCl_6)^{2-}$ has a high reduction potential of 0.718V at basic pH 9 when employing strong reducing agent of N_2H_4. [37] One way to prevent the thermal reduction of $(PtCl_6)^{2-}$ is to pump N_2H_4 into the ED bath, denoted as semi-continuous ED, since all $(PtCl_6)^{2-}$ is initially added to the ED bath. In addition to semi-continuous ED, continuous ED has been developed to address unstable baths and make ED more attractive for large scale use.[38] By adding controlled concentrations of a metal salt and RA from two independent syringe pumps, as shown in Fig. 1.5, neither metal salt nor reducing agent concentration accumulates in the ED bath, which minimizes thermal reduction. Continuous ED gives more kinetics control over ED, it provides an easy way to

deposit desirable amounts of metals as large as needed. The relative simplicity and versatility of continuous ED suggests that to simultaneously deposit two or more different metal salts on a base catalyst could be achieved simply by adding extra syringe pump for the addition of other metal salt. [39] Three syringe pumps containing two different salts and one RA are used to synthesize Pd-Cu bimetallic catalysts on Ag plasmon in this dissertation.

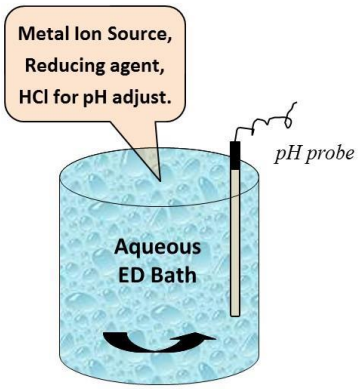

Figure 1.4 Schematic representation of batch ED bath

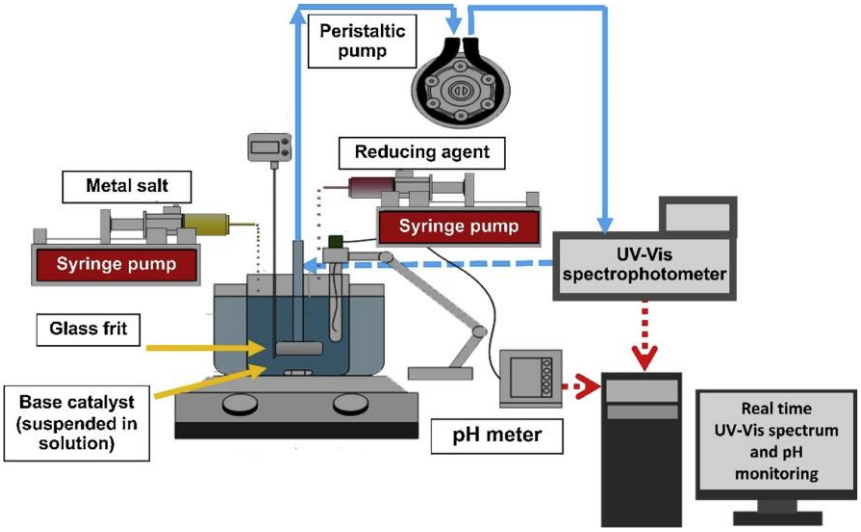

Figure 1.5 Configuration of continuous ED apparatus

1.3 catalyst characterization

Quantitative characterization of the exposed, reactive surface is of great importance in the study of catalytic reactions on supported metals. The fraction of metal available on the surface is reported as dispersion and its measurement can be done with various techniques in catalyst characterization. Chemisorption is one of the classic and most frequently used techniques. It is based on the formation of a strong chemical bond between the adsorbate gas molecules and the exposed metal surface. O_2 precover- H_2 titration method is commonly used for measuring the metal dispersion. The useage of other methods, such as XRD and electron microscopy, to obtain the surface information is strongly advisable. Size discrepancy between different analytical methods is expected since the XRD measurements are also recording dislocations in the crystal structure which are not registered by chemisorption. Due to the theory difference behind the crystallite size calculations, the calculated size from XRD is always smaller than the chemisorption methods. Extra information about the crystallite size distribution can be derived from XRD measurements, which are additionally suitable for the development of new or improved catalysts. TPX (X = oxidation, reduction or desorption) is used to study the surface property of the catalyst. For instance, surface contamination of carbon species or residual reactant from the catalyst preparation. Apart from these methods, X-ray photoelectron spectroscopy (XPS) is one of the other most valuable surface science tools for the studies of the chemical state and surface composition of heterogenous catalysts.

1.4 Thesis layout

The purpose of this dissertation is to focus on the field of catalyst synthesis through ED with desired composition and size to produce target products. By understanding the ED

process, synthesis engineering can aid in controlling metal particle size on support. Also, catalytic properties can be tailored rationally by carefully tuning of catalyst size and composition. In chapter 1, background of this work and review on different synthesis method are discussed. Chapter 2 discusses size control of carbon supported Pt particle being prepared by ED. Uniformly dispersed Pt particle is produced by transferring from semi-continuous ED to continuous ED. Better size control is achieved by extending the deposition time. This work led to a CeRCaS funding project of precision control of supported nanoparticle size via ED. Chapter 3 studies the effect of Al_2O_3 supported Ag size on the ethylene epoxidation. Variable Ag size ranging from 44 nm to 381 nm is obtained by increasing the length of deposition time using developed percolating ED bath. Catalytic activity evaluation under real reaction condition demonstrates that the TOF of EO formation is a function of the Ag size. Chapter 4 studies the synthesis of bimetallic Pt-Ru catalysts on multi-wall carbon nanotubes by ED. The prepared catalysts exhibit higher mass activities than the commercial Pt-Ru catalysts in direct methanol fuel cells. Chapter 5 extends the ED application to deposit two metals (Pd and Cu) simultaneously. Unique catalysts with predicted metal composition are tested in catalytic CO_2 reduction. Chapter 6 summarized this dissertation and provides outlook for future work on ED.

CHAPTER 2

SIZE-CONTROLLED SYNTHESIS OF PLATINUM PARTICLES BY CONTINUOUS ELECTROLESS DEPOSITION

2.1 Abstract

In catalysis with supported metal nanoparticles, the size and distribution of particles are critical in catalyst design to obtain optimized performance. This work demonstrates a straightforward synthesis methodology of controlling carbon-supported Pt nanoparticles size. Firstly, SEA is used to make ultrasmall core Pt particles (2.1nm). By using ED to deposit additional metal over these existing particles, larger sizes are systematically prepared without producing any additional particle and maintaining the original site density. Continuous ED exhibits better stability against thermal reduction by simultaneously pumping the metal salts and reducing agent. Same Pt wt% samples were prepared by manipulating the deposition time. Size measurements by XRD, chemisorption, and STEM show that Pt size distribution depends on the deposition time. Longer deposition time gives tighter size distribution.

2.2 Introduction

The study of catalyst structure sensitivity is to investigate the effect of the supported metal particle size on the reaction activity and selectivity.[40-43] In 1966, Boudart and coworkers found that the reaction rate of cyclopropane hydrogenolysis is a function of the size of the supported Pt catalyst, and based on the work, he classified catalytic reactions into two types: structure sensitive and insensitive.[44] After that, the interest on study the effect of catalyst size on activity and selectivity has been intrigued. For instance, on Pt/Al_2O_3 catalysts, the optimal CO oxidation activity was found in a 2−3 nm particle size range.[45-47] For the Pt particle with a size of 1−9 nm, the catalyst activity towards propane dehydrogenation increases with decreased size. [48-50] The activity and the selectivity towards Methylcyclopentane (MCP) hydrogenolysis ring-opening products

(ROP) is also found to be a function of Pt catalysts size since the active sites responsible for n-H production are corners and a proportion of edge sites while 2-MP and 3-MP are produced on faces and a part of the edge sites[51]. Besides, the oxygen reduction reaction (ORR) on carbon supported Pt particles is a typical structure-sensitive reaction in electrocatalysis, and the optimal Pt particle sizes were found to be 2–3 nm. [52-54]

Recently, significant progress in the size-controllable synthesis of uniform and precisely tunable Pt particle has been made to understand the nature of particle size effect. Especially, the widespread utilization of careful the advanced characterization methods, such as transmission electron microscopy and gas chemisorption, have greatly promoted the size effect study. Metal particles synthesized by traditional preparation method, such as incipient wetness or impregnation, however, often exhibit a broad size distribution which greatly restrain the systematic studies of particle size effects.[55, 56] The grand challenge of synthesizing size-controllable metal particles by colloidal chemistry is to thermally remove the surfactants without losing original particle size distribution.[57] Although several more synthetic procedures are now available to synthesize metal nanoparticles with good particle size control, most of these procedures can only produce nanoparticles with a limited range of size. To synthesis catalyst with a wide range of size, a combination of various methods may be required. However, each of those individual synthetic procedures may influence the catalytic performance of the catalyst,[49, 58-60] which may make it difficult to interpretate the catalysis reaction results. Electroless deposition (ED) methods, on the other way, may serve as a promising alternative in precise size control synthesis of metal nanoparticles. ED is a catalytic or autocatalytic process that certain amount of metal atoms can be selectively deposited onto pre-existing core particles

in a controlled manner. ED has been used to deposit a wide variety of metals, including Ag [61], Ru [36], Cu, Au [38], and Ni, Co[62]. Various Pt particle size can be generated with careful tuning of the ED process by gradually depositing Pt atoms on Pt core. Recent work [38, 39] demonstrated that continuous ED can enlarge the thermal stability of ED bath and permit greater control over the ED reaction.

To conduct the catalysts synthesis by ED in this work, firstly, strong electrostatic adsorption (SEA) [14, 17]was used to produce small and uniform Pt nanoparticles on carbon support as a core for ED. The ED process begins with this Pt core by continuously pumping Pt salt and reducing agent into the ED bath forming Pt layer over the Pt core. ED experiments reported here vary from semi-continuous ED which first loads the metal salts and continuously pumps reducing agent into the reaction bath, while the metal salts and reducing agent are simultaneously pumped into the continuous ED bath to increase the ED bath thermal stability. The resulting catalyst was then characterized by a variety of analytical techniques, including scanning transmission electron microscopy (STEM), XRD and selective chemisorption to measure the Pt particle size. The procedure was repeated with a wide range of concentration of Pt salt and reducing agents and deposition time. We found that the average size of the deposited Pt depends strongly on the deposition time and that thus could be tuned to control the average size of the particle and prepare catalyst with specific particle size.

2.3 Experimental methods

2.3.1 Pt/C catalyst synthesis with SEA

Preparation of Pt/C catalyst was conducted by SEA method. Vulcan XC72 carbon (C) with a surface area of 250 m^2/g and PZC of 8.5 was used as the support. Chloroplatinic

acid (H_2PtCl_6) from Sigma-Aldrich was diluted in 1005 ml de-ionized water (18.2 M-cm) resulting in a Pt concentration of 200 ppm. The H_2PtCl_6 solution was then adjusted to an initial pH of 3 with NaOH base to achieve maximum uptake as reported previously[20]. The solution was then aged for two days before being readjusted to the same starting pH. This aging procedure was repeated twice until the pH of the solution gets stable. After that, 5ml aliquot of this solution was taken as initial sample and 2g carbon was added into the solution, corresponding to 500 m^2/L surface loading. The slurry was then shaken vigorously (~120 rpm) for an hour. The pH of the slurry was measured and then filtered. A sample of the filtered liquid was taken as the final sample. Pt wt% was calculated by measuring the Pt concentration of the initial and final sample with Inductively Coupled Plasma (ICP). The filtered powder was then dried in an oven at 120 °C overnight, followed by a reduction at 200 °C for 1 h with a heating ramp of 2.5 °C/min under 10% H_2 - balance He flow (200 sccm total) in a horizontal tubular furnace. The resulting 6.4% Pt/C catalyst was cooled to room temperature prior to being stored. Another 6.4% Pt/C was made by dry impregnation (DI) to compare with the Pt/C catalyst prepared by continuous ED.

2.3.2 Pt/C catalyst prepared by ED

More Pt was added to the Pt/C base catalyst to grow large size Pt particle using continuous ED method as described in early studies[37, 39]. H_2PtCl_6 and hydrazine (N_2H_4) was chosen as the Pt salt and the reducing agent, respectively. (EN) was selected as the stabilizing agent to prevent the unwanted thermal reduction of H_2PtCl_6 and N_2H_4. The detailed setup of ED is shown in Fig 2.1. EN was mixed with the H_2PtCl_6 solution before loading to one syringe pump at a molar ratio of [EN] / [（$PtCl_6$）$^{2-}$] = 2 / 1. Another syringe pump contains the N_2H_4 solution at a molar ratio of [N_2H_4] / [$PtCl_6^{2-}$] = 5 / 1 after the period

of ED. Both Pt salt and N_2H_4 were continuously pumped into the well-stirred ED bath within different deposition time as listed in Table 2.3 which also shows the reactants concentrations. Target amount of Pt salts pumping into the ED bath were selected based on the Pt final wt%. The base catalyst (0.25g Pt/C) was added to 100 ml DI water and the pH of the ED bath was maintained at 9 by adding concentrated NaOH solution, and all depositions were conducted at room temperature. To measure the kinetics of $PtCl_6^{2-}$ deposition, liquid aliquots (1 mL) were collected and filtered using 0.2 um mesh syringe filter to remove catalyst particles at different time intervals to monitor the time-dependent concentrations of $PtCl_6^{2-}$ in the ED bath. The collected liquid samples were analyzed to calculate the $PtCl_6^{2-}$concentrations by ICP-OES spectroscopy (Perkin-Elmer Optima 2000 DV). After the completion of ED, the slurry was filtered and washed thoroughly with excess DI water. The wet sample cakes were dried in vacuum at room temperature and stored at ambient conditions.

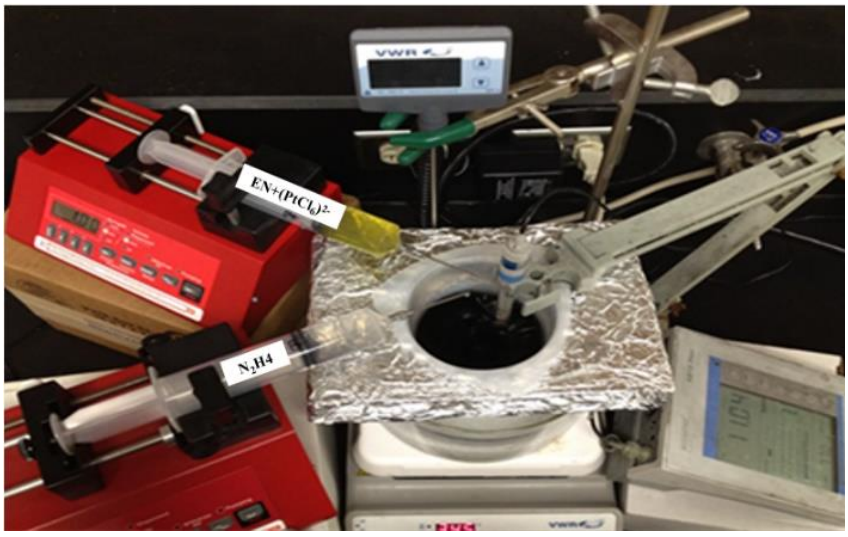

Figure 2.1 Continuous ED setup for Pt catalyst preparation

2.3.3 Pt/C catalyst characterization

Chemisorption was conducted in a Micromeritics Autochem II 2920 analyzer for all the prepared catalysts. About 0.1 g sample was used for analysis and 3 successive analyses of O-precover and H_2 pulse titration were conducted to determine Pt particle size. Catalysts were subjected to reduction pretreatment at 200 °C in 10% H_2/ balance Ar and cooled down to 45 °C before being contacted with 10% O_2/balance He for 30 min. Once the catalyst is cooled down, Ar is flowed to purge physisorbed O_2, and at the same temperature, 10% H_2/balance Ar is pulsed which reacts with the chemisorbed oxygen to form water and chemisorbed H. The stoichiometry of the chemisorption is 0.667 surface metal: 1 H_2. Particle dispersion was then obtained from the hydrogen consumption and catalyst loading while particle size estimation was calculated assuming a hemispherical geometry. Uptake was determined by the summation of pulse area and gas loop volume. This procedure was repeated three times per sample to ensure reproducibility, with average values and standard deviation being reported.

Particle size can also be obtained from STEM images taken by an aberration corrected JEOL 2100F STEM which is equipped with a 200kV field emission gun and a double tilt holder for tilting the sample across a range of angles (± 20°). Particle size distributions were obtained by counting about 1000 particles on each sample. Based on the STEM images, the volume average sizes (D_V) and surface average sizes (D_s) are determined based on the following equations, where d_i represents the particle size and n_i is the number of particles in each size increment.

$$D_V = \frac{\sum n_i d_i^4}{\sum n_i d_i^3}$$

$$D_s = \frac{\sum n_i d_i^3}{\sum n_i d_i^2}$$

The volume average will be compared with the results from the XRD analysis, and the surface average data will be compared with data from the chemisorption results. [63]

A Rigaku Miniflex II equipped with a high sensitivity D/teX Ultra silicon strip detector and Cu Kα radiation (λ=1.5406 Å) was applied to investigate the crystallographic properties of powder catalysts. Scans were made in a 2θ range of 20˚-80˚ with a scan rate of 2.0˚ 2 θ /min. Metal diffraction patterns are deconvoluted using Gaussian peak shapes. Average particle sizes are estimated by the Scherrer equation with a shape factor of 0.94.[64]

Temperature Programmed Oxidation (TPO) was conducted in a custom TPX System fitted with an inficon transpector 2 Mass Spectrometer. About 0.1 g sample was loaded in the reaction tube. Moisture was removed by heating the sample at 200 °C inflowing Helium until the water signal is diminished. TPO was done immediately afterwards with a ramp of 10 °C /min from 35°C to 250 °C, flowing 10% O_2 in Helium at 20 sccm. The CO_2, H_2O and N_2 or CO signals were primarily monitored during the experiment.

2.4 Results and discussions

The Pt weight loading of the Pt/C base catalyst made by SEA is determined to be 6.4 %. Representative STEM image and size distribution of the 6.4% Pt/C catalyst made by SEA are shown in Fig. 2.2 (a) and (b), respectively, and well dispersed particles with narrow size distribution were observed. The XRD profile of base Pt/C catalyst, hereby denoted as 6.4 % Pt, SEA, demonstrates a peak position for FCC phase Pt as shown in Fig. 2.2. Broad peaks which correspond to metallic Pt phase were observed, indicating well

dispersed Pt particles. Deconvolution of these Pt phase peaks from carbon support signal contribution and using Scherrer formula XRD line broadening calculated an average particle size of 2.1 nm. SEA produces much smaller particle than DI sample (3.7 nm from XRD calculations), designated as 6.4% Pt. The volume and surface average particle sizes from the STEM are summarized in Fig. 2.2 (d), and comparison between results from XRD and chemisorption are also shown. A good agreement in the determined particle size was found between various characterization methods.

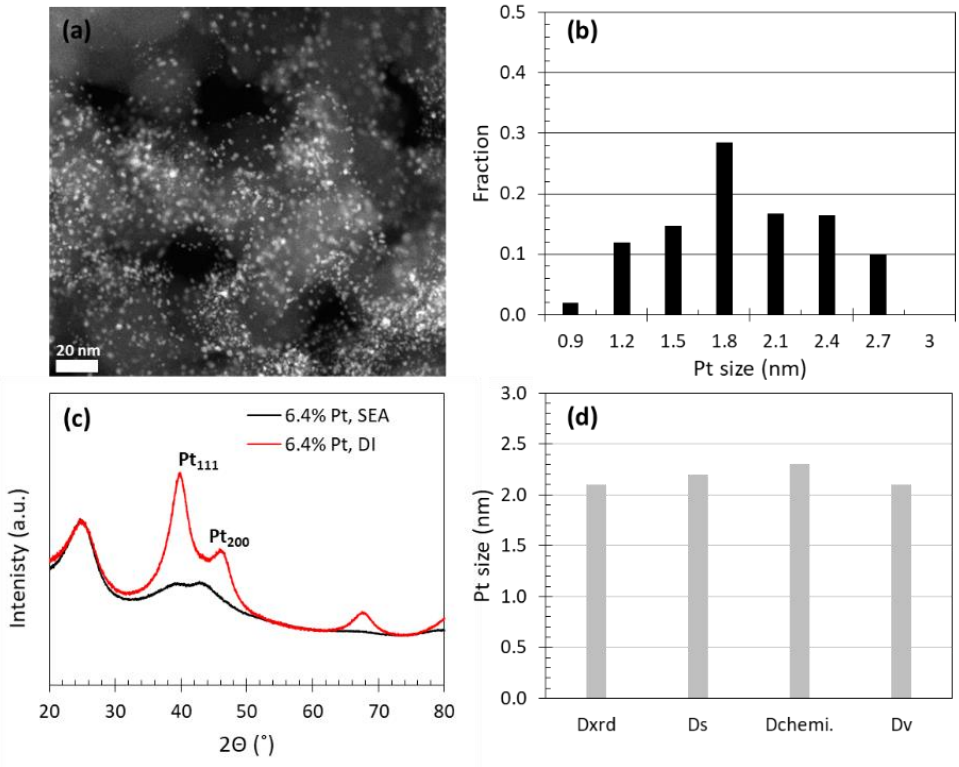

Figure 2.2 STEM image (a), particle size distribution (b) and XRD patterns (c) of the 6.4% Pt/C sample prepared by SEA and DI, (d) Comparison of the particle size of the 6.4% Pt/C sample determined from XRD, Chemisorption and STEM.

In the following, various ED parameters are investigated to explore the effect on the catalyst preparation. Firstly, deposition time is studied since it is one of the most important ED parameters (as discussed in section 1.2.5). Fig. 2.3 shows the change of the amount of

deposited Pt along with time during ED process for the synthesis of 9.0% Pt/C and 7.7% Pt/C sample from base catalyst (6.4% Pt/C). The final Pt wt% was calculated by adding the amount of deposited Pt to the base catalyst. Left plot in Fig. 2.3 shows the time-dependent Pt deposition for the 9.0% Pt/C sample preparation with a deposition time ranging from 10 mins to120 mins, while the left plot shows the trend for the 7.7% Pt/C sample preparation with a deposition time ranging from 30 to 480 mins.

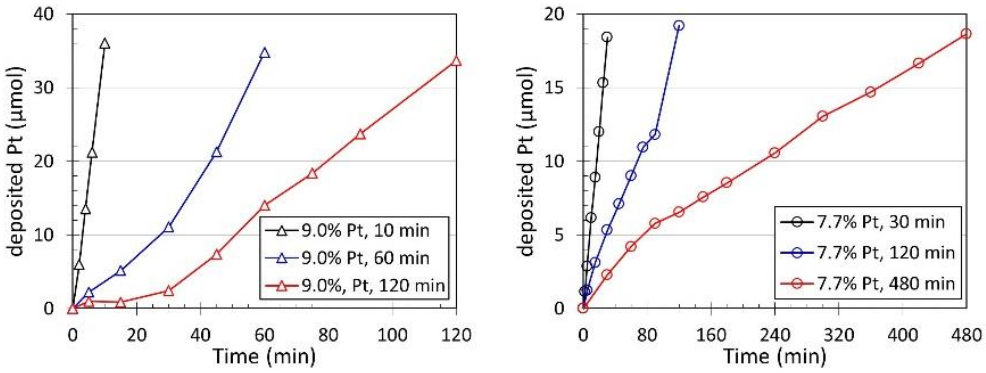

Figure 2.3 Time dependent ED profiles of 9.0% Pt/C (left) and 7.7%Pt/C (right).

TPO was employed as a diagnostic technique to determine the Pt surface contamination caused by the synthesis and exploit the cause of the difference between the chemisorption data and that from other methods. For instance, the TPO profile of the 9.0% Pt sample as shown in Fig. 2.4., reveals that CO_2, H_2O and N_2 or CO signals start to take off at about 150°C, demonstrating demonstrates that ethylenediamine (NH_2-CH_2-CH_2-NH_2) which is a residual from ED process, produces CO_2, H_2O and N_2 or CO in the O_2 rich environment. Besides, TPO result confirms the hypothesis that residual ethylenediamine blocked the Pt surface site and chemisorption data estimated bigger Pt particle size than the actual size.

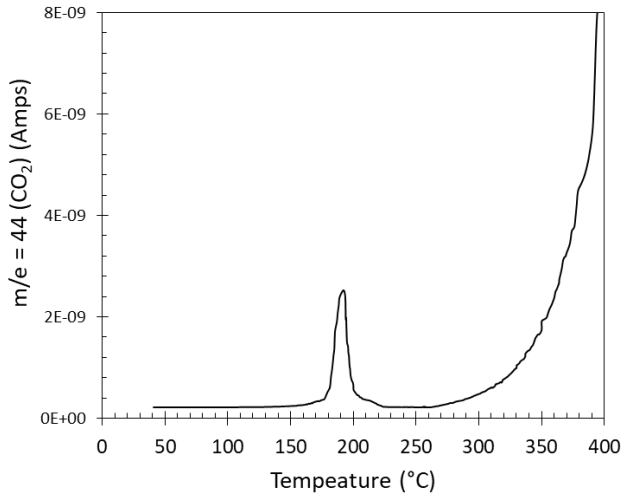

Figure 2.4 TPO profile of 9.0 % of Pt/C sample

Prior to the selective chemisorption, 9.0% Pt/C and 7.7% Pt/C samples were preheated in 10% O_2 at 250 °C to burn off the residual EN and other impurity, followed by reduction in 10% H_2 at 200 °C to remove oxidation layer. The Pt size was then calculated from H_2 uptake by assuming 0.667 H_2 molecule was chemisorbed on a Pt surface atom. Pt particle size was also estimated with XRD data from the same sample taking out from the chemisorption sample tube. The XRD characterization profile of these two samples is shown in Fig.2.5. For the 9.0% Pt/C sample, with the deposition time decreasing from 10 to 120 mins, FCC Pt peaks became sharper and bigger, and the particle size was estimated to increase from 3.3 to 4.6 nm with decreasing deposition time as shown in Table 2.1. For the 7.7% Pt/C catalyst, the process with deposition time of 480 and 120 mins produces the same size of Pt particle (2.5 nm), while the particle size from the ED process with 30 mins deposition was estimated to be 2.8 nm.

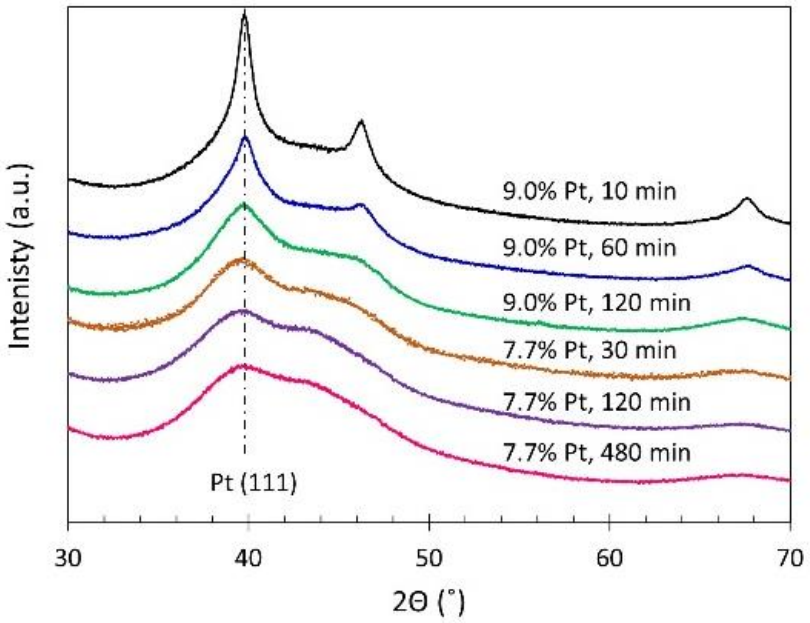

Figure 2.5 XRD patterns of 9.0%Pt/C and 7.7%Pt/C sample.

Besides, STEM analysis on these samples was performed to gauge the effect of deposition time on particle size and also on breadth of the size distribution. Representative STEM Z-contrast images and particle size distributions are shown in Fig.2.6 (a), (b), (c) for 9.0%Pt/C catalyst, and (d), (c), (f) for 7.7%Pt/C catalyst with various deposition time. The smaller average size and wider distribution of catalyst particle prepared with longer deposition time for 9.0% Pt/C is confirmed, and the particle size follows the order of 10 min (4.5 nm)>60 min (3.8 nm)>120 min (3.3 nm). Same analysis result from XRD, STEM images for the 7.7% Pt/C sample shows no significant change in the particle size with deposition times varying from 120 to 480 minutes. What's more, Pt nanoparticles are uniformly distributed on the surface of carbon substrates and the observed metallic particle sizes are predominately in the range of 1.5–3.0 nm. Interestingly, boarder particle size distribution was found when the ED process was conducted at a deposition time of 30 mins.

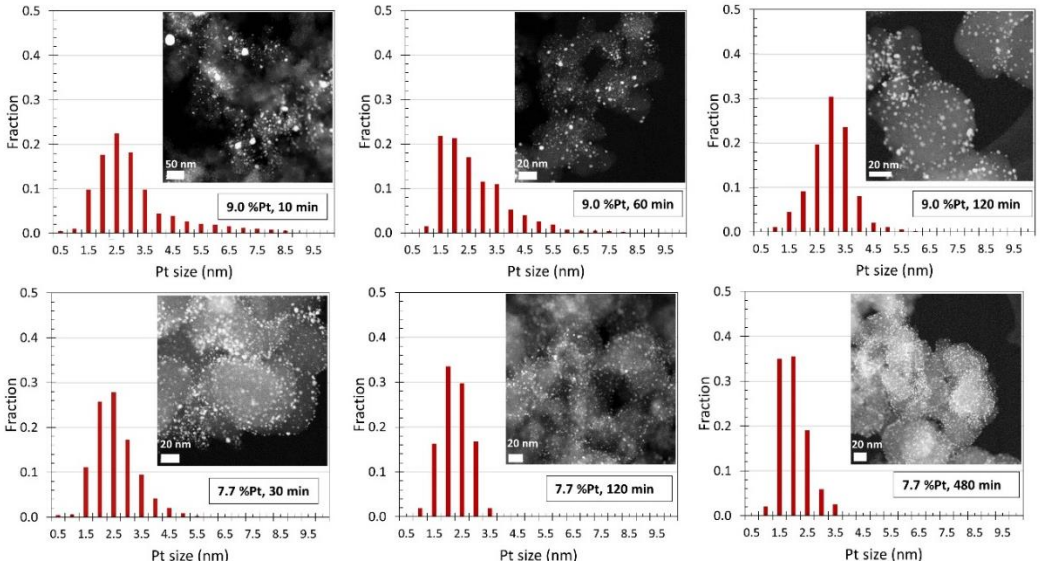

Figure 2.6 STEM images and particle size distribution with decreased deposition time of (a) 10 mins, (b) 60 mins, (c) 120 mins for 9.0%Pt/C catalyst; (d) 30 mins, (e) 120mins, for 7.7%Pt/C catalyst.

What shown in Table 2.1 are the Pt particle size determined by chemisorption, XRD and STEM. A comparison of the obtained data lead us to the following conclusions as expected,

1) Pt particle size increases with increasing Pt wt %. Adding more Pt by kinetics control during ED on Pt core produces bigger particles.
2) Pt size distribution depends on the deposition time, and faster deposition results in boarder size range.
3) Good agreement on particle size estimation is found between XRD, chemisorption, and STEM. However, the Pt crystallite sizes measured by XRD are smaller than the crystallite sizes calculated from chemisorption, which is not surprising since the XRD measurements also record the dislocations in the crystal structure which are not registered by chemisorption.[65]

Table 2.1 ED parameter and size measurements of the 9.0 % Pt/C and 7.7 % Pt /C samples.

sample#	Pt initial wt%	deposition time(min)	Pt final wt%	chemi., nm	XRD, nm	Ds, nm	Dv, nm
1	6.4	0	6.4	2.3	2.1	2.1 ± 0.4	2.2 ± 0.5
2	6.4	10	9.0	4.6	4.6	4.6 ± 2.3	5.4 ± 2.5
3	6.4	60	9.0	4.0	3.8	3.8 ± 1.7	4.5 ± 2.1
4	6.4	120	9.0	3.5	3.3	3.3 ± 1.3	3.5 ± 1.5
5	6.4	30	7.7	3.4	2.8	3.0 ± 0.7	3.3 ± 0.9
6	6.4	120	7.7	3.0	2.5	2.5 ± 0.7	2.6 ± 0.8
7	6.4	480	7.7	2.8	2.5	2.3 ± 0.6	2.4 ± 0.7

2.5 Conclusions

This chapter investigated the synthesis of Pt nanoparticles by continuous ED. Pt particle size is found to increase with increasing Pt wt%. Continuous ED of simultaneously pumping both the Pt salt and reducing agent into the ED bath can better control the Pt salt concentration and more careful tunning of the ED kinetics. During the continuous ED process, $PtCl_6^{2-}$ is gently reduced step by step with N_2H_4 and can result in more uniform deposited Pt shell on the pre-existing Pt core. In the case of 9.0 % Pt and 7.7 % Pt sample preparation, it is found that the average size and size distribution depends strongly on the deposition time. It is also found that high Pt wt% sample with narrow size distribution can be achieved by manipulating the deposition time. This seed particle growth by continuously

pumping, which was pioneered in the field, has been established as a powerful tool for tuning the size of metal nanoparticles. The versatility and simplicity of ED make it readily for precise size control of other metal particles, for instance, Pd, which is undergoing studying in our lab. Also, in the next chapter of this dissertation, we will discuss about the tuning the Ag particle growth through continuous ED.

CHAPTER 3

STRCUTURE SENSITIVITY OF ELECTROLESS DEPSOTION DRIVEN SILVER CATALYSIS ON ETHYLENE EPOXIDATION[1]

[1] Xiong W., Egelske B. and Monnier J. R., to be submitted to *Journal of Catalysis.* (co first author).

3.1 Introduction

Ethylene Oxide (EO) is currently a 35M metric ton/year chemical that is expected to continue to grow at a 5 – 7% annual growth rate for the foreseeable future[66]. This is a remarkably healthy growth rate, particularly for a mature chemical like EO. Several billion pounds of additional capacity have recently been added in the Texas and Louisiana gulf coast due to the supply of cheap ethylene from cracking of natural gas[67]. It is the largest volume product prepared by a heterogeneously catalyzed oxidation process and accounts for almost 50% of the volume of all oxidation products. Modern high performances catalysts no longer resemble the unpromoted Ag catalyst discovered by Lefort in 1933[68]. Catalyst developments to improve selectivity to EO have gone through several phases as detailed in a Shell company magazine[69]. The Cs-promoted, Ag catalyst boosted selectivity to the 80% level and then was replaced based on the work of Lauritzen [70] that described the addition of Re^{7+} and other high valent salts including Mo^{6+}, W^{6+}, S^{6+} (as the primary promoters) existing as high valent oxyanions. EO selectivity is now as high as 90 – 92% for initial time online periods. Because the active Ag surface is loaded with multiple promoters to boost selectivity, the Ag surface site concentrations are often too low for acceptable space time yields, forcing Ag weight loadings to be increased to 30 – 40 wt% on non-acidic, fused α-Al_2O_3 supports. These supports typically have surface areas < $1 m^2/g$, so the resulting Ag particle sizes are very large and exist in a wide size distribution of surface and various surface morphologies. The scanning electron micrograph (SEM) in Fig.3.1 illustrates the variety of Ag particle sizes for "only" 12 wt% Ag supported on older generation fused α-Al_2O_3 rings with a surface area of 0.73 m^2/g, determined in our laboratory using Kr BET surface area analysis. The Ag is shown as white particles on the

dark gray α-Al_2O_3 surface. Even at the low 20K magnification, the α-Al_2O_3 surface appears rather featureless and not likely to anchor Ag particles as well as higher surface area and more interactive supports. However, to achieve the low acidity required to maintain the epoxide ring structure, low surface area is a basic requirement of all catalyst supports used for ethylene epoxidation. Note the wide distribution of Ag particle sizes and the presence of different morphologies including triangles, spheres, and faceted cuboctahedrons (Ag is an fcc metal).

One of the obvious questions that has not been clearly resolved is whether ethylene epoxidation is a structure-sensitive reaction; that is, does the rate of reaction per Ag site, more commonly known as the turnover frequency, change with the Ag particle size. It is not possible to answer this question if Ag particle sizes exist over a wide range as in Fig.3.1, since reaction rates are the sum of all particle sizes. Likewise, it is critical to have an accurate way to measure active Ag surface site concentrations. Monnier showed in earlier work [71]that a comparison of four typical techniques to measure active Pt surface site concentrations of a PEM fuel cell, specifically selective chemisorption, electrochemical surface area (ESA), x-ray line broadening, and electron microscopy, by far the two preferred methods were selective chemisorption and ESA because they actually measured, or counted, either H_2 molecules or electrons, respectively. X-ray line broadening worked only until XRD peaks became too narrow and insensitive to reflect further changes in the sizes of small crystallites. Of course, the problem with electron microscopic methods is the small number of particles actually measured and whether they represent the entire surface.

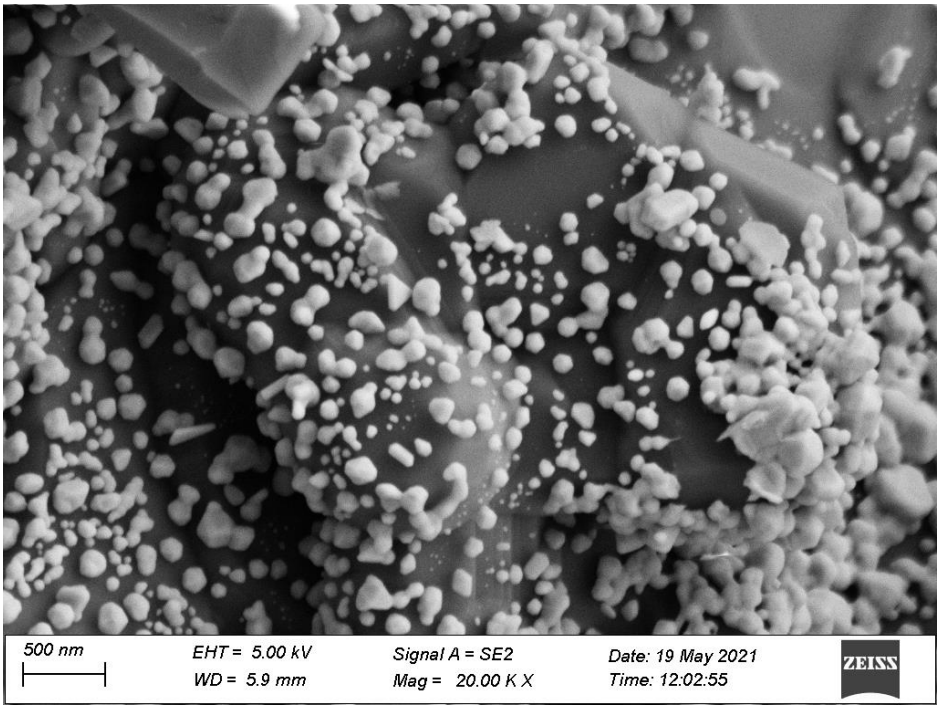

Figure 3.1 12wt% Ag supported on SA5562 alpha alumina.

Regardless, structure-sensitivity on α-Al_2O_3 supports has been investigated by a number of groups whose particle size determinations are shown in Table 1. Ag particle sizes were determined by both chemisorption and particle counting of microcopy images. In some cases, the numbers of particles countered were < 200, and in all cases less than 500. It was also not stated whether the observed size distributions were assumed to be representative of the entire sample and whether the distribution was assumed for the full Ag weight loading to determine the Ag site concentrations for spherical or hemispherical (same result) particles.

For instances where chemisorption has been reported, the data are typically based on dissociative O_2 adsorption and use 1 Ag to 1/2 O_2 stoichiometry. Both O_2 chemisorption and H_2 titration of O precovered Ag sites have been used by Vannice but results were shown to be more consistent with H_2 titration where the only species capable of undergoing

reaction with H_2 to form H_2O was monoatomic oxygen bound to the Ag surface.[72] While there are possibly and likely more than metallic Ag sites capable of adsorbing atomic oxygen, particularly for heavily promoted Ag catalysts containing Cs, Re, Mo, W, S after a high temperature reduction treatment, only Ag-O species are likely to be reactive for H_2 titration at 170 ˚C. The high valences of Re and its co-promoters and the very low ionization potential of Cs^0 make it difficult for reduction by H_2 at low temperatures such as 170 ˚C. Furthermore, the 1 : 1 H_2 to Ag-O stoichiometry doubles the sensitivity of detection improving sample-to-sample repeatability specifically for systems with low Ag site concentrations such as EO catalysts with large particle sizes.

Many have examined the EO reaction for structure sensitivity, but problems exist not only for sensitive and accurate methods of measuring Ag active sites, but also the preparation of catalysts with narrow particle size distribution. The listing of some of the more recent studies is shown in Table 3.1. Verykios [73] prepared Ag particle sizes between 35 and 170 nm using four different α-Al_2O_3 supports with surface areas ranging from 0.2 to 3.0 m^2/g. Samples were characterized by selective oxygen chemisorption at 200 ˚C and evaluated between 180 and 240 ˚C at 220 psig in an oxygen-rich feed. For one series, EO selectivity decreased as Ag particles increased from 120 to 170 nm diameter; however, with a different α-Al_2O_3, selectivity increased as particles grew from 50 to 130 nm. In later work Lee et al. [74] re-examined Ag particle size effects for a wide range of oxide supports and found that some of the oxides strongly contributed to the rate of combustion with only SiO_2 and α-Al_2O_3 having significant activity for EO formation. Contrary to their work where a minimum in EO formation rate was identified at 70nm, the α-Al_2O_3 supported samples in this study exhibited a maximum rate of formation between

40 and 80nm. Danilyuk et al. later noted the difficulty of obtaining tight particle size distributions on low surface area α-Al_2O_3. Even using a higher surface area of 7 m^2/g for alumina prepared in their laboratory which should help in narrowing particle size distributions, Ag particles between 19 and 140nm were formed by incipient wetness. Ag particle sizes were determined by TEM imaging of approximately 100 particles and compared with oxygen chemisorption whose experimental parameters were referenced in earlier work [75]. Evaluation for an C_2H_4-lean feed containing 2% C_2H_4, 7% O_2, balance N_2 at 230 ºC and 14.7 psia pressure gave a linear increase in the rate of EO formation with increasing Ag particle size over the range 19 to 140 nm; selectivity values were not discussed. In 2017 de Jongh [76] examined the effect of gas compositions on precursor decomposition for Ag particle sizes during preparation of 15wt% Ag samples supported on 8.0 m^2/g α-Al_2O_3. Particle size measurements were determined using a combination of TEM and SEM for 100 - 170 particles per sample. These results were supplemented with UV/VIS spectra to examine the Ag plasmon peak positions in the 300-750 nm range to infer Ag particle diameters assuming spherical geometry. Catalyst evaluation was conducted in a C_2H_4-rich feed and the authors concluded that at constant C_2H_4 conversions of ~2.8%, the EO selectivity was independent of particle size. However, in the analysis it was assumed that selectivity was dependent only on the competitive rates of epoxidation versus C_2H_4 combustion and that the rate of sequential EO combustion was zero and independent of the temperature used to reach 2.8% C_2H_4 conversion. Recently, Hoof et al [77] studied a series samples supported on 1.04 m^2/g α-Al_2O_3 with loadings between 1.7 and 14.0 weight % Ag. Particle sizes between 20 and 185 nm were determined from STEM for 200 – 485 particles per sample. For an oxygen-rich feed (10% O_2, 5% C_2H_4, balance

He at 225 ºC and 290 psig), it was concluded that O_2 dissociation does not occur on the external Ag surface and instead only proceeds at defect sites to form subsurface monatomic oxygen which is the responsible species for selective epoxidation. The authors note a theoretical maximum of EO selectivity of 75% for particles < 100 nm and 80% for Ag particles > 100 nm as C_2H_4 conversion approached 0% C_2H_4. In summary, there have been no agreements in activity or selectivity trends, likely because of the methods used to measure Ag particle sizes, methods of catalyst preparation, and variety of supports that were used.

Table 3.1 Literature reported Ag particle size and preparation parameters for epoxidation catalysts supported on α-Al_2O_3.

Ref	Ag Precursor	α-Al_2O_3 Support	Synthesis	SA (m^2/g)	Ag (wt %)	Max Synthesis Temperature (ºC)	Fresh SizeChemi (nm)	Fresh $Size_{TEM}$ (nm)	n
Verykios 1980	$AgNO_3$	MAG-99	Note 1	0.2	1	200	36	-	-
				0.2	1	400	43	-	-
				0.2	1	480	47	-	-
				0.2	1	600	53	-	-
				0.2	1	750	59	-	-
		NortonSA-5202		0.63	13.92	200	120	-	-
				0.63	13.92	400	141	-	-
				0.63	13.92	500	166	-	-
		Carborundum SAH7-99-Series		0.97	5.6	200	55	-	-
				0.97	5.6	400	70	-	-
				0.97	5.6	500	78	-	-
				0.97	5.6	600	100	-	-
				0.97	5.6	700	121	-	-
		Prepared by Authors		3.03	6.43	200	31	-	-
				3.03	6.43	410	43	-	-
				3.03	6.43	510	75	-	-
				3.03	6.43	700	108	-	-
				3.03	6.43	850	123	-	-
Pitchai 1989	$AgNO_3$	Source Not Specified	Note 2	0.5	0.5	200	13	10	100-200
				0.5	1	200	26	20	100-200
				0.5	2	200	41	35	100-200

				0.5	5	200	80	78	100-200
				0.5	10	200	100	88	100-200
Danilyuk 1995	Ag Amine in Ethanolamine	Prepared by Authors	Note 3	7	0.4	240	13	16 ± 9	100
				7	0.6	240	-	20	-
				7	1.5	240	-	24.3	-
				7	2.4	240	20	18.4	-
				7	2.7	240	30	30.6	-
				7	3.7	240	25	40	-
				7	5.2	240	-	56	-
				7	6.5	240	56	45	-
				7	13.8	240	126	100 ± 32	100
de Jong 2017	$Ag_2C_2O_4$	BASF AL4196E	Note 4, H_2	8	15	215	-	28 ± 19	170
			Note 4, N_2	8	15	215	-	62 ± 21	105
			Note 4, O_2	8	15	215	-	76 ± 37	104
Hensen 2019	$Ag_2C_2O_4$	Saint-Gobain NorPro SA 5102	Note 5 He / O_2 (100/0)	1.04	1.3	400	-	19 ± 9	200
				1.04	1.7	275	-	23 ± 11	400
				1.04	4.5	275	-	41 ± 16	400
			Note 5 He / O_2 (90/10)	1.04	1.7	275	-	48 ± 19	400
				1.04	4	275	-	57 ± 21	400
				1.04	8.7	275	-	99 ± 32	400
				1.04	8.2	275	-	106 ± 47	199
				1.04	10	275	-	127 ± 47	349

			Note 5 He / O_2 (90/10)	1.04	7.8	500	-	167 ± 58	291
				1.04	14.4	275	-	183 ± 8	484

1. Incipient Wetness -> Atmospheric Drying (50 ºC) -> Water Wash -> Atmospheric Drying (50 ºC) -> H_2 Reduction (200 ºC, 60 hours) -> N_2 Sintering (6-70 hours).
2. Incipient Wetness -> Atmospheric Drying (70 ºC) -> H_2 Reduction (200 ºC, 6 hours).
3. Incipient Wetness -> Contact Drying (25 ºC) -> Vacuum Reduction (90 ºC) -> Water Wash -> Dry in Static Air (100 ºC) -> Calcination (240 ºC, 2 hours).
4. Incipient Wetness -> Drying in Static Air (60 ºC, 24 hours) -> Heating in H_2, O_2, or N_2 (215 ºC, 5ºC/min, 2 hours)
5. Incipient Wetness -> Vacuum Drying (25 ºC, 1 hour) -> Calcination in He/O_2 (275, 400, or 500 ºC, 10 ºC/min, 4 hours).

Thus, in this communication, we prepare a series of supported Ag catalysts using our method of electroless deposition (ED) [78] to deposit Ag on pre-existing Ag nuclei prepared by dry impregnation of 0.1 wt% Ag/α-Al_2O_3 to give better control of resulting Ag particles. We also use an authentic older generation α-Al_2O_3 ring that has been used as a commercial EO catalyst support that was ground and sieved to 20/40 mesh (420 - 840 μm) size before Ag was deposited. Interestingly, this process is much like development of silver halide photographic films where Ag particles of 2 – 6 atoms (called latent images) produced by the photoreduction of AgCl during light exposure were reduced further (by unexposed AgCl particles adjacent to the latent image) during film development by a formaldehyde-containing developer solution to form a negative film [79]. In this study we also use formaldehyde as the reducing agent in the ED bath and $AgNO_3$ as the reducible Ag salt. The principal difference here is we begin with ultra-small Ag particles prepared by dry impregnation.

Ag particles have been analyzed by H_2 titration of oxygen-precovered Ag surface sites at 170C using the Vannice [72] method and compared with SEM micrographs to determine Ag particle size distributions which independently infer Ag active site concentrations. The catalysts have been evaluated using an automated reactor system operating at authentic reaction conditions like those used industrially. By knowing the number of active surface Ag sites and accurately measuring reaction rates and EO selectivity, it should be possible to determine to substantial accuracy whether ethylene epoxidation is structure sensitive and if EO selectivity has an optimum Ag size range. Finally, the TOF's in this manuscript are reported for site concentrations determined before and after 150 hours of reaction to determine sintering characteristics of different Ag particle sizes on the α-Al_2O_3 support.

3.2 Experimental Methods

3.2.1 Catalysts preparation

The 0.1 wt% Ag and 12 wt% Ag catalyst were prepared by wet impregnation of clear precursor $AgNO_3$ instead of silver oxalate as previously publication.[80] The impregnation volume was calculated using the pore volume of the carrier plus 5% excess. The α-Al_2O_3 catalyst carrier (SA5562, 8-mm rings, BET surface area = 0.60 m^2/g using Kr adsorption, and pore volume = 0.53 cm^3/g) was crushed and sieved to 20-40 mesh (425-850 um). 18g SA5562 20-40 mesh and the appropriate $AgNO_3$ amount of the impregnation solution were transferred to a 400ml round bottom flask and tumble dried under vacuum (10 inHg) at 70 ºC until free tumbling was observed. Samples were transferred to a vacuum oven, evacuated to 20 in Hg below and heated to 110 ºC, for 12 hours prior to reduction in 125 sccm of 50% H_2 with balance He at 200 ºC (ramp rate 5ºC/min) for 4 hours in a separate vertical split tube furnace. All temperatures used in this study are maintained at $\leq$ 200 ºC to minimize sintering of Ag particles.

The 0.1% Ag/SA5562 catalyst was used as the base material for all electroless deposition (ED) derived samples. Different wt% of Ag were added to pre-existing Ag surface using continuous ED. In the standard continuous electroless deposition process, two separate syringe pumps (New Era NE-300) were used to accurately pump the reducing agent and reducible metal salt ($AgNO_3$) to a bath containing a pH adjusted, aqueous slurry of the base catalyst. Typical continuous ED apparatus used in this work has been shown previously in Fig. 1.5. The pH of the ED bath was maintained at 11 by adding concentrated NH_4OH solution. All depositions were conducted at room temperature. Formaldehyde (HCHO) Hydrazine and silver nitrate ($AgNO_3$) were selected as the reducing agent and

Ag^{2+} source, respectively. The $AgNO_3$ solution and HCHO solution were added from two separated different motor-driven syringe pumps at a fixed molar ratio of [HCHO] / [Ag^+] = 2 / 1. The Ag weight loadings deposited by ED were controlled by increasing the duration of RA (6.0 X 10^{-2} M) and Ag salt (2.9 X 10^{-2} M)/ syringe pumped (HCHO at 11.30 ml/h; $AgNO_3$ at 11.45 ml/h). Initial attempts using a magnetic stirrer bar in the ED vessel resulted in attrition of the catalyst particles to produce fines, which changed diffusion characteristics during catalytic reaction. As shown in Fig. 3.2, percolating ED bath is developed to avoid the damage of 20-40 mesh support by sit bar. The bath solution was peristaltically pumped into the bottom of a vertically mounted 15 ml tube and the flow rate adjusted until the 420 - 840 μm particles behaved as a percolating catalyst bed to give good convective mixing of the catalyst particles with the ED components. At the top of the tube, the solution was filtered through a glass frit to remove and maintain the fines in the tubular percolating bed and then recirculated back to the stirred bath. During the period of deposition time, aliquots of the ED bath were taken in 20-30 min intervals and analyzed by inductively coupled plasma-optical emission spectroscopy (ICP-OES) to confirm metal salt concentrations remaining in the bath. Added Ag amount was determined from the difference of what was added by syringe pump and the amount of metal salt in solution. After the completion of ED, the slurry was filtered and washed repeatedly with excess DI water. The wet sample cakes were dried under vacuum at room temperature and stored at ambient conditions. Thus, a series of Ag catalysts with incremental Ag metal weight loadings and designated as xAg/SA5562, where x represents the mass loading of Ag, listed in see Table 3.2. All vessels, tubing, and the pump liner were constructed from inert plastic or Teflon and were cleaned with 37% nitric acid, and thoroughly rinsed with DI water, between samples.

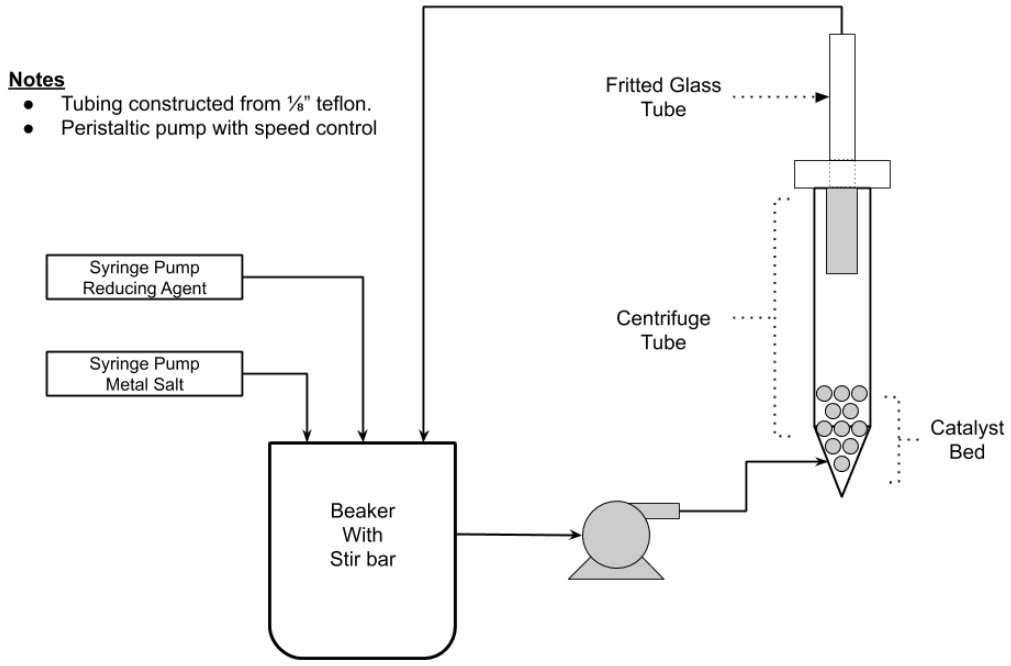

Figure 3.2 a schematic representation of the percolating bed configuration

Following electroless deposition, all samples were filtered and washed with 1 L/g cat of DI H2O to remove residual ED byproducts and unreacted components. The catalysts were then dried overnight in vacuo at 110 °C and reduced at 200 °C using the same conditions used for the 0.1% Ag/SA5562 base catalyst. Nominal Ag loadings on α-Al_2O_3 that determined from analysis of periodic aliquots were confirmed to match results after digestion of the catalyst in concentrated 37% nitric acid and ICP analysis.

3.2.2 Catalyst Characterization

Temperature programed oxidation (TPO) and temperature programed reduction (TPR) experiments were performed using Brooks 5850E mass flow controllers to deliver specific feed compositions to < 200 mg samples in a quartz micro-reactor in a high wattage, split-tube furnace connected to an Inficon Transpector 2 Mass Spectrometer by means of a Varian 951 variable leak valve customized for fast detection [81]. Samples were loaded

into a ¼-inch quartz tube supported on a quartz plug, dried in-situ at 120 ºC for 1 hr, then cooled to room temperature in flowing (30 sccm) Ar. For TPO, 10% O_2 with balance Ar was introduced to the system and samples were ramped at 20 ºC/min to 600 ºC while monitoring for CO_2 (m/e = 44) and H_2O (m/e = 18). For TPR, samples were heated to 500 °C at 20 ºC/min or, alternatively, heated in a separate experiment to 200 ºC at 20 ºC /min, maintained for 4.5 hours, and then ramping to 260 ºC and 340 ºC to verify the absence of residual nitrates from $AgNO_3$ decomposition (NO at m/e = 30).

A Micromeritics ASAP 2020 was used for Kr BET analysis, and for chemisorption of exposed Ag sites, H_2 titration of oxygen precovered Ag (Ag-O) was performed on a Micromeritics 2920 pulsed chemisorption apparatus using a modified version of the method of Vannice et al. [72] Prior to analysis, samples were ramped to 200 ºC at 10 ºC/min in flowing 10% O_2 balance Ar and held for 10 hours to remove residual formaldehyde fragments from ED. After this, the samples were reduced for an additional 2 hours at 200 ºC in 10% H2, balance Ar before cooling to 170 ºC and purging with flowing Ar. Samples were then exposed to 10% O_2, balance He for 30 min to saturate the Ag surface with Ag-O species before conducting the pulsed H_2 titration, also at 170 ºC. Each sample was given two additional sequences of H_2 titration and results are reported as an average; error bars represent the standard deviation between in-situ titration cycles and show good agreement for H_2 uptakes.

Aberration-corrected JEOL 2100 F scanning transmission electron microscopy (STEM) was used to do Z-contrast imaging with a 200 kV field emission gun and a double tilt holder for tilting the sample across a range of angles (± 20°) for obtaining images. Sample preparation involved direct deposit of ground powder on a copper TEM grid with a thin

holey carbon coating. Scanning electron microcopy (SEM) was also performed using a Zeiss Gemini 500 equipped with a secondary electron detector (SE2). SEM samples were crushed, applied to carbon backed adhesive tape, and coated with a thin layer of Pd-Au using a Denton Desk II sputter coater with global rotation and tilt. SEM images were collected using the SE2 detector at 5KV beam energy and particle counting was performed with ImageJ software version 1.8.0-172. Great care was taken to ensure that each sample was well represented with ~20 different images collected at various positions.

3.2.3 Catalyst evaluation

Catalyst evaluation was performed in a parallel flow system consisting of six stainless-steel reactors. Reactors were constructed of 0.25" OD, 0.035" wall thickness seamless tubing and loaded with 3.0g of size 420 - 840 μm catalysts supported on a plug of glass wool. Each reactor tube was jacketed with a 1" OD aluminum sheath to improve isothermal performance which was heated with a custom-fitted 1" ID x 15" long Brisk Heat heating mantle. Temperatures were controlled and recorded using a 1/16" thermocouple embedded in the Al sheath. The master reaction feed stream consisted of 25% C_2H_4 (Praxair, EY 2.5-T), 8% O_2 (Praxair, OX 4.3UH-T), balance CH_4 (Praxair, ME3.7UH-T) and was blended using Brooks 5850E mass flow controllers. No ethyl chloride (EtCl) feed modifier was added to the feeds in this series of experiments to avoid potential issues that might arise from unequal rates and extent of Ag site modifications for different weight loadings of Ag. The master feed composition was plumbed to a second manifold of mass flow controllers which provided 50 sccm (GHSV 1000 hr^{-1}) to each reactor at a pressure of 250 psig. All product streams were heated to 120 °C to avoid condensation and were individually sampled automatically using a six-stream Valco sample valve at 2 hours

intervals using an Agilent 7890A gas chromatograph (GC) equipped with an FID for hydrocarbon compounds (EO) and a TCD for CH_4, CO_2, and H_2O analyses. Both detectors were fitted with a Poraplot-Q column. Carbon calculations between the feed and the product streams accounting for CO_2, EO, and C_2H_4 indicated a carbon balance of basically 100%. All kinetic studies were performed at less than 10% C_2H_4 conversion and Weisz-Prater calculations indicated the absence of internal mass transfer limitations.

EO isomerization studies were performed in the same reactor system used for catalyst evaluation, except a 2.1 % EO balance He mixture was blended with O_2 and CH_4 to give a concentration of 0.5 %EO, 8 % O_2, and balance He + CH_4; 100 sccm of mixed gas was supplied to each reactor containing 2.0 g of sample at atmospheric pressure. One reactor was left empty to determine EO conversion and mass balance of the isomerization reaction; isomerization was measure at 220, 245, and 270 ºC, respectively.

3.3 Results and Discussion

3.3.2 Isomerization Experiments

SA5562 is tested for EO activity under the feed of 0.5% C_2H_4 and 8% O_2. Kinetics results are obtained from 220-270 ºC as shown in Fig. 3.3 along with 12wt% Ag/SA5562 catalyst. At 245 and 270 ºC, EO conversions for SA5562 were 5.1% and 13.5%, respectively. Acetaldehyde was the sole product detected for metal free SA5562 α-Al_2O_3. However, at similar conditions for 12 wt% Ag/ α-Al_2O_3, considerably more EO underwent combustion to form CO_2 and H_2O, indicating that consecutive combustion of both EO and HAc had occurred. The absence of HAc indicated complete, Ag-catalyzed oxidation of HAc and additional combustion of EO had also taken place; at 245 ºC, EO conversion had increased from 5.1 % to 20.0 % when 12% Ag was present. No significant EO

consumption was found on SA5562 at temperature lower than 210 ºC compared to supported 12% Ag sample. These results indicate that SA5562 does not measurably catalyze the isomerization reaction at 200-210 ºC range. Based on these observations, it can be reasonably assumed that the conversion of EO at 210 ºC on 12%Ag/SA5562 catalyst is only assigned to Ag. Thus, 210 ºC is selected as the ethylene epoxidation evaluation temperature in this study.

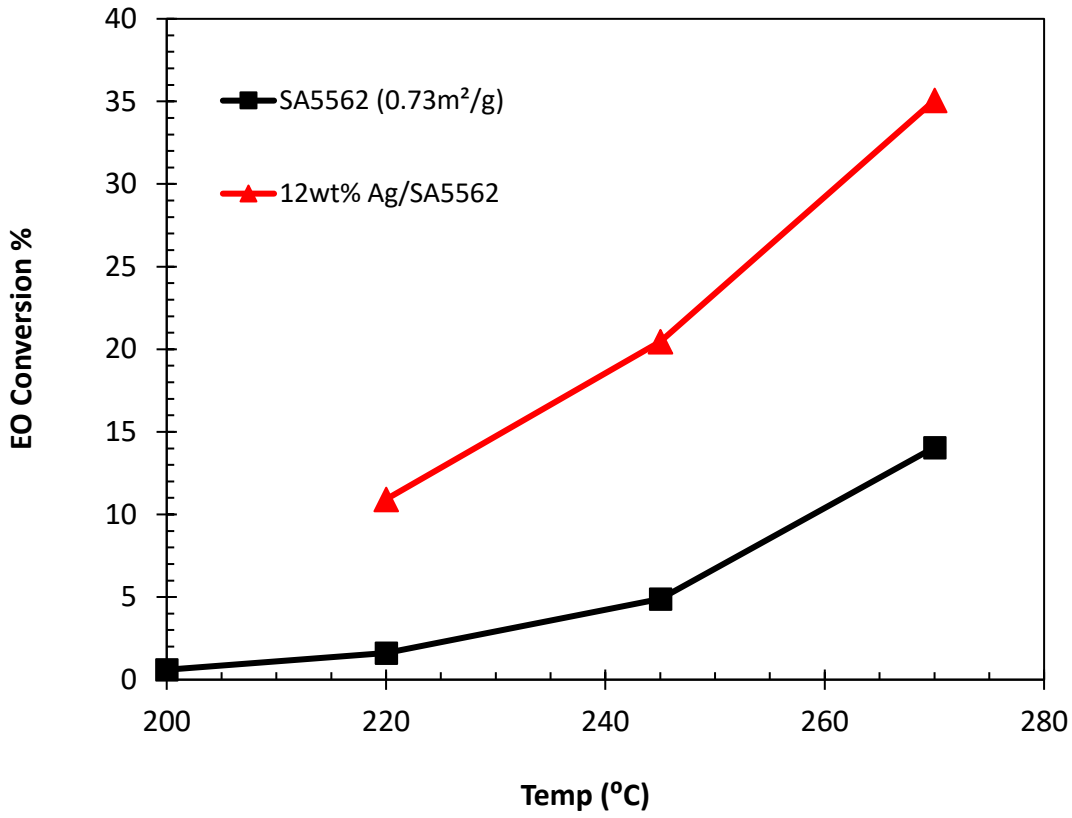

Figure 3.3 EO isomerization activity as a function of reactor temperature.

3.3.2 Electroless Depostion

Due to the low surface charge of α-Al_2O_3 with 0.7 m^2/g surface area, it is not able to produce uniform and small Ag particles by SEA as base catalyst for ED. To address this challenge, small amount of $AgNO_3$ were added to 20-40 mesh (425-845 um) SA5562 by

incipient wetness impregnation at 7% excess water accessible power volume which has been shown to be an effective method for obtaining small uniform Ag nanoparticles. Clean $AgNO_3$ precursor was selected as the Ag source due to the complete reduction of $AgNO_3$ to Ag and gas NO_2 and H_2O. Temperature programed reduction (TPR) was performed on the 12Ag/SA5562 sample to determine the reduction temperature. The sample was heated from 25 to 500 ºC at 20 ºC/min, as shown in the Fig. 3.4 left figure, $AgNO_3$ starts to decompose at temperature 160 °C and maximum temperature appears at peak 250 °C. Normally, 250 °C would be selected as the reduction temperature of $AgNO_3$ precursor. However, higher temperature would sinter small Ag particles. In another TPR experiment, the catalyst was heated in flowing 50% H_2 balance Ar up to 200 °C and NO_2 was monitored at m/e = 30 for a soak duration of 4.5 hours. Following the 200 °C soak, the sample was heated in-situ to 260 °C then 340 °C to confirm the absence of residual compounds demonstrating the 200 °C reduction temperature was sufficient for totally reducing $AgNO_3$. The 0.1wt% Ag sample was used as a base catalyst for electroless deposition.

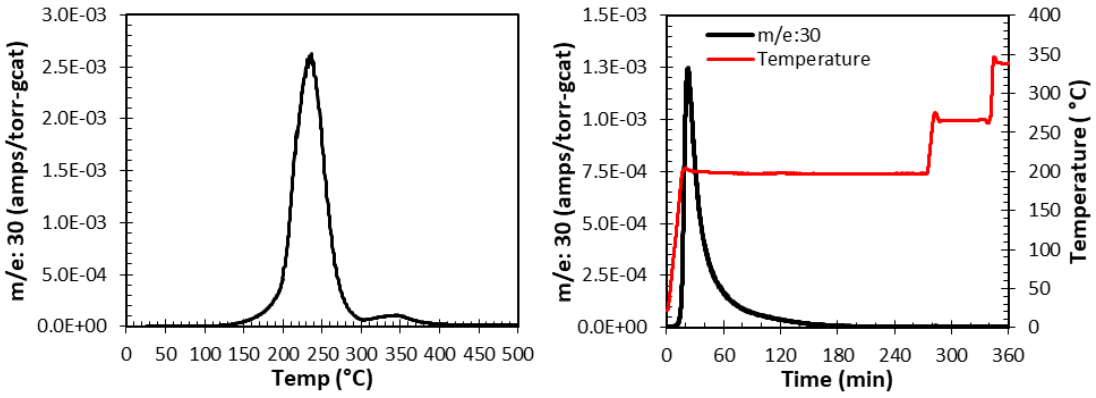

Figure 3.4 Nitrate decomposition by reduction of 12%Ag/SA5562 in 20 sccm of flowing 10% H_2 balance Ar.

The electroless deposition (ED) bath was developed based on prior work from our group. Formaldehyde was chosen as a reducing agent for its ability to release molecular hydrogen on Ag surfaces and relative stability compared with other common reducing agents such as hydrazine (N_2H_4). NH_4OH was selected for pH adjustment following control experiments where precipitation of the $AgNO_3$ was observed at pH 11.0 using NaOH. Initial experiments were performed using a continuous ED bath whose experimental setup is described in previous literature. However, agitation issues were encountered when substituting powders for the 20-40 mesh Ag base catalyst. ~ 60% of the 20-40 mesh base catalyst was grinded as powder due to autonomous grinding by the stir bar in solution for 1 hour experiment. To improve sample recovery while maintaining sufficient agitation, the percolating ED bed was developed, as shown in Fig. 3.2. In this configuration, the RA and $AgNO_3$ solutions are syringe pumped into a catalyst free beaker, containing DI water. A peristaltic pump then transfers well-mixed solution into a vertically mounted plastic 15ml centrifuge tube where the upward motion of fluid causes convective mixing of the base catalyst. Catalyst fines are removed from the recycle stream using a glass frit mounted on top of the centrifuge tube. Mass recovery of the 20-40 mesh material approached 100% for all samples used in this study.

Chapter 2 discussed carbon supported Pt particle size distribution could be tightly controlled by extending the deposition time. In the current work, similar approach was adopted to the synthesize Ag on α-Al_2O_3. For standard ED procedure, thermal stability of developed ED bath should be satisfied to make sure Ag precursor is catalytic deposited on supported pre-existing Ag nuclei, not thermally reduction to suspended particle in the solution. As shown in the dash line in Fig. 3.5, in the absence of a base catalyst, the rate of

thermally reduction is very limited, indicating a stable ED bath. Different deposition time has been studied herein regard to Ag deposited amount. As shown in Fig. 3.5, different targeted Ag wt% was obtained by enlarging the deposition time (as listed in the legend) by maintaining the pumping speed of the precursor and RA. The ED kinetics profiles clearly demonstrate this process is reproducible, for example, 5.0%Ag sample exhibits the same deposition rate with 2.1%Ag up to 197 mins. Moreover, the deposition behavior follows the same trend from 197 mins to 420 mins. Thus, electroless deposition can be assumed to greatly exceed the rate of thermal instability since the Ag^0 surface will kinetically favor activation of HCHO and Ag salt. Theoretical Ag weight loadings were confirmed by digestion and ICP analysis of the ED samples following ex-situ reduction in flowing H_2 indicating that none of the reduced Ag existed as nanoparticles in solution.

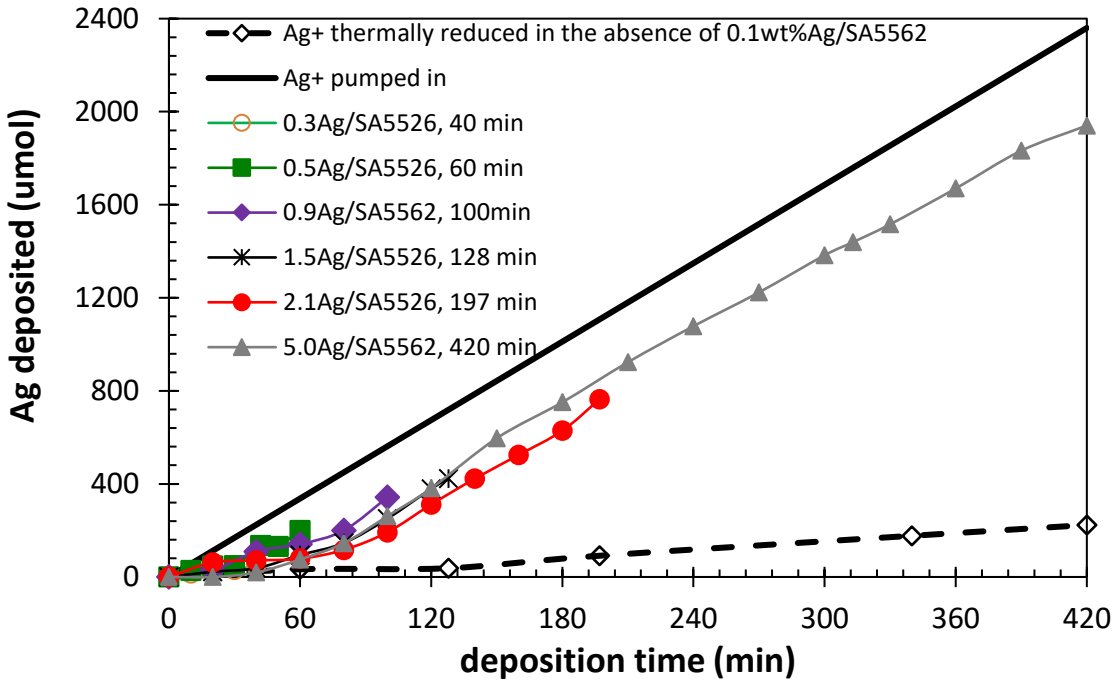

Figure 3.5 thermal stability control experiment and time dependent Ag deposition profiles compared to the total quantity of Ag syringe pumped into solution.

3.3.3 silver size measurement

The concentration of surface Ag sites of 0.1% base catalyst, a series of Ag fresh sample after ED and 12% Ag sample were determined using two different methods. Firstly, SEM imaging was used to examine Ag particle sizes and distribution, visually showing the ability of ED to increase Ag particle size. Determined Ag surface average sizes (D_s) of all Ag catalysts are analyzed using approximately 1000 particle, summarized in Table 3.1. Representative SEM images of 0.1%Ag, 0.5%Ag, 1.5% Ag and 5.0% Ag are shown in Fig. 3.6. 0.1% Ag made by impregnation has small particles with tighter size distribution. Ag particle size increased when we put more Ag down by electroless deposition from 0.5Ag all the way to 5.0Ag.

Secondly, concentrations of Ag surface sites are determined by pulse chemisorption using 10% H_2 titration of oxygen-precovered at 170 °C. For example, the pulse chemisorption result of 0.1% Ag is shown in Fig. 3.7, gives the average Ag dispersion of 7%, which corresponds to an average Ag particle size of 19 nm. Regardless, both methods provide valuable information and are included in Table 3.1 for all Ag catalysts. For 0.1%Ag, 44 nm size from SEM measurement is much higher than the value from chemisorption. This may be due to the low resolution of SEM of missing some smaller particles, which can be detected by gas adsorption in chemisorption.

3.3.4 activity and selectivity on different Ag size

Ethylene epoxidation rates were measured in a hydrocarbon rich feed consisting of 25% C_2H_4, 8%O_2, balance CH_4. Turnover frequencies (TOFs) are reported at steady state conditions, using the surface area average particle size derived from SEM images and hydrogen titration for samples characterized. Comparing the size dependency for TOF, the

microscopy and titration calculations are in general agreement with slopes of 0.0002 1/nm-s and 0.0003 1/nm-s respectively, as shown in Fig. 3.8. However, a clear discrepancy exists between the two methods of size determination for the following reactions, where a volcano curve with TOF decreasing for particles greater than 400 nm based on size estimation from SEM while the titration results indicate that the TOF literally reaches the maximum at around 1400 nm. The unsupported -10 to 20 mesh Ag with a particle size of about 1430 nm being estimated from BET have a TOF of 0.01 s^{-1} confirming an eventual decrease in site specific activity at the extreme of Ag particle size.

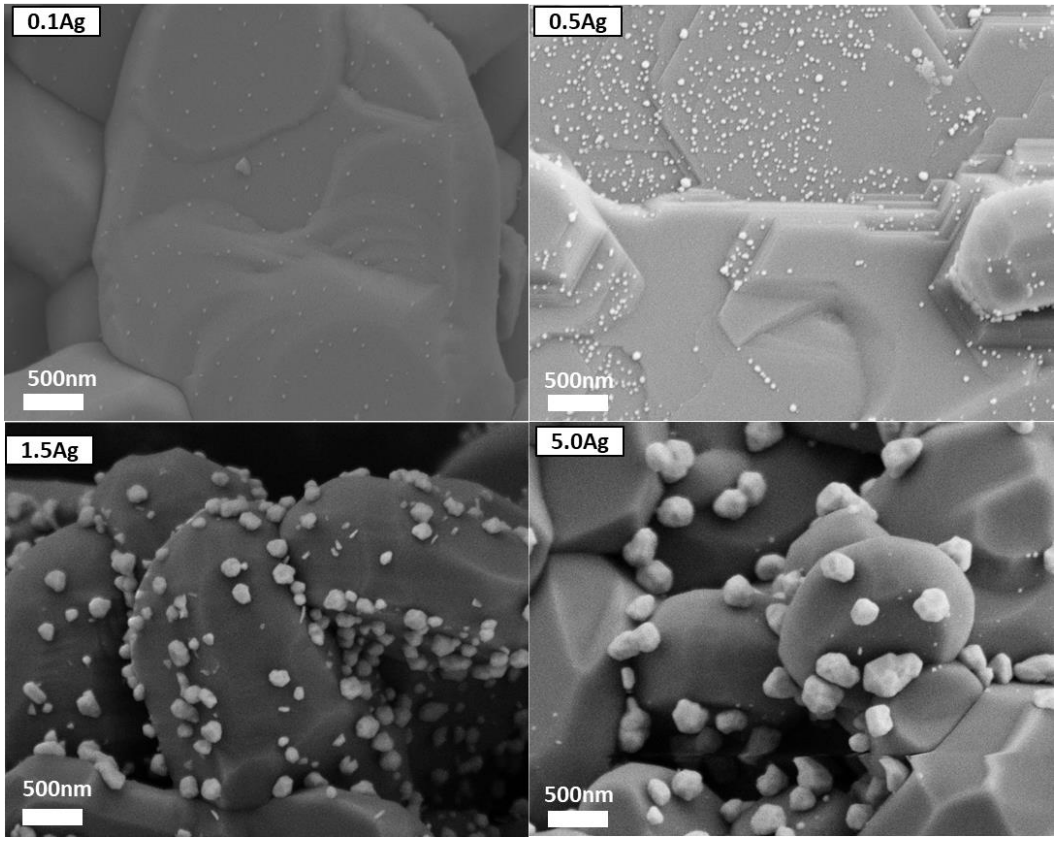

Figure 3.6 SEM images of 0.1%, 0.5%, 1.5% and 5.0%Ag catalyst

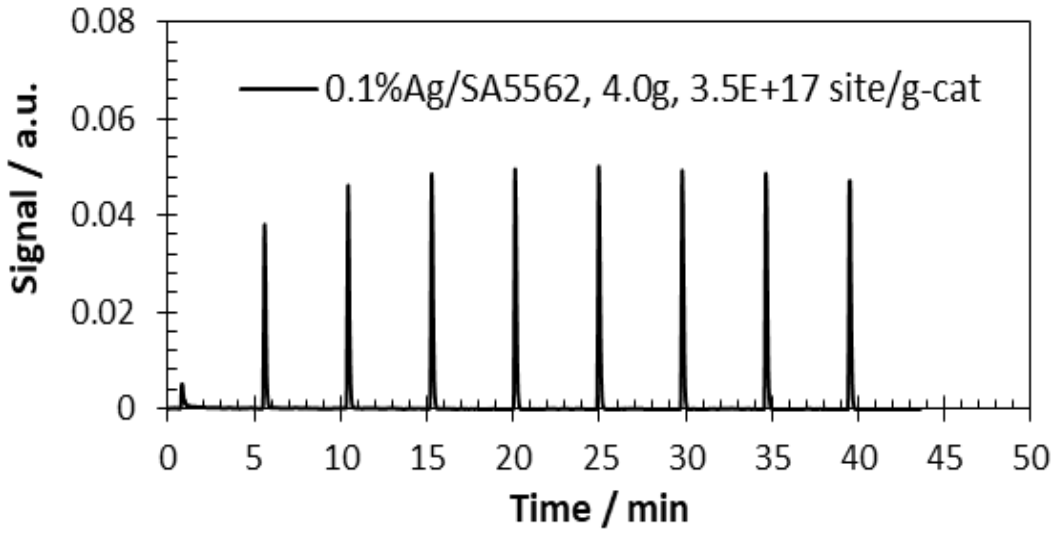

Figure 3.7 H_2 pulse titrations for O precovered Ag site at 170 °C

Table 3.2 Ag Particle sizes as determined by SEM and chemisorption

Catalyst	$Size_{Chemi}$ (nm)	$Size_{SEM}$ (nm)
0.1Ag/SA5562, DI	19	44 ± 12
0.3Ag/SA5562, ED	80	84 ± 30
0.5Ag/SA5562, ED	85	90 ± 26
0.9Ag/SA5562, ED	148	160 ± 54
1.5Ag/SA5562, ED	201	138 ± 46
2.1Ag/SA5562, ED	220	211 ± 67
5.0Ag/SA5562, ED	292	381 ± 154
12Ag/SA5562, DI	1291	683 ± 239

The results that have been obtained at constant 210 ºC temperature but with different oxygen concentrations (4%, 8%, 12%) show that EO selectivity is principally dependent

on formed EO mole %, as shown in Fig. 3.9. Fig. 3.9 shows the strong dependence of EO selectivity on EO mole %. The decrease in EO selectivity with increasing EO mole % n is likely due to consecutive reactions of the primary EO product. We can estimate the intrinsic EO selectivity by extrapolating to zero ethylene conversion. It is also observed that, smaller particles exhibited a lower EO selectivity in comparison to catalysts containing larger particles. Smaller Ag particles (44-90 nm) has lower selectivity of around 55-60% while larger particles (211-381 nm) explore high selectivity (~75%). Importantly, the value of 75% is approaching that of unsupported Ag powder. The effect of particle size on the product distribution in a catalytic process is usually explained in terms of the particle size dependent reaction. EO can isomerize on hydroxyl groups of the support to acetaldehyde, which is prone to rapid combustion on the silver surface. Differences in EO selectivity may therefore also be due to the amount of support surface exposed, which depends among other things on the silver loading. The higher silver loading used to obtain catalysts with larger silver particles can thus explain the higher EO selectivity as well as the less pronounced decrease in the EO selectivity with increasing EO mole %. In summary, larger silver particles gave rise to a higher activity and EO selectivity. In this study, the method adopted for varying average crystallite size was by increasing the loading of silver through ED. The conventional sintering technique used by others was not used to avoid the possibility of morphology change and impurity segregation. SEM clearly shows that there is no morphology change with increase in the average particle size. Furthermore, the participation of the support has been considered, Fig. 3.3 shows that α-Al_2O_3 is inactive in ethylene oxide reactions. Therefore, the observed changes in specific activity and selectivity must be attributed to changes in the size of the metal particle. Herein, the

sensitivity of ethylene oxidation reaction to Ag particles size has been observed in the average size range of 44-381 nm, where the silver particles are expected to behave like bulk metal. Since the average particle sizes used are greater than 10 nm, it is impossible that the variation in activity corresponds to the changes in the coordination number of surface atoms. In order to explain the results of this study, in light of published results, it must be recalled that the particles in supported catalysts have a wide distribution and that the proportion of small crystallites can have a profound influence on the overall performance of the catalyst. SEM analysis indicates that the particle size distribution in these catalysts is rather broad. As the average crystallite size increased, the population of crystallites smaller than 10 nm is expected to decrease and hence the contribution to activity from small crystallites decrease. The small silver crystallites are less active in ethylene epoxidation and combustion due to the fact that the surfaces of these particles are more oxidic in nature, which is in agreement with the observation that Ag_2O is not very active and selective in ethylene oxidation. As shown in Fig. 3.8, activities are low on small Ag particles. As far as the dependence of selectivity on silver particle size on $Ag/\alpha\text{-}Al_2O_3$ is concerned, it will be low in the case of small particles due to the formation of Ag_2O on these. Therefore, small Ag size favors combustion of ethylene while large Ag particle selectively produces EO.

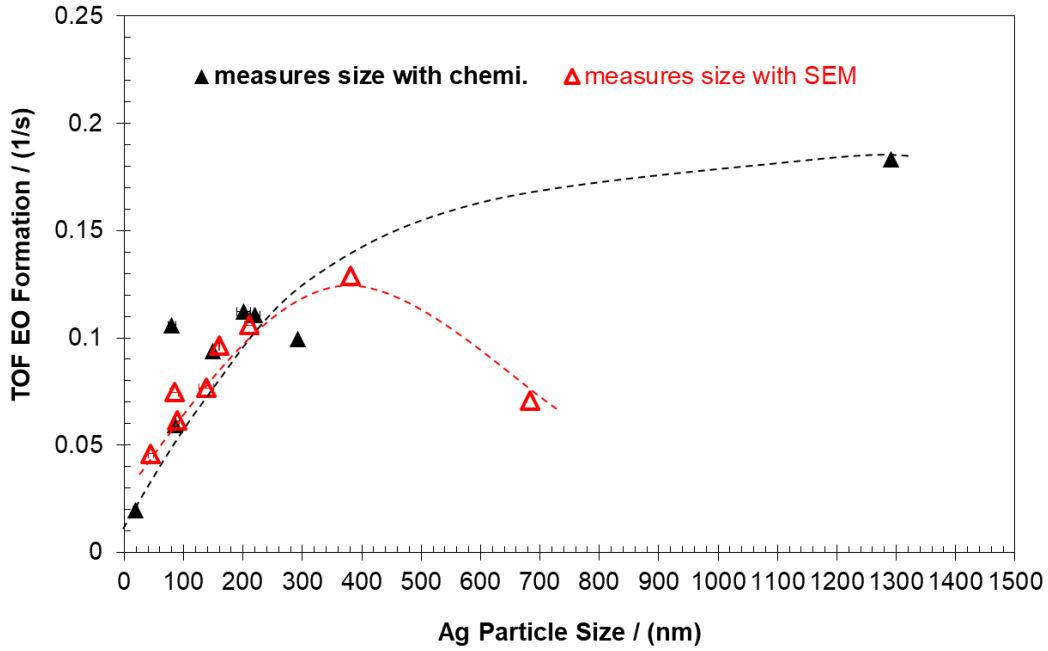

Figure 3.8 Turn over frequency for EO formation as a function of particle size. H_2 titration Dashed lines are added to guide the eye.

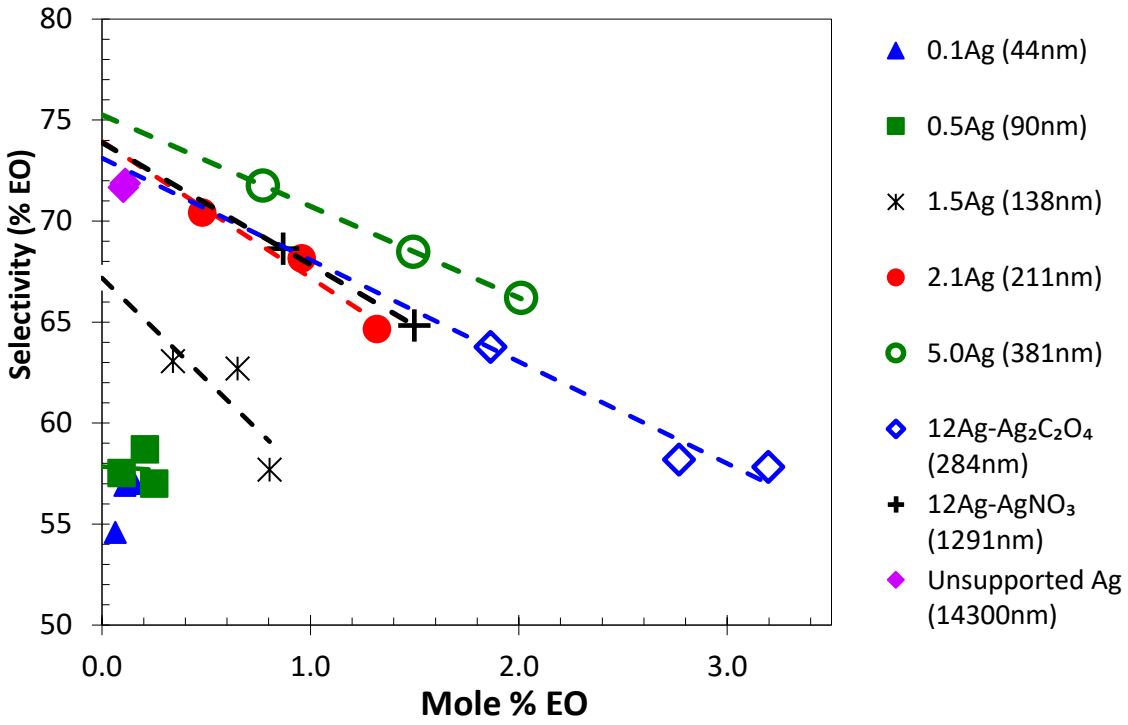

Figure 3.9 Activity-Selectivity plot generated by varying oxygen concentration between 4 and 12%.

3.4 Conclusions

A study of the synthesis of supported silver catalysts by ED showed that different silver particle size can be obtained by controlling the extra Ag being deposited on base Ag catalyst. The obtained particle sizes were in a range of 44-381 nm from selective chemisorption and SEM estimation. The influence of silver particle size on ethylene oxidation has been investigated. It is found that the activity of the supported silver catalysts on the ethylene epoxidation is strongly dependent on the silver particle size, which is in good agreement with previous studies. The study demonstrates the precisely control of the ED in synthesis metal particles without changing the morphology of the particle surface. Additionally, the selectivity was found to be strongly dependent on the conversion, and smaller Ag size exhibits lower selectivity than larger Ag particles. Out study therefore provides a possibly to manipulate the reaction selectivity by controlling the size of Ag catalyst particles.

CHAPTER 4

ENHANCED PERFORMANCE OF OXYGEN-FUNCTIONALIZED MULTI-WALLED CARBON NANOTUBES AS SUPPORT FOR PT AND PT-RU BIMETALLIC CATALYSTS FOR METHANOL ELECTROOXIDATION [2]

[2]Xiong W. and Monnier J. R., *ACS Applied Energy Material,* 3 (2020) 5487-5496

Reprint here with permission of publisher.

4.1 Abstract

The performance of Pt-Ru catalysts for methanol electrooxidation has been greatly enhanced by replacing the standard carbon XC72 support with oxygen-functionalized multi-wall carbon nanotubes (MWCNTs). Highly dispersed, intimately contacted Pt-Ru nanoparticles were synthesized on the MWNT supports by a combination of strong electrostatic adsorption (SEA) and electroless deposition (ED) methods. The catalysts have been characterized by x-ray diffraction (XRD), scanning transmission electron microscopy (STEM), chemisorption, x-ray photoelectron spectroscopy (XPS), and evaluated by cyclic voltammetry (CV) for the methanol electrooxidation reaction. The results showed that oxygen-functionalized MWCNTs influenced not only the chemical nature and morphology of the surfaces relative to XC72 but also enhanced the electrocatalytic properties of the resulting Pt and Pt-Ru electrocatalysts. STEM images revealed homogeneous dispersion of uniformly sized nanoparticles (NPs) for the two types of functionalized MWCNTs with relatively high particle density and no noticeable aggregation. The results also showed that the activities of Pt-Ru on functionalized MWCNTs catalysts prepared by SEA and ED for methanol oxidation were much higher than for commercial catalysts. The activities of –OH and –COOH terminated Pt-Ru/MWCNTs-OH and Pt-Ru/MWCNTs-COOH catalysts for methanol oxidation were up to seven times higher than commercial Pt/XC72 and up to four times higher than a commercial Pt-Ru/XC72 catalyst with 1:1 = Pt: Ru bulk atomic ratio.

4.2 Introduction

Direct methanol fuel cells (DMFCs) are one promising alternative energy storage solution that circumvents the challenge of current hydrogen fuel cell technology, by eliminating the hydrogen storage step (liquid being far more easily handled and transported

than compressed gas). Despite many efforts devoted to DMFC development, there still remain limitations to be overcome in efficiency and power density. A significant reason is the relatively slow kinetics of the methanol oxidation reaction at the anode, which leads to high over-potentials[82-84]. Because of this, improved catalysts are required. Much of current research has focused on developing new catalyst synthesis methods for bimetallic catalyst formation.

Research has shown that bimetallic Pt-Ru alloys have the best combination of activity and stability for electrocatalytic methanol oxidation, and in previous work, [23]we have shown that bimetallic Pt-Ru catalysts prepared by the electroless deposition (ED) of variable and controlled amounts of Ru onto a base Pt catalyst supported on Vulcan XC 72 was in fact much more active than either commercial Pt/Vulcan XC 72 or commercial Ru-Pt/Vulcan XC 72 catalysts. Current rationale is that Ru-Pt bimetallic catalysts exhibit lower levels of carbon monoxide (CO) poisoning on the active Pt sites. As methanol is oxidized, CO is formed as an intermediate that is strongly chemisorbed on Pt sites, reducing the turnover frequency for Pt and the operating efficiency of the fuel cell. This problem is solved by the introduction of Ru sites, preferably contiguous to the Pt sites that dissociatively adsorb H_2O to promote formation of CO_2, which readily desorbs from the Pt surface. Alternatively, e^- transfer between Ru and Pt may also lower the adsorption strength of CO to assist the desorption of CO.[85]

A second area of research is to use improved carbon supports for the Pt-Ru particles, in particular to enhance the formation and stabilization of smaller metallic/bimetallic particles as well as to possibly provide higher electrical conductivity of the support from the metallic/bimetallic particles to the anode collector. One particular carbon black, denoted

as Vulcan XC 72 is commonly used, because of its high electrical conductivity and moderate, internal pore diameters.[86, 87] However, carbon blacks typically corrode under normal fuel cell operating conditions, so new materials are being sought for use as electrically conductive and more corrosion and sintering-resistant supports. New types of carbon supports have appeared in the literature over the past few decades, including carbon nanotubes, carbon nanofibers, ordered mesoporous carbons, and carbon xerogels and aerogels. These supports have been evaluated as candidates for more stable and more active catalyst systems at low platinum loadings (< 0.1 mg/cm^2) and, therefore, lower cost.[88] Carbon nanotubes (CNTs) have been evaluated as supports in heterogeneous catalysts for fuel cell applications, since they also have high electrical conductivity and are more corrosion resistant. Their higher surface areas may also give rise to higher dispersion of metal nanoparticle catalysts and the smooth graphitic surface may contribute to better accessibility of metal nanoparticles to the reactants in a non-mass transfer limited regime. [89] Results [90] from DMFC using Pt supported on single wall carbon nanotubes (SWNTs) have shown enhanced mass activities (mA/mg Pt) than conventional Pt catalysts supported on Vulcan XC 72 carbon supports. The authors stated the higher activities may have been due to oxygen-containing functional groups on the surface of the SWNTs, higher surface areas of the support, or lower e^- resistance of the nanotubes between the carbon and electrolyte interfaces. Their results also showed that SWNTs-supported Pt catalysts were more active than multi-wall carbon nanotubes (MWCNTs)-supported Pt catalysts; both were more active than Vulcan XC 72. However, MWCNTs are much cheaper than SWNTs and are easier to modify with oxygen functionalities.

Thus, the present study focuses on characterization and evaluation of Pt and Pt-Ru catalysts supported on MWCNTs for methanol electrooxidation that are prepared using the combination of Strong Electrostatic Adsorption (SEA) and Electroless Deposition (ED) methods. Specifically, MWCNT carbons with different surface functional groups have been chosen because they offer the possibility of providing anchor sites for deposition and stabilization of supported Pt and Pt-Ru particles and are readily available. Further, their cost compares reasonably favorable to Vulcan XC 72, the standard support. Firstly, Pt monometallic catalysts with extremely small average particle sizes have been produced using SEA methods and then Ru deposited on the Pt surface by ED of appropriate Ru salts. Previously, [23]we observed that ED of $Ru(NH_3)_6^{3+}$ on a commercial 20wt% Pt/XC72 catalyst at a theoretical 1:1 atomic surface ratio of Pt : Ru gave the best performance for methanol oxidation,[82, 91] so this ratio has been used in this study for Pt supported on different MWCNT supports. A comparative evaluation of the structure, composition and electrochemical performance of the Pt-Ru/MWCNTs catalysts are discussed and compared to commercial Pt-Ru/XC72.

4.3 Experiment

4.3.1 Carbon Supports

The surface area and points of zero charge (PZC) of MWCNTs, OH and COOH functionalized MWCNTs, and Vulcan XC72 employed in this study are summarized in Table 4.1. BET measurements were conducted by linearly 5 points from relative pressure 0.01 to 0.10 at liquid N_2 temperatures with N_2 as the adsorbate using an ASAP 2020 Micrometrics Analyzer. The PZC of the supports, which corresponds to the pH value where the charge of the support surface is zero (neutral surface), was measured by the method of

Park and Regalbuto. [92] multi-walled carbon nanotubes with terminal -OH groups (MWCNTs-OH) and multi-walled carbon nanotubes with terminal -COOH groups (MWCNTs-COOH) were obtained from Carbon Nanotubes Plus© (Madisonville, TX, USA). The Vulcan XC72 was provided by Cabot© (Billerica, MA, USA) and the commercial Pt/XC72 and Pt-Ru/XC72 were purchased from Premetek.

Table 4.1 Summary of support properties.

Support	BET Area (m^2/g)	PZC
MWCNTs	196	8.0
MWCNTs-OH	236	3.6
MWCNTs-COOH	274	3.7
XC72	250	8.5

4.3.2 Preparation of the carbon-supported catalysts

SEA was used to prepare the monometallic Pt catalysts on different carbon supports. On the basis of the SEA protocol, chloroplantinic acid ($H_2(PtCl_6)$) was chosen as the precursor; 200 ppm $H_2(PtCl_6)$ solution was contacted with different carbon supports for 1 h followed by filtration and subsequent drying overnight in ambient air. The sample was then reduced in a flowing 10% H_2 (balance He) for 1 h with a ramp rate of 2.5 °C/min at 200 °C after drying in an oven at 120 °C for 12 h. A previous study showed that a catalyst with a theoretical coverage of 0.5 ML Ru on a Pt surface had the maximum activity for the methanol oxidation reaction.[23] Therefore, catalysts with theoretical 1:1 atomic surface ratios of Pt:Ru supported on different carbons were prepared by the ED method. Metal weight loadings were determined from inductively coupled plasma-optical emission spectroscopy (ICP-OES) analyses (Perkin-Elmer Optima 2000 DV) of the initial and final

concentrations of $(PtCl_6)^{2-}$ in the SEA solution and $Ru(NH_3)_6^{3+}$ in the ED bath. Weight loadings of Pt and Ru are shown in Table 4.2.

Table 4.2 Metal loadings of catalysts prepared by SEA and ED. Loadings for commercial Pt/XC72 and commercial Pt-Ru/XC72 are also included.

Sample	Pt loading (wt%)	Ru loading (wt%)
Pt/MWCNTs (SEA)	5.2	-
Pt/MWCNTs-OH (SEA)	6.5	-
Pt/MWCNTs-COOH (SEA)	7.3	-
Pt/XC72 (SEA)	6.3	-
Pt/XC72 (Commercial)*	20	-
Pt-Ru/MWCNTs-OH (SEA/ED)	6.5	0.7
Pt-Ru/MWCNTs-COOH (SEA/ED)	7.3	0.7
Pt-Ru/XC72 (SEA/ED)	6.3	0.7

4.3.3 Catalyst Characterization

Chemisorption using H_2 pulse titration of oxygen-precovered Pt was conducted using a Micromeritics Autochem II 2920 analyzer, and the concentration of accessible Pt active surface sites and Pt particle size were determined from the chemisorption results. STEM images were also used to measure the distributions and sizes of the particle sizes for all catalysts. An aberration corrected JEOL 2100F STEM equipped with a 200 kV field emission gun and a double tilt holder for adjusting samples across a range of angles of ± 20 ° was used to obtain the STEM images. The images were recorded using Digital Micrograph software and the particle size distributions were obtained by manually measuring about 1000 particles on each catalyst sample. Based on the STEM images, the volume average sizes (D_V) and surface average sizes (D_s) were determined based on the following equations,

$$D_V = \frac{\sum n_i d_i^4}{\sum n_i d_i^3}$$

$$D_s = \frac{\sum n_i d_i^3}{\sum n_i d_i^2}$$

where n_i is the number of particles with a diameter of d_i.[63]

A Rigaku Miniflex II equipped with a high sensitivity D/teX Ultra silicon strip detector and Cu Kα radiation (λ = 1.5406 Å) was used investigate crystallographic properties of the different catalysts on the carbon supports.[93] Scans were made in a 2θ range of 20 ˚ - 80 ˚ at a scan rate of 2.0 ˚/min. Diffraction patterns were also obtained for the supports alone, in addition to the supported metal catalysts. Metal diffraction patterns were deconvoluted using Gaussian peak shapes. Average particle sizes were estimated by the Scherrer equation with a shape factor of 0.94.[64]

Various carbon-supported Pt and Pt-Ru catalysts particles were analyzed by X-ray photoelectron spectroscopy (XPS) to determine properties of carbon surfaces and to examine possible interactions between metal particles and functional groups on the carbon support. XPS analyses were carried out on a Kratos AXIS Ultra DLD XPS system with a monochromatic Al Ka source at 15 keV and 150 W at pressures below 10^{-9} torr. The X-rays were incident at an angle of 45 ° with respect to the surface normal. High resolution core level spectra were measured with a pass energy of 40 eV and analysis of the data was carried out using XPSPEAK41 software. The XPS experiments were conducted while using an electron gun directed on the sample for charge neutralization.

4.3.4 Electrochemical Evaluation

A three-electrode electrochemical cell was used to evaluate catalytic activities by cyclic voltammetry (CV). A 5 mm diameter glassy carbon disk coated with the prepared catalyst was used as the working electrode, while a Pt wire functioned as the counter electrode and

a luggin capillary of $Hg/HgSO_4$ was used as the reference electrode. Preparation and application to the glassy carbon disk of a typical suspension of the catalyst samples has been previously described.[23] All potentials are given with respect to that of the standard hydrogen electrode (SHE). Electrolytic solutions were purged with high-purity N_2 to remove all traces of O_2 before measurements were made. The CV experiments were conducted in an electrolyte of 0.5 M H_2SO_4 and 1 M methanol at 25 °C for electrochemical surface area (ESA) measurements. All catalysts were conditioned at 50 mV/s between 0.0 and 1.2 V vs. SHE for 50 cycles before CV measurements were made using three cycles at 5 mV/s between 0.0 to 1.2 V vs. SHE for determination of the catalyst electrochemical surface area. The average peak currents of multiple scans corresponding to catalytic activity were calculated.

4.4 Results and discussions

Four different Pt catalysts supported on MWCNTs, -OH and -COOH functionalized MWCNTs and Vulcan XC72 were synthesized by SEA and designated as Pt/MWCNTs, Pt/MWCNTs-OH, Pt/MWCNTs-COOH and Pt/VXC72, respectively. Following the same procedure in previous work, [4] bimetallic Pt-Ru/MWCNTs-COOH, Pt-Ru/MWCNTs-OH and Pt-Ru/VXC72 bimetallic catalysts were made. The concentration of surface Pt sites on the monometallic Pt catalysts were determined using three different methods. Firstly, STEM imaging was used to examine Pt particle sizes and distribution. The results are shown in Fig. 4.1, and corresponding Pt size distributions are shown as insets for each analysis; approximately 1000 particles were measured for each distribution plot. Based on the STEM images, the volume average sizes (D_V) and surface average sizes (D_s) were determined and are included in Table 4.3. Because of severe agglomeration of Pt particles

for Pt/MWCNTs, no particle analysis was conducted. The basically uniform distribution of Pt particles in Fig.4.1(a-d) indicates strong attachment of the Pt nanoparticles to the surface of the oxygen-functionalized carbon nanotubes and carbon VXC72. However, the Pt particles in Fig.4.1(e) show that Pt has both low dispersion and broad size distribution on the non-functionalized MWCNTs support, likely due to the lack of strong binding sites. Because of the agglomeration of Pt at the surface of non-functionalized MWCNTs, Pt particle sizes could not be measured from STEM images. Overall, the agreement of Pt particle sizes determined from XRD, STEM, and chemisorption measurements is very good and shows that when Pt particles are well-dispersed and have narrow size distributions, good agreement exists between these diverse methods of analysis. XRD and STEM (volume average) measurements are volume methods of particle size measurements and STEM (surface average) and chemisorption are surface methods of analysis. When particle sizes have a narrow distribution of sizes and are dispersed, all measurements merge to the same value, as in this case.

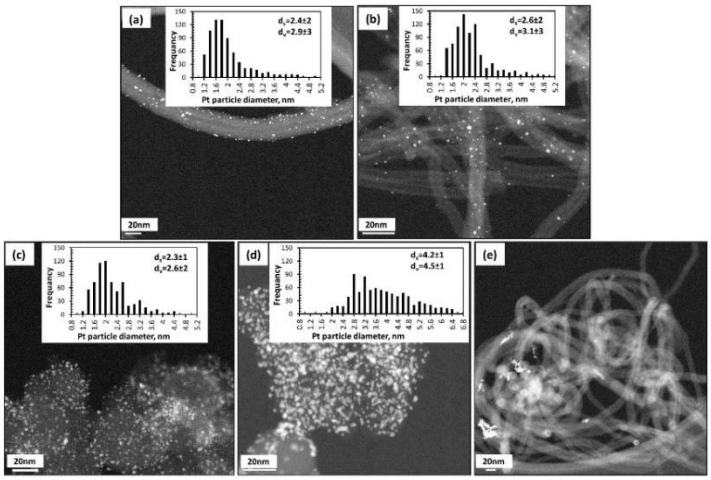

Figure 4.1 STEM images with particle size distributions for (a) Pt/MWCNTs-OH, (b) Pt/MWCNTs-COOH, (c) Pt/VXC72, (d) Pt/VXC72 (commercial) and (e) Pt/MWCNTs catalysts.

Secondly, selective chemisorption, specifically H_2 titration of O-precovered Pt sites (Pt-O), was conducted using the titration stoichiometry based on the following equation, 3/2 H_2 + Pt-O → H_2O + Pt-H. The uptake of H_2 was quantified using Micromeritics software to calculate the number of Pt surface sites and the average Pt particle diameters were determined. [71] Pt particle sizes were determined by assuming Pt exists in a hemispherical or spherical shape (same results); however, the real strength of chemisorption is that the number of active Pt surface sites are directly measured and not inferred as in the case of both XRD and STEM measurements. Regardless, all three methods provide valuable information and are included in Table 4.3 for the four Pt samples made by SEA as well as a commercial 20 wt% Pt/VXC72 catalyst. For the commercial 20 wt% Pt/VXC72 catalyst, chemisorption gave an average Pt particle diameter of 4.3 nm. Interestingly, similar values determined from chemisorption were also observed in previous studies for other commercial samples of 20 wt% Pt/VXC72 catalyst. Punyawudho [71]found average Pt particles of 3.9 nm, and in another study [94], an average Pt size of 4.4 nm was determined, indicating reproducibility of Pt sizes for different lots of the commercial catalyst. In fact, with the exception of Pt/MWCNTs, each sample gave excellent agreement for all three methods (XRD, STEM, and chemisorption) of particle size determination. Agglomeration of Pt particles for Pt/MWCNTs to give much larger particles over a wide range of sizes (Fig.4.1(e)) made it meaningless to determine an average particle size. Only chemisorption, which measures the actual concentration of surface Pt could be used.

Table 4.3 Particle sizes as determined by XRD, STEM and chemisorption

Sample	Pt (wt%)	XRD size (nm)			STEM volume average Pt particle size (nm)	STEM surface average Pt particle size (nm)	Chemi. average Pt size (nm)
		Pt°	Pt_3O_4	Pt° + Pt_3O_4			
Pt/MWCNTs-OH (SEA)	6.5	1.5	1.4	2.9	2.9±3	2.4±2	2.9
Pt/MWCNTs-COOH (SEA)	7.3	1.7	1.2	2.9	3.1±3	2.6±2	3.2
Pt/MWCNTs (SEA)	5.2	3.7	0.8	4.5	-	-	26.8
Pt/VXC72 (SEA)	6.3	1.7	0.8	2.5	2.6±2	2.3±1	2.5
Pt/VXC72 (Commercial)	20	2.5	0.7	3.2	4.5±1	4.2±1	4.3

Thirdly, Pt particle sizes can be determined from X-ray diffraction analysis. Detailed examination of the XRD patterns of Pt/MWCNTs-OH, Pt/MWCNTs-COOH, Pt/VXC72 and commercial Pt/VXC72 is shown in Fig. 4.2. In earlier work, Banerjee [95] suggested that the surface oxidation of ultra-small Pt particles had to be considered during fitting. A simple model that the Pt_3O_4 phase resides as a thin skin on the Pt^0 nanoparticle core was considered. The detailed background subtractions and peak fits are shown in the insets of Fig. 4.2. Resulting sizes of metallic and oxidized Pt phases are estimated from the deconvoluted Pt (111) and Pt_3O_4 (210) peaks and calculated from the Scherrer equation. The sum of Pt^0 and Pt_3O_4 average particle size is summarized in Table 4.3 to give an overall particle diameter. Platinum particle sizes for all samples are less than 2.5 nm. After deconvolution, the intensities of the graphite peaks at 2θ = 26-27 ° are larger after Pt deposition on the nanotube samples, such as Pt/MWCNTs-OH (Figure 2(a)) and Pt-MWCNTs-COOH (Fig. 4.2 (b)). This may due to the graphitization of the nanotubes since it has been reported that transition metals can accelerate the graphitization of carbon.[96]

The XRD particle size of Pt/MWCNTs sample is about 4.5 nm, much smaller than the value of 26.8 nm from chemisorption. This may be due to agglomeration of smaller Pt particles to form a larger array of fused Pt particles, each particle having its own crystalline array. XRD measures the crystal size of individual aggregated or non-aggregated particles while chemisorption measures the outside surface of the entire agglomerated particle and not the internal, fused particle interfaces. For the Pt/MWCNTs sample, the STEM image in Fig. 4.1(e) provides evidence that Pt particles are agglomerated together to give larger effective particle sizes relative to surface Pt sites.

In order to better understand the role of O-functionality of MWCNTs for Pt stabilization, high resolution XPS was used to examine the O 1s region of the XPS spectrum. The results are shown in Fig. 4.3 for the relevant supports. The complex spectra are broken down into three regions: 531.5 eV for O single-bonded to C (C-O), 533.1 eV for the carbonyl (C=O) group, and 534.0 eV for O-H, as in water.[97, 98] These samples were analyzed by XPS with no drying before analysis and the potential amounts of H_2O adsorbed on the carbon supports made it difficult to separate intensities of O-H and C=O, so only the more resolved C-O contribution was used to measure the normalized O concentrations of the different carbons. The results in Fig.4.4 confirm higher concentrations of –C-O functionality exist for the –OH and –COOH modified MWCNTs compared to the standard VXC72 or non-functionalized MWCNTs supports. If the O-containing sites on the functionalized MWCNTs are where SEA occurs and subsequently act as an “anchor” for Pt particle formation, the O 1s region following Pt deposition should have lower normalized O concentrations. The lower concentration of –C-O on MWCNTs is consistent with the Pt particle aggregation seen in Fig. 4.1(e).

The results in Fig. 4.5 for MWCNTs-COOH and MWCNTs-OH supported catalysts are consistent with the O-functionalized sites acting as binding sites for the Pt and Pt-Ru particles; the surface concentrations of C-O decrease after SEA of Pt and even more after ED of Ru on the Pt core sites. Thus, functionalization of MWCNTs seems to be an important requirement for uniform distribution of Pt particles. Antolini [99] and Hernández-Fernández [100] have both reported that Pt supported on non-conventional carbon supports such as carbon nanotubes and carbon nanofibers function as better supports than conventional carbon supports, presumably linked to better crystallinity of the nano components. These more crystalline supports gave better dispersion of Pt particles and also improved electron transfer between Pt and the electrode. Hull [101] also supported Pt particles onto surfaces of multi-walled carbon nanotubes functionalized by ultrasonic agitation of MWCNTs in a HNO_3/H_2SO_4 bath to form surface –C=O, -COO-, -C-O-C-, and –C-OH groups and concluded that indeed Pt particles interacted with the O-functionalized MWCNTs to form PtO_x species that helped to anchor and maintain smaller Pt particles. Extended x-ray absorption fine structure (EXAFS) measurements of the Pt L_{III} edge of the same structures confirmed Pt coordination with oxygen of the functionalized MWCNTs surface.

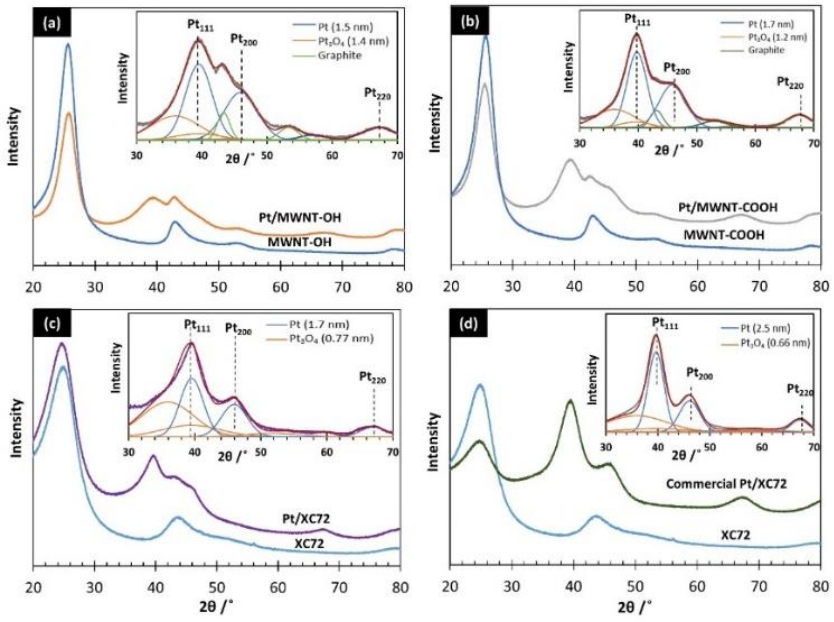

Figure 4.2. Powder X-ray diffraction profiles with deconvoluted patterns in the inset for (a) Pt/MWCNTs-OH, (b) Pt/MWCNTs-COOH, (c) Pt/VXC72 and (d) Pt/VXC72 (commercial) catalyst).

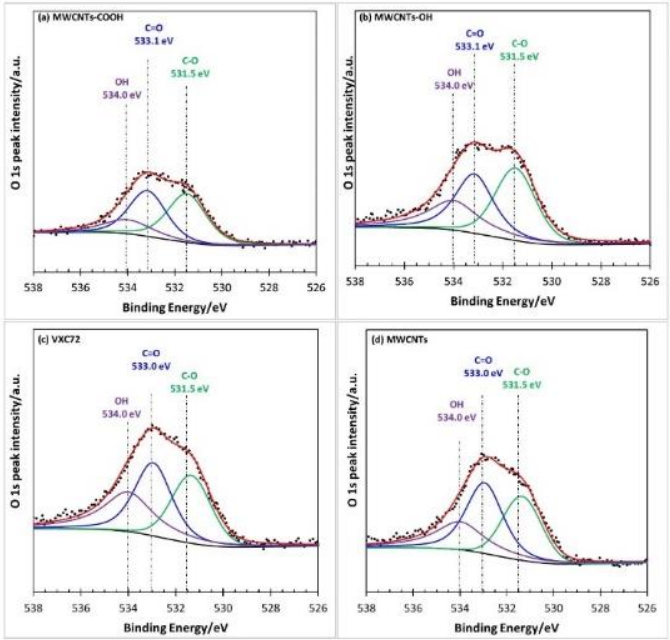

Figure 4.3 XPS O 1s peak intensities of carbon supports (a), MWCNTs-COOH, (b), MWCNTs-OH, (c), VXC72 and (d), MWCNTs

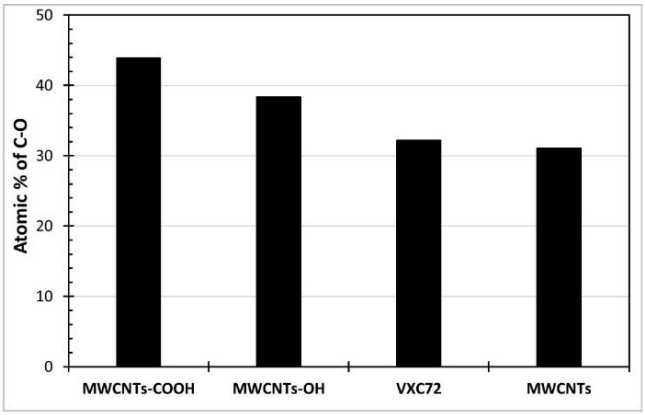

Figure 4.4 C-O bond atomic ratio (%) of O 1s peak intensity for all the support: (a) MWCNTs-COOH, (b) MWCNTs-OH, (c) VXC72 and (d) MWCNTs.

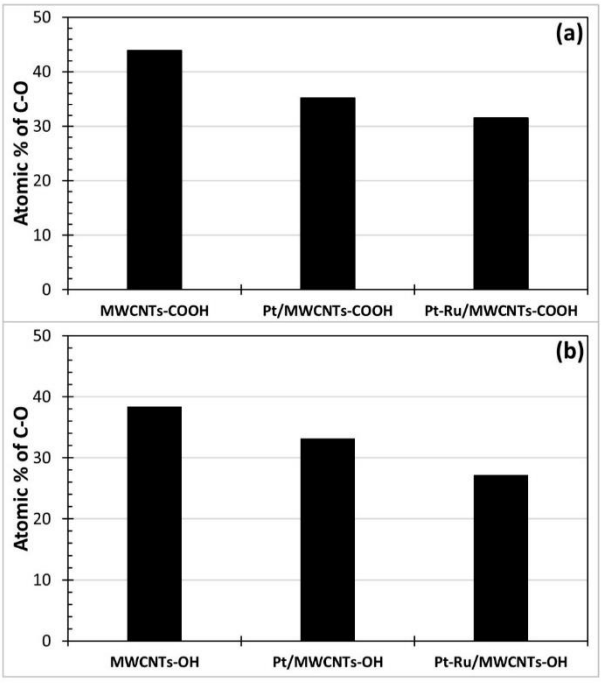

Figure 4.5 C-O atomic concentration (%) of O 1s peak for support, Pt/support and Pt-Ru/support; (a), MWCNTs-COOH and (b), MWCNTs-OH supports.

We also used XPS to examine the electronic states of surfaces of the Pt particles as a measure of the interaction between the Pt metal particle and different carbon supports. The Pt 4f XPS spectra of selected catalysts are shown in Fig. 4.6 The Binding Energy (BE)

positions of all peaks were referenced to the C 1s peak at 284.6 eV of the carbon supports, in very close agreement to the standard BE of 284.5 eV for conductive carbon surfaces. [102] The Pt $4f_{7/2}$ peak at 71.40 eV represents metallic Pt for the Pt/MWCNTs sample. The shift to higher BE for Pt/VXC72 (71.63 eV), Pt/MWCNTs-COOH (71.66 eV) and Pt/MWCNTs-OH (72.08 eV) is indicative of e^- shift from Pt to the O-functionalized MWCNT support to give $Pt^{\delta+}$ species which are intrinsically more active for methanol electro-oxidation as stated by others. Wu [90] reported that this effect was even higher for Pt-SWNTs catalysts, which exhibited the highest mass activity (expressed in mA/mg Pt) in the electro-oxidation of methanol. Thus, we believe the oxygen functionality provides two beneficial roles. The first is to provide anchoring sites for the Pt nanoparticles. Both C-O and C=O sites should provide this benefit. The second role is to provide sp^3 "defect" sites on the normally sp^2 hybridized nanotube surface (fused aromatic carbon rings). Surface carboxylic acid groups also contain carbon in the sp^2 hybridization state, which does not electronically increase the activity of the Pt site. The interaction of the sp^3 carbon surface with Pt nanoparticles increases activity of the Pt surface by shifting Pt 4f BE to higher values to enhance the positive character of the Pt surface sites. For maximum performance, the Pt particles must be small (oxygen functionality) and exhibit higher BE shifts, i.e., exhibit more positive character (sp^3 carbon). Previous studies [103] have found that the catalytic activity of Pt supported on functionalized CNTs is controlled by the functional group(s), which is consistent with the experimental results in this study. Although the C-O bond atomic ratio for MWCNTs-COOH is higher than that for MWCNTs-OH (44% vs 38%, as shown in Figure 4), the sp^3 atomic concentration of the surface carbons of MWCNTs-OH surface is higher than for MWCNTs-COOH, 20.1% vs.

18.7% (as shown in Fig. 4.7), respectively. In fact, the shift to higher Pt BE for Pt supported on the O-functionalized MWCNTs would likely be larger, but the penetration depth of x-rays extends to 10 – 20 atom layers of Pt which gives an average BE value for both surface and near surface atoms. Regardless, the XPS results agree well with STEM results that MWCNTs-COOH and MWCNTs-OH exhibit stronger Pt-support interactions than non-functionalized MWCNTs. This stronger interaction should increase the mass activity of these catalysts.

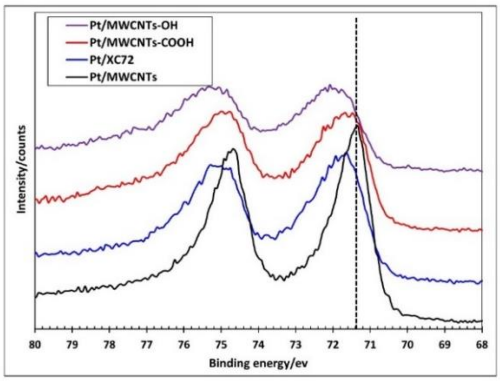

Figure 4.6 Pt 4f XPS spectra of Pt/MWCNTs, Pt/VXC72, Pt/MWCNTs-COOH and Pt/MWCNTs-OH catalysts. The dashed line at 71.40 eV represents metallic Pt and is the same as reported by others.

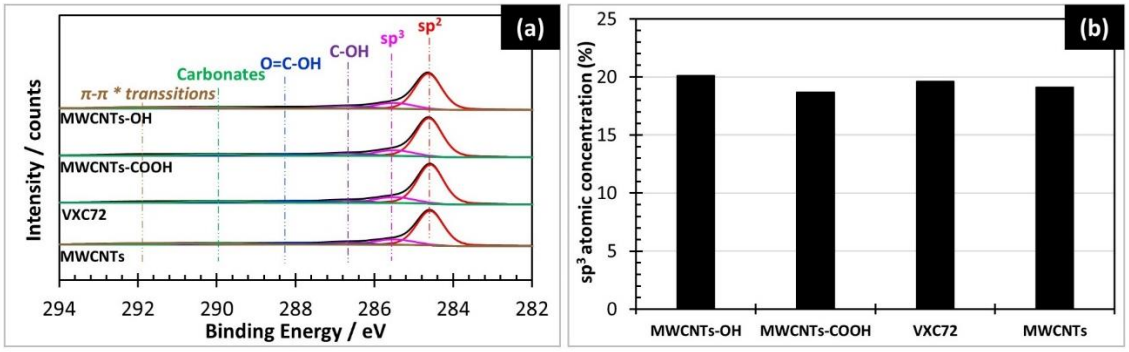

Figure 4.7 (a) surface C 1s XPS spectra peak deconvolution and (b) sp^3 atomic concentration of the surface carbons for all the supports: MWCNTs-OH, MWCNTs-COOH, VXC72 and MWCNTs

Cyclic voltammograms for methanol oxidation of Pt-Ru/MWCNTs-OH, Pt-Ru/MWCNTs-COOH, Pt-Ru/VXC72 and the commercial Pt/VXC72 are shown in Fig. 4.8. Voltammograms used for methanol oxidation correspond to the third cycle obtained at 5 mV/s were recorded after catalysts had been conditioned at 50 mV/s for 50 cycles. Two anodic peaks (one in the forward scan direction and one in the backward scan direction), typical for methanol electrooxidation, are observed for all samples. During the forward scan, a shoulder is observed at around 0.75 V, corresponding to the oxidation of methanol to form a Pt-CO complex, which is further oxidized to gaseous CO_2 at approximately 0.85 V vs SHE. At higher potentials (> 1.2 V), oxidation of the clean Pt surface sites is observed. During the reverse scan, the adsorbed oxygen then reacts with adsorbed CO to form CO_2. [91] The forward peak current density (I_f) and the backward peak current density (I_b) are marked in Fig.4.8. The current densities in the forward scan are normally used to evaluate the electrocatalytic activity towards methanol electro-oxidation. The ratio of the forward anodic peak current (I_f) to the reverse anodic peak current (I_b) can be used to describe the tolerance of a catalyst to accumulation of carbonaceous species. [104] A higher ratio indicates more effective removal of the poisoning species on the catalyst surface. As an index for the ability of electrocatalysts in complete oxidation of methanol, the ratio of the peak current density in the forward to backward scans (I_f/I_b) has been tabulated in Table 4.4. For the current study, a value of the ratio >1 indicates the electrocatalyst exhibits a high tolerance for CO adsorbed on Pt surface sites and the effectiveness of Ru for assistance in removal of the strongly adsorbed CO that acts as a poison. [105] The higher values of I_f/I_b for Pt/MWNTs-OH and Pt/MWNTs-COOH indicate the functional oxygen (-OH and –COOH) species on these MWCNTs increases the ability of the electrocatalysts to

oxidatively remove strongly-adsorbed CO species. These findings are in agreement with Hernández-Fernández [100] who demonstrated that for CNT-supported catalysts, the oxygen-containing groups play a beneficial role on the overall electro-oxidation of methanol.

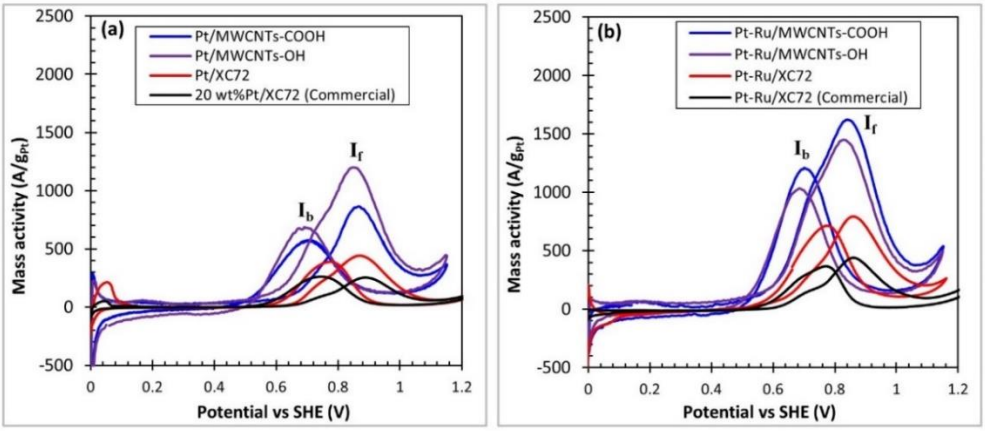

Figure 4.8 Voltammograms for methanol oxidation vs. standard hydrogen electrode (SHE) for carbon supported Pt, Pt-Ru and commercial Pt samples.

Table 4.4 I_f/I_b values for methanol oxidation for Pt-Ru/MWCNTs-OH, Pt-Ru/MWCNTs-COOH, Pt-Ru /VXC72 samples and commercial 20 wt% Pt/VXC72.

Sample	I_f/I_b
Pt-Ru/MWCNTs-OH (SEA/ED)	1.7
Pt-Ru/MWCNTs-COOH (SEA/ED)	1.6
Pt-Ru/MWCNTs (SEA/ED)	1.1
Pt/VXC72 (commercial)	1.0

Fig. 4.9 shows the comparison of mass activities calculated from forward scans peaks for the different catalysts. The SEA-derived Pt/MWCNTs-OH and Pt/MWCNTs-COOH catalysts for methanol oxidation have much higher mass activities than the SEA-derived Pt/VXC72 and commercial Pt/VXC72 catalysts in Fig. 4.9 (a). Further, the SEA/ED-derived Pt-Ru/MWCNTs-OH and Pt-Ru/MWCNTs-COOH catalysts exhibit even higher

Pt mass activities, 1655 A/g Pt and 1530 A/g Pt, respectively, compared to commercial Pt-Ru/VXC72 (435 A/g Pt) and Pt/VXC72 (238 A/g Pt). The smaller Pt particle sizes on the O-functionalized MWCNTs obviously increase the concentration of surface Pt sites and the higher electrical conductivity of carbon nanotubes (fewer ohmic, carbon-carbon interfaces) support may contribute to higher current density for methanol oxidation on Pt/MWCNTs-COOH and Pt/MWCNTs-OH catalysts.

Determination of differences in intrinsic activities for the different catalysts requires measurement of the surface concentrations of surface Pt sites. The specific activities of the electrocatalysts are shown in Fig. 4.9 (b) and (c) based on the concentrations of Pt surface sites (expressed as m^2 of Pt surfaces and the conversion factor of 8×10^{-20} m^2/Pt surface site). To determine the specific Pt surface site concentrations of the Pt monometallic catalysts, chemisorption and electrochemical surface area (ESA) were used and are summarized in Table 4.5. In an earlier study by Punyawudho [71] Pt surface site concentrations determined by chemisorption and cyclic voltammetry were found to be superior to the methods of x-ray diffraction and STEM, since chemisorption and CV directly measure surface site concentrations with fewer assumptions. Of the two methods, chemisorption data are usually more accurate and reliable because of the larger sample sizes; CV measurements typically use < 0.01 g, and any loss of sample during application as an alcohol suspension to the 5 mm diameter (20 mm^2) glassy carbon electrode transfer could have a dramatic effect on the calculation of Pt surface site concentrations. On the other hand, CV data directly reflect the accessible Pt sites during the electrochemical process. [106] Thus, Pt surface site concentrations determined from both chemisorption and electrochemical surface area (ESA) analyses were used in this work to calculate

specific activities and are shown in Table 4.5. With the exception of the Pt/MWCNTs sample, the ESA and chemisorption values agree reasonably well with the chemisorption values being higher in all cases. The lower values for CV measurements may be due to electrical resistances between the Pt surfaces and the electrodes. For Pt/MWCNTs the electrochemical surface area (79 m^2/g Pt) is much higher than the surface area determined from chemisorption (10.9 m^2/g Pt). This may be due to some combination of non-uniform distribution of Pt particles and the wide variation of sizes on the MWCNTs surface. Since it was different from the other samples, we have chosen not to include these data in further discussion.

The specific activities in Fig. 4.9 (b) and (c) clearly show that activities of surface Pt sites for particles supported on O-functionalized MWCTs are higher than all other comparable electrocatalysts. The differences are even more pronounced for the Pt-Ru bimetallic catalysts. The stronger interaction between Pt particles and the carbon nanotube support of MWCNTs-COOH and MWCNTs-OH from XPS of Pt 4f BE (Fig. 4.6) may be another possible reason for the enhanced electrocatalytic activity. In Fig. 4.9 (b), specific activities based on ECA results of the COOH or OH group functionalized MWCNTs-supported samples were three to four times higher than that of the analogous Pt/VXC72 and commercial Pt/VXC72 catalyst. The difference in specific activities is apparently linked to support interactions between Pt and the surface of the -COOH or -OH functionalized MWCNTs or possibly the enhanced electrical conductivity of the nanotubes. Specific activities based on chemisorption results in Fig. 4.9 (c) have the same trend as specific activities based on ECA results.

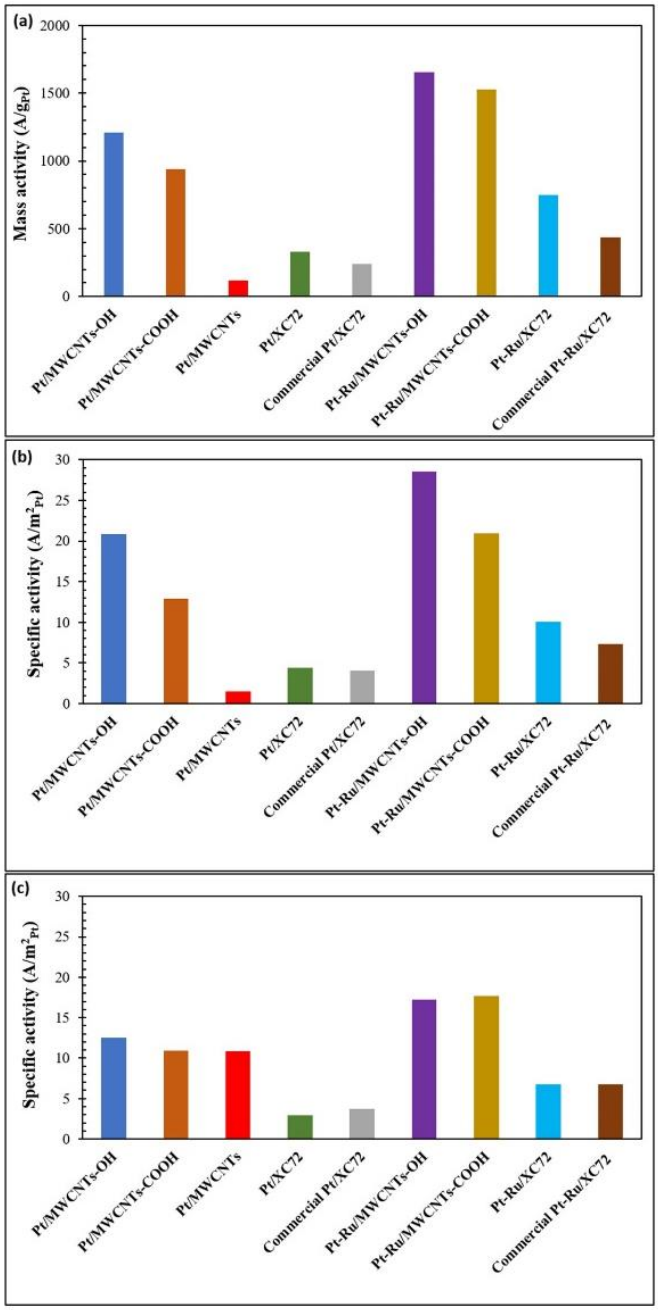

Figure 4.9 Direct methanol fuel cell (a) mass activities, (b) specific activities based on ECSA results and (c) specific activities based on chemisorption results for supported MWCNTs or VXC72 supported Pt and Pt-Ru catalysts. Comparisons are also made for commercial Pt/VXC72 and Pt-Ru/VXC72.

The three metrics of mass activity, specific activity, and I_f/I_b ratios show that O-functionalized MWCNTs serve as much more active supports for Pt and Pt-Ru than the conventional VXC72 carbon support. Studies by others have also addressed the roles of supports with oxygen-containing groups for electrochemical reactions. Most of the other work correlate the general increase in mass activity for CO and methanol oxidation with smaller Pt nanoparticles. [100, 107] We also find the functional groups on the MWCNTs surfaces increase the dispersion of Pt nanoparticles to give more Pt surface sites and higher mass activities for methanol oxidation.[102] The reason for the performance enhancement is more complicated than simply because of smaller Pt particles. Other factors including higher hydrophilicity of the O-functionalized surface making H_2O diffusion more favorable with greater availability of H_2O to create a more favorable reaction environment for removal of adsorbed CO must also be considered.[100, 108] In addition, the higher conductivity of sheet-like MWCNTs can lower inter-particle resistance (fewer e^- transfers across grain boundaries) during methanol electrooxidation. Certain oxygen functionalized MWCNTs also provide high concentrations of sp^3 "defect" sites on the normally sp^2 hybridized nanotube surface (fused aromatic carbon rings). Surface carboxylic acid groups also contain carbon in the sp^2 hybridization state, which does not electronically increase the activity of the Pt site. The interaction of the sp^3 carbon surface with Pt nanoparticles increases activity of the Pt surface by shifting Pt 4f BE to higher values to enhance the positive character of the Pt surface sites. Finally, this study has shown that rational catalyst design and preparation using SEA and ED methods can be translated to give real gains in performance for this very important application of catalysis to generate alternative energy. It also indicated that the support is an integral part of this complex catalyst system.

4.5 Conclusions

In summary, we studied electro-catalytic activity of MWCNTs supported Pt and Pt-Ru catalysts supported on MWCNTs towards methanol oxidation. The preliminary results obtained provide useful information for optimizing electrochemical performance of metal catalyst supported on MWCNTs. Consequently, in comparison with Pt/MWCNTs, Pt/VXC72 and Pt/VXC72 (commercial), Pt/MWCNTs-COOH and Pt/MWCNTs-OH catalysts as well as Pt-Ru/MWCNTs-OH and Pt-Ru/MWCNTs-COOH exhibit higher mass activity due to more Pt or Pt-Ru active site as inferred from the I_f/I_b ratios. This excellent performance may be attributed to the higher electric conductivity of the layered structure of MWCNTs and a stronger metal and support interaction in Pt or Pt-Ru/MWCNTs-OH, MWCNTs-COOH catalysts. Functionalized MWCNTs may be good candidates for catalyst support in potential fuel cell application. However, this synthesis method is not limited to Pt and Pt-Ru. It may be also used to prepare a variety of metal nanoparticle on functionalized MWCNTs surface for catalysis application. These catalysts will also be used for preparation and operation for a complete DMFC fuel cell in our laboratories to evaluate the electrochemical activity and the long-term stability of the catalysts.

In addition, Pt-Ni and Pt-Co bimetallic catalysts prepared by co-continuous ED have been studied in filed patent. [62] Predicted mixed-metal composition have been achieved and it is able to determine the optimal performance. Therefore, ED has been successfully applied for the creation of methanol electrooxidation catalysts for DMFC applications.

CHAPTER 5

SILVER PLASMONIC RIBBON™ SUPPORTED CU-PD BIMETALLIC CATALYSTS SYNTHESIZED BY CO-CONTINUOUS ED AND ITS APPLICATION IN CARBON DIOXIDE REDUCTION

5.1 Introduction

The constant global generation of carbon dioxide is cited as a primary cause for the climate change and global warming, with most of the CO_2 emissions stemming from traditional fossil fuel consumption. This makes the utilization of carbon dioxide as a building block for fuel production a very attractive and promising field. Methods for carbon capture and utilization present both business and environmental opportunities in the scenarios where industrial CO_2 is stored and used as a raw material for the synthesis of fuels, chemicals, and other valuable resources. The hydrogenation of carbon dioxide to methanol is an attractive route in this regard, as methanol can be utilized as a fuel, a vehicle for hydrogen storage, and a constituent in the synthesis of olefins. The process of synthesizing methanol from captured CO_2 and sourced H_2 is performed under catalytic reaction conditions, employing high-pressures and temperatures and requiring sophisticated process equipment that consumes large amounts of energy[109, 110]. The limiting factor in current reactors is the high activation energy required to reduce carbon dioxide. Traditionally, thermal energy is applied to a vessel containing the catalyst and reactants that operates at a temperature and pressure suitable to promote the desired reaction. In the case of CH_3OH formation from CO_2 and H_2, promoting the forward reaction while limiting the reverse reaction is crucial and requires costly, multi-stage reaction vessels operating at threshold pressures > 40 Bar and temperatures > 200 °C. [110] Innovative catalytic materials that utilize unconventional energy sources and reaction methods are fundamental to make the synthesis of CH_3OH from CO_2 and H_2 an economically viable reality. Plasmonic materials can effectively couple radiation into subwavelength sized metallic nanostructures resulting in novel phenomena that can be

exploited for enhancing catalytic processes. When electron oscillations are optically excited through plasmon resonance and decay non-radiatively, it leads to localized photothermal heating and the injection of high-energy hot electrons.[111] This makes the surface of the nanostructure catalytically active both thermally and through the energetic hot electrons that can transfer into a molecule adsorbed on the surface. In the case of H_2, this will trigger facile dissociation and consecutive reactions of the hydride and the hydrogen atom with CO_2 or other molecules in the pathway of CO_2 reduction to methanol (CH_3OH) or even methane (CH_4). [112] Recent work by Halas demonstrated that light-driven plasmonic photocatalysts can be used to convert CO_2 into CO at significantly milder operating conditions than its thermally activated counterpart.[113] Remarkably, this work demonstrated that the plasmon-induced, carrier-driven reaction occurs at a higher rate and lower temperature (175 °C vs 400°C) than the thermally driven one; and further it occurs below the thermal threshold temperature of 200°C. Thus, plasmonic materials for catalysis provide a mechanism, through light-activated photocatalysis, that lowers the activation energy by injecting high-energy electrons (hot-carriers) into adsorbates.

In addition, Cu-Pd bimetallic catalysts are reported to have superior CH_3OH formation rates than either Cu or Pd monometallic catalysts and work cooperatively in a bifunctional manner to promote the desired reaction.[114] The Pd sites will provide active locations for the dissociative adsorption of H_2, while the adjacent, or vicinal Cu sites, will promote dissociative adsorption of CO_2 to form adsorbed CO and O species, which subsequently undergo facile reduction to form CH_3OH and H_2O as products. The primary technical objective of the project is to produce controlled catalyst layer of Cu-Pd bimetals on the silver surfaces and test the photocatalytic activity of CH_3OH formation from CO_2 and H_2.

Traditional synthesis methodologies, for instance, co-impregnation, provide inadequate control over metal placement and require absorption of aqueous metal salt solutions on the support, which cannot be transferred to bimetal deposition on silver surface. A novel co-continuous ED catalyst preparation program developed by our group will be utilized to achieve this technical objective.[38] Kinetic ED process results in the formation of only bimetallic surfaces of Cu and Pd sites, and not a wide range of compositions associated with current methods of catalyst preparation. The exposed Ag surfaces on the nanorods of Plasmonic Ribbon™ will be used as support for the deposition of thin bimetallic Cu-Pd catalytic layers.

5.2 Experimental procedure and methods

5.2.1 Catalyst preparation

The silver plasmonic ribbon™ samples used in this work are provided by *Aquaneers Inc* and are synthesized by depositing the silver metallic nanorod arrays on the surface of flexible Corning® Willow® and Display® Glass via roll-to-roll nanomaterial manufacturing techniques. When illuminated in the vicinity of the nanorods plasmon resonance energy (frequency), light is absorbed with extraordinary efficiency.

Then silver plasmonic ribbon™ nanorods are coated with bimetallic Cu-Pd using co-continuous ED. As shown in Fig. 5.1, the ED bath consists of a beaker set, a pH probe that operates at room temperature and three programmable microcontroller syringe pumps (New Era NE-300). The microcontroller syringe pumps are capable of feeding solutions at rate ranging from 1.2 μl/min to 25 ml/min and therefore can be used to accurately control the amount of the reducing agent, Cu and Pd metal salts added to the ED bath. Liquid aliquots of the bath were periodically taken throughout the reaction and analyzed by

Inductively Coupled Plasma-Optical Emission Spectroscopy (ICP-OES) (Perkin-Elmer Optima 2000 DV) to confirm metal salt concentrations in the bath. Metal deposition was determined from the difference of what was added by syringe pump and the amount of metal salts left in solution. Finally, the ED coating sample is dried in the hood overnight at room temperature and stored in a vacuum oven.

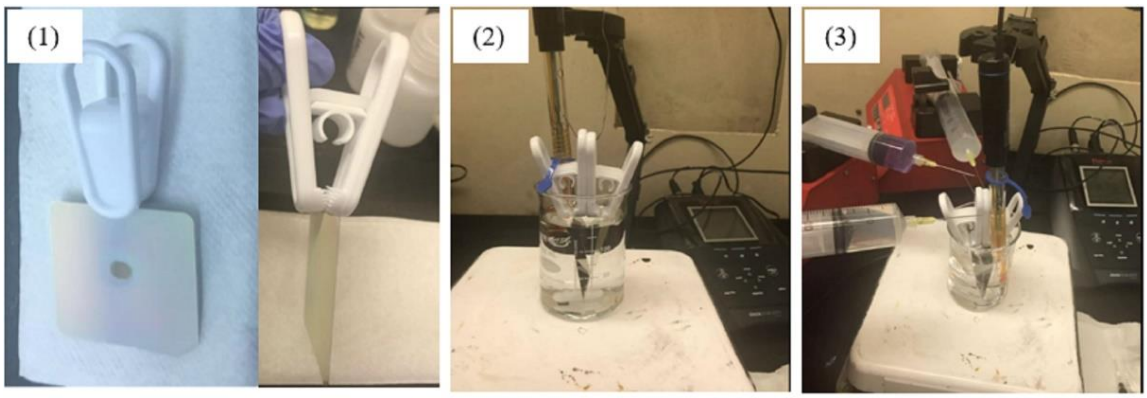

Figure 5.1 co-continuous Cu-Pd ED setup: (1) silver plasmonic ribbon^{TM}, (2) adjust pH value, (3) three syringe pumping of reducing agent, Cu and Pd metal salts.

5.2.2 Catalyst characterization

Catalysts were characterized by powder XRD, Scanning Electron Microscope (SEM), (Energy Dispersive X-ray (EDX) analysis and XPS. SEM micrographs and EDX analysis are conducted by ZEISS Gemini FE-SEM at different magnitudes. Powder x-ray diffraction (XRD) was performed using a Rigaku Miniflex-II outfitted with a high sensitivity D/teX Ultra silicon strip detector and a Cu-Kα radiation source (k=1.5406 Å). Scans were run from 20°-80° 2θ values.

5.2.3 Catalyst evaluation

The Catalytic plasmonic ribbon^{TM} samples were tested for CO_2 or CO reduction in the presence of H_2. Catalysts were evaluated in a single pass, 4 inches length and 1inch width

bed, plug flow reactor as shown in Fig. 5.2. The reactor was heated to 250 or 300 °C by cartridge heater when the catalyst was pretreated in situ. In all evaluations, the reactor was loaded with one sheet of catalyst. A thermocouple was inserted into the catalyst bed to accurately monitor the reaction temperature and to ensure isothermal behavior. Catalysts were pretreated in situ at 250 °C with flowing 20% H_2/balance He for 2 h. All gas flows were maintained by mass flow controllers. Feed gas consisted of 20% CO_2 (or CO), 60% H_2, balance He was fed at a total flow rate of 48 sccm. Both reaction feed and product streams were measured through an automated, on-line Hewlett-Packard 5890 Series II gas chromatograph based on thermal conductivity detection. The feed composition was collected before reactions. Product analysis was made periodically at a specific frequency. In addition to CO_2 (or CO), CH_4 or CH_3OH were identified and quantitatively analyzed. 365nm LED light with 3 inches or 5 inches distance from the reactor surface was irradiated on/off during the reaction process. Finally, the reaction activity data (amount of gas out from the reactor) was plot with time on stream based on GC recording.

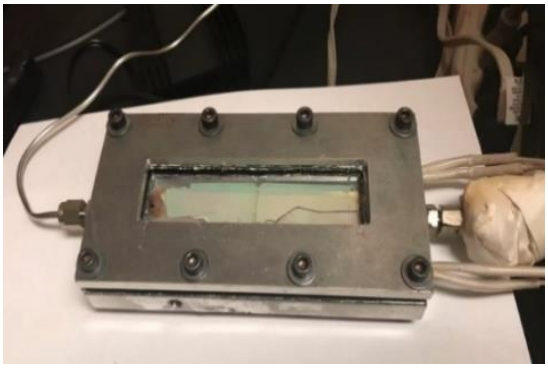

Figure 5.2 A single pass plug flow reactor

5.3 Results and discussions

Aquaneers Inc. fabricated the silver plasmonic ribbon™ and confirmed the silver nanorods are about 700 nm in length and 150 nm in diameter through SEM, as shown in

Fig. 5.3. No significant difference has been observed between the display and willow glass supports. *Aquaneers Inc*. also tested the plasmon resonance, and the optical spectra of silver plasmonic ribbon™ is shown in Fig. 5.4. Based on their test, we chose 100W, 365 nm LED light from *Dongguan Houke Electronic Co.,LTD* as the irradiative light source.

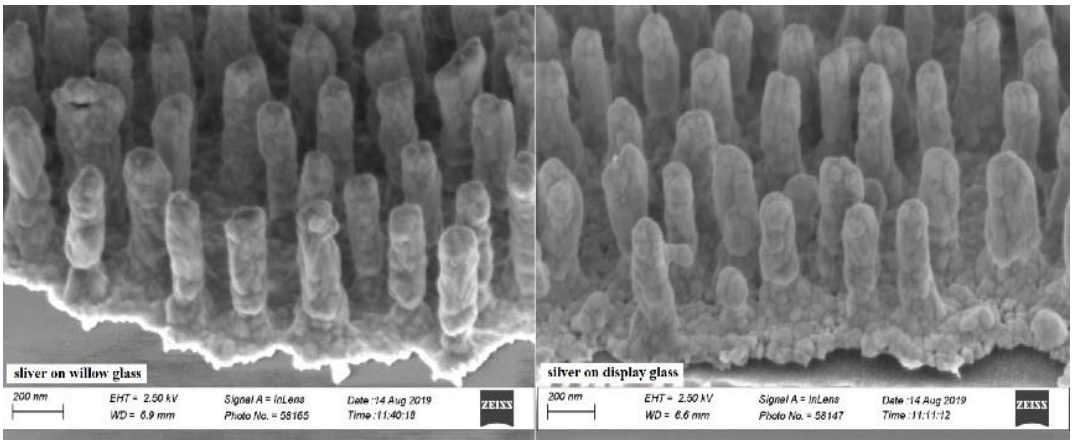

Figure 5.3 SEM images of silver on willow glass and display glass

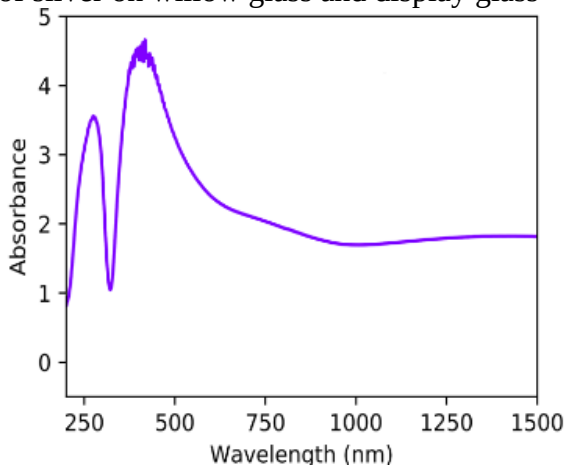

Figure 5.4 Absorbance spectrum of silver plasmonic ribbon™

We developed the co-continuous ED bath conditions for Cu and Pd deposition on 5 wt% Ag/silica, made by dry impregnation. The Ag surface site concentration of the 5 wt% Ag/silica has been measured by both XRD peak broadening and selective O_2-H_2 chemisorption. Dispersion values from chemisorption are typically lower than that from

XRD peak broadening (0.035 vs 0.092). We chose the chemisorption value of 0.035, since it was directly measured and not inferred from x-ray line broadening of the Ag^o (111) peak at $2\theta = 38.5^o$. Then one theoretical monolayer (ML) of Cu and 1ML Pd salts was added to the prepared 5 % Ag/SiO_2, using the co-continuous ED method. The ED bath is thermodynamically unstable, but kinetically stable in the absence of a catalytic surface, Ag in this case. Before doing co-continuous ED on the Ag base catalyst, all baths were checked for thermal stability (no catalyst present in the bath) to ensure only deposition of Cu and Pd on the Ag surface by ED, rather than thermal reduction of Cu^{2+} and Pd^{2+} by the reducing agent (N_2H_4) in the ED bath. All ED baths here exhibited good thermal stability of both Cu^{2+} and Pd^{2+} salts. The summary for co-continuous ED results is shown in Table 5.1. All ED baths contain Cu and Pd reducible metal salts, reducing agent (RA) and stabilizer in pH-adjusted water. Baths and ED conditions that have been tested for deposition of Pd^{2+} and Cu^{2+} salts are also shown in Table 5.1.

As shown in Table 5.1, a near complete deposition of Cu^{2+} and Pd^{2+} at 25°C has been reached using hydrazine (N_2H_4) as the reducing agent and ethylenediamine (EN) as the stabilizer, as shown in the 8^{th} row of Table 5.1, and the conditions of which is used for catalyst preparation on Ag plasmonic ribbon™.

Secondly, we characterized the Ag plasmonic ribbons on both display and willow glasses. We have measured the PZC values, the pH at which the charge of the surfaces is neutral. At higher pH values, the surfaces are negatively charged, while at lower pH values, the surface is positively charged. The PZC of the display and willow glasses are 8.1 and 8.2, respectively. The surface area of the display glass was measured by physical adsorption of N_2 at liquid N_2 temperatures using the BET method and approximately to be

0.38 m^2/g. XRD analyses were conducted for Ag supported on display glass and on willow glass to calculate Ag particle sizes. The sizes of Ag on the display glass and willow glass are very similar, which are 22.2 nm and 22.4 nm, respectively. The XRD peak intensities of Ag^o (111) at $2\theta = 38.5^o$ show ample signal strengths and the sharpness correspond to very similar Ag particle diameters of 22.4 and 22.2 nm for Ag "particles" supported on willow and display glasses, respectively, as shown in Fig. 6.5. No meaningful uptake of H_2 during the titration sequence was observed in the chemisorption analyses due to the very low concentrations of surface Ag sites of the supported Ag samples. However, dispersion values determined from XRD line broadening usually overestimate Ag dispersion values and thus the concentration of Ag surface sites. For 5% Ag/silica mentioned above, the Ag dispersion determined from XRD was 0.092 and 0.035 from chemisorption. If we make ratio of 0.035/0.092 = 0.38 to be a normalization factor, we can calculate more reasonable values of Ag dispersion on display and willow glass, being 0.02 and 0.02, respectively.

Thirdly, different MLs of Cu and Pd are then added to the Ag plasmonic ribbon^{TM} by co-continuous ED. ED kinetics for target 4 MLs of Cu and Pd are show in Fig. 5.6 as an example. From the plots, we can see that about 52 % of Cu^{2+} and 44% of Pd^{2+} have been deposited on Ag. The properties of all the prepared bimetallic Cu-Pd ED samples have been summarized in Table 5.2.

Table 5.1 summary of co-continuous ED experiments

No.	Precursor	RA	stabilizer	[RA]/[stabilizer]/[metal]	pH	Temp.	deposited%	Θ_M
1	$Cu(NO_3)_2$	DMAB	EDTA	5/1/1	9	70C	31%	0.31
	Na_2PdCl_4	DMAB	EDTA	5/1/1	9	70C	42%	0.42
2	$Cu(NO_3)_2$	DMAB	EDTA	2/1/1	7	70C	29%	0.29
	Na_2PdCl_4	DMAB	EDTA	2/1/1	7	70C	28%	0.28
3	$Cu(NO_3)_2$	HCHO	EDTA	5/1/1	10	70C	14%	0.14
	Na_2PdCl_4	HCHO	EDTA	5/1/1	10	70C	4.6%	0.05
4	$Cu(NO_3)_2$	HCHO	EDTA	5/1/1	12	70C	35%	0.35
	Na_2PdCl_4	HCHO	EDTA	5/1/1	12	70C	20%	0.2
5	$Cu(NO_3)_2$	HCHO	EDTA	10/1/1	10	70C	9.0%	0.09
	Na_2PdCl_4	HCHO	EDTA	10/1/1	10	70C	4.4%	0.04
6	$Cu(NO_3)_2$	HCHO	EDTA	10/1/1	12	70C	80%	0.8
	Na_2PdCl_4	HCHO	EDTA	10/1/1	12	70C	40%	0.4
7	$Cu(NO_3)_2$	N_2H_4	EDTA	5/1/1	10	25C	55%	0.55
	Na_2PdCl_4	N_2H_4	EDTA	5/1/1	10	25C	48%	0.48
8	$Cu(NO_3)_2$	N_2H_4	EN	5/2/1	9	25C	100%	1.0
	$Pd(NH_3)_4(NO_3)_2$	N_2H_4	EN	5/1/1	9	25C	98%	1.0

DMAB = dimethylamine borane; EDTA = ethylenediaminetetraacetic acid; EN = ethylenediamine.the

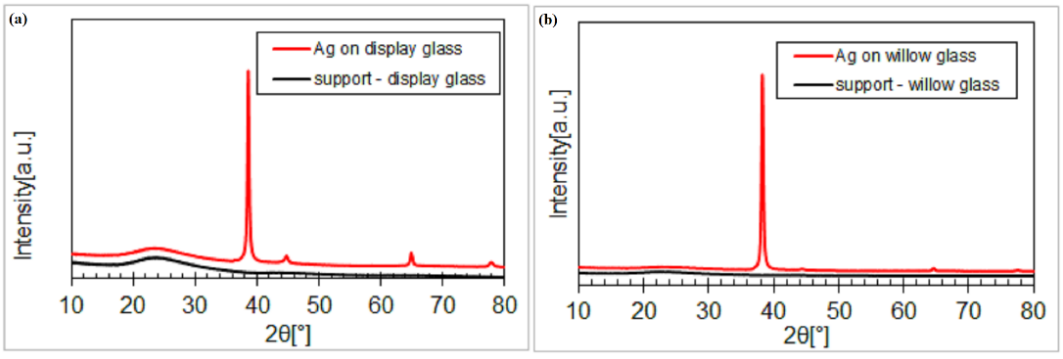

Figure 5.5 XRD patterns of Ag plasmonic ribbon^{TM} on(a) display glass, (b) on willow glass

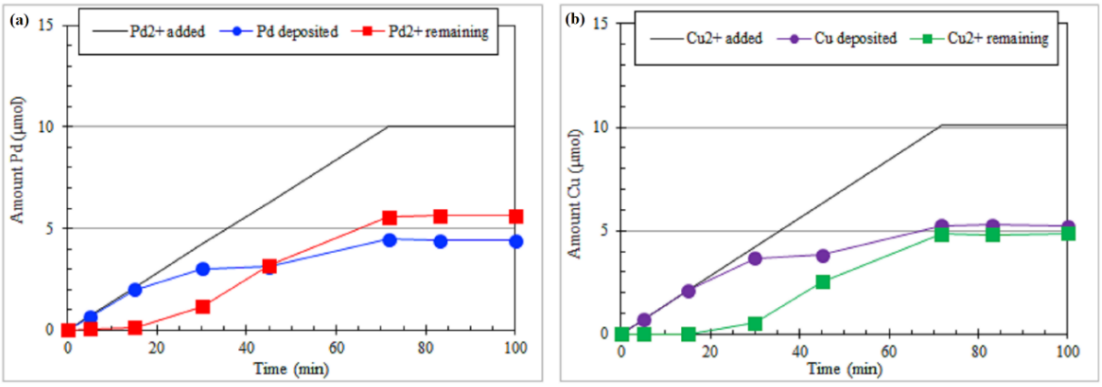

Figure 5.6 ED kinetics of target 4ML coverage of (a) Pd and (b) Cu

Sample 1 (2.5 MLs Cu and 2.1 MLs Pd) and sample 3 (6.2 MLs Cu and 5.4 MLs Pd) are selected to do XRD analysis and check the existence of Cu and Pd on Ag. in Fig. 5.7, there are no significant differences between the XRD patterns for the ED catalysts and their corresponding base catalysts, revealing that deposition of Cu and Pd by ED bath formed only thin overlayers, which are lower than the XRD detect limitation. In addition, the peaks observed in the XRD patterns were not shifted relative to the standard positions of the primary metals and the similar lattice parameters suggest no alloy formation. Besides, EDX analysis were applied to sample 2 and sample 3 to measure the distribution of Cu and Pd over Ag nanorod. As we can tell from Fig. 5.8, both Cu and Pd were coated uniformity on Ag surface. In addition, XPS analysis results as shown in Fig. 5.9 indicate sample 2 and sample 3 have large amount of metallic silver, trace amount of Pd^{2+} or Pd^{0} and some Cu^{2+}. In a short summary, from the above XRD, EDX and XPS analysis, we concluded that both Cu and Pd have been uniformly deposited on Ag plasmonic ribbon^{TM} through co-continuous ED.

Table 5.2 bimetallic Cu-Pd coverage on Ag

Sample	**Ag sample #**		**target coverage (MLs)**		**Deposited %**		**θ_M on Ag**	
#	Sheet 1	Sheet 2	Cu	Pd	Cu	Pd	Cu	Pd
1	AQ502	AQ504	4	4	52%	44%	2.5	2.1
2	AQ498	AQ499	4	4	58%	45%	2.3	1.8
3	AQ497	AQ501	10	10	62%	54%	6.2	5.4
4	ST525	BB517	4	4	60%	51%	2.4	2.1
5	BB521	BB522	10	10	54%	42%	5.4	4.2
6	AQ527	AQ528	2	2	49%	40%	1.0	0.8
7	BB523	CL487	10	10	56%	50%	5.6	5.0
8	AQ542	AQ548	3	3	61%	49%	1.8	1.5
9	AQ547	AQ534	6	6	60%	54%	3.6	3.2
10	CL488	CL490	0	4	0	79%	0	3.2
11	AQ503	AQ500	4	0	64%	0%	2.5	0
12	AQ545	AQ540	6	6	71%	57%	4.2	3.4
13	AQ551	AQ554	3	3	58%	51%	1.7	1.5

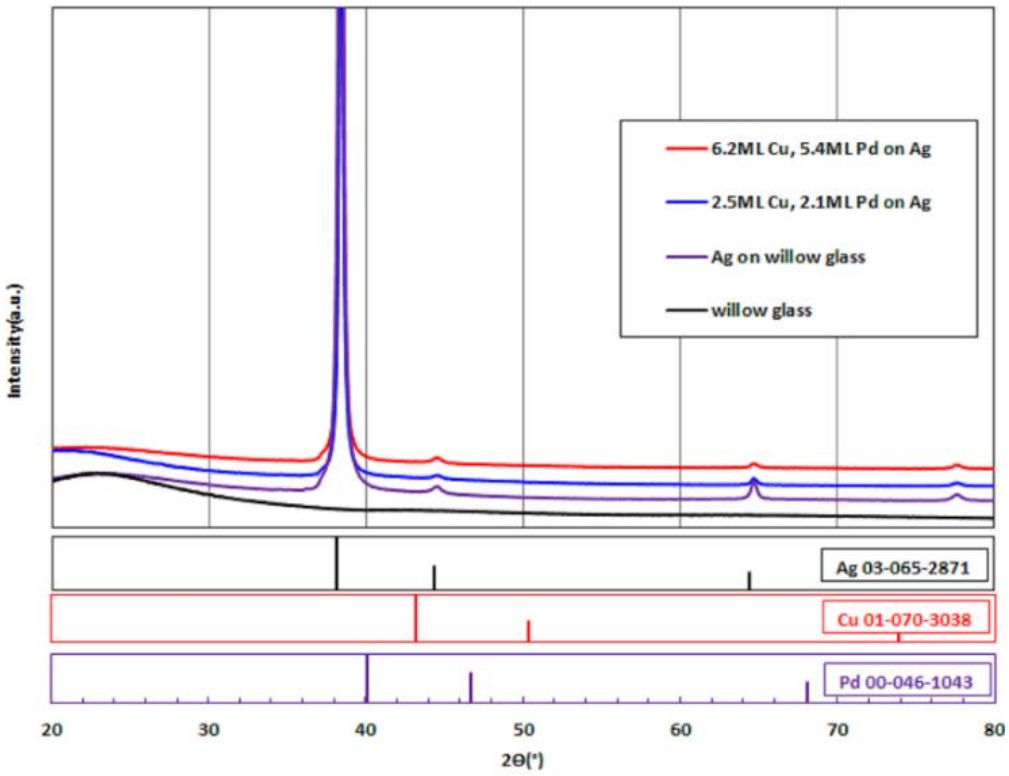

Figure 5.7 XRD patterns of co-continuous ED samples with different MLs on Ag

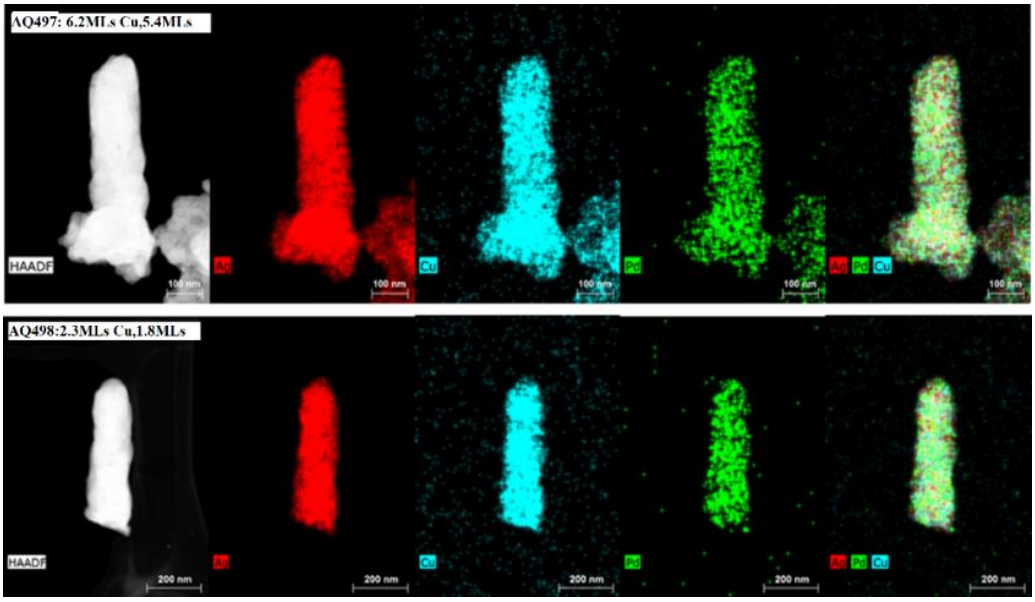

Figure 5.8 EDX analysis of Cu and Pd coating distributions on Ag nanorod.

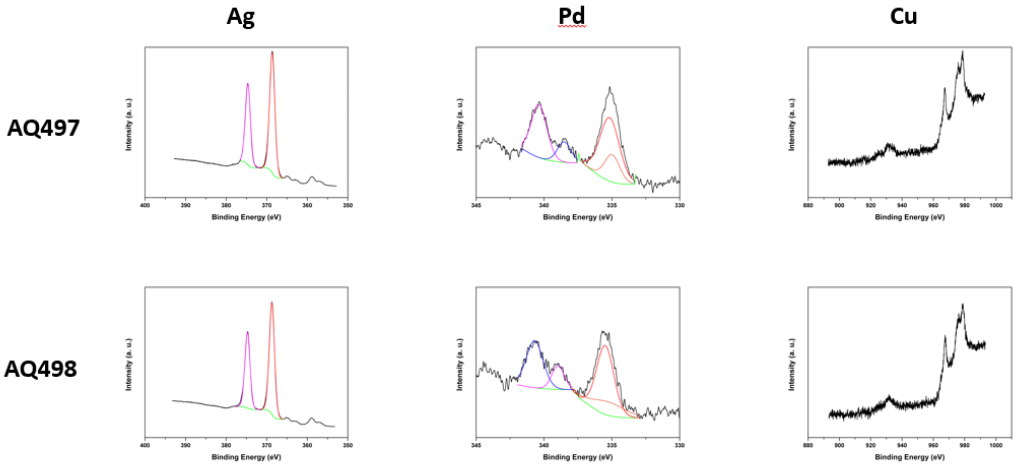

Figure 5.9 Spectra of XPS analysis of sample 2 and sample 3.

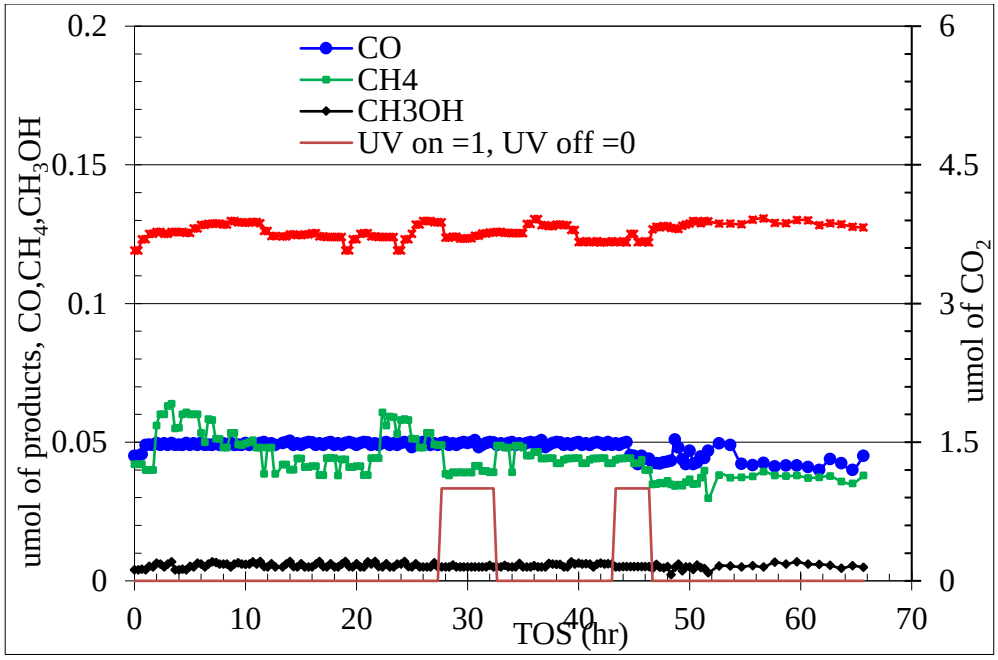

Figure 5.10 An example of a typical run for the evaluation of the catalytic activity of the plasmonic ribbon^{TM} samples (conditions: 20% Helium, 20% CO_2, 60% H_2, total flow=15sccm at 60 psig and 250°C, the distance between the 365nm LED and reactor surface is 3 inches; catalyst: CL487, 5.6MLs Cu and 5.0MLs Pd on Ag/willow glass).

Following the synthesis of the above bimetallic Cu-Pd catalysts, we applied the prepared catalyst to the carbon oxide reduction in our plug flow reactor system and runs for catalyst

evaluation are summarized in Table 5.3. The results shown in Fig. 5.10 demonstrate the standard protocol for evaluation of the catalytic activity of the plasmonic ribbon^{TM} samples. In this case, a representative example of a run performed using CL489 catalysts is provided. The catalyst consists of 5.6 MLs of Cu and 5.0 MLs of Pd on Ag/willow glass. The reaction ran at a constant pressure of 60 psig and a temperature of 250 °C. Values for CO_2 conversions, CH_4 and CH_3OH concentrations were recorded for each catalyst. The reactor performance data at different conditions (overall 17 runs with different catalysts, temperature, gas flow rate and UV light conditions) included in subsequent sections of this work were collected using the same protocol and reported after steady state operation had been reached. We initially ran CO_2 reduction reaction at 200°C with no UV radiation and no products were observed. No CH_3OH was formed until the reaction temperature was increased to 250 °C (Run2). The UV light showed negligible effect on CH_3OH formation in the reduction of CO_2 and CO since the amount of CH_3OH doesn't change with UV light on/off (Run 2, 4, 5, 6, 9, 10, 11). When lowering the flow gas rate (longer contact time), the amounts of CH_3OH increased. For instance, the amount of CH_3OH formed in Run 6 which was conducted at a flow rate of 15 sccm is about 3 times larger than that of Run 7 which was conducted at a flow rate of 48 sccm, demonstrating that the reaction is kinetically controlled. Comparing the results of Run 6 and 9 in which the catalysts have different Cu and Pd loading, we can find that increase the Cu and Pd loading cannot necessarily increase the CH_3OH formation. However, the amount of formed CH_3OH from both CO_2 reduction reaction (Run 9,10) and CO reduction reaction (Run 8,11) increased with increasing temperature (from 250°C to 300°C).

For Cu/Ag catalyst, no effect of UV light on CH_3OH formation was observed for the reduction of CO_2 at low temperatures (Run 12, 250°C). However, the amount of CH_3OH formation increased by about four times (from 0.03 µmol to 12µmol) with the UV light on at a higher temperature (Run 13, 300°C). In addition, co-continuous ED of Cu and Pd on Ag catalyst in Run 1 (230°C) and Run 5 (250°C) reached a near complete CO conversion (> 99 %) with CH_4 being the main product and only trace amounts of CH_3OH being formed. From Run 14-17, we found that Pd/Ag sample has no activity towards the CH_3OH formation in either CO_2 or CO reduction since supported Pd has been known to be a good methanation catalyst.

5.4 Conclusions

Bimetallic Cu-Pd layers were applied to the silver nanorods using continuous co-ED. ED produces homogeneous bimetal catalyst with Pd having uniform coverage over Ag surface and with Cu being more enriched near the nanorod tip. This co-ED coating uniformly attaches to all exposed metallic surfaces and can be deposited with uniform thickness. Furthermore, the thickness and composition of the bimetal layer can be controlled with sub-monolayer accuracy. These bimetallic catalysts are evaluated in custom optical flow-reactor system to investigate the photocatalytic activity of CH_3OH formation from CO_2 reduction. No significant discernable light enhancement is observed on CH_3OH formation for the reduction of CO_2 at 250 ˚C with the catalysts prepared by co-continuous ED method. However, at 300 ˚C, the amount of CH_3OH formation increases by four times with UV light on.

Table 5.3 run summaries for catalyst evaluation.

Run no.	Cat. ID	Analyzed catalyst composition	Pretreat in H_2 at 250°C ,2 hours	Dist o UV lamp from cat, (in)	Feed CO_X	Flow rate, sccm	Temp. (°C)	CO_X conversion	µmol reacted	CO amount (µmol)	CH_4 amount (µmol)	CH_3OH amount (µmol)
0	AQ527	1.0ML Cu+ 0.8ML Pd	N	No UV	CO_2	48	200	-	4.01	0	0	0
1	AQ527	1.0ML Cu+ 0.8ML Pd	N	5	CO	48	230	99%	3.98	0	3.97	0.003
2	AQ527	1.0ML Cu+ 0.8ML Pd	N	5	CO_2	48	250	1.3%	0.06	0.05	0.01	0.002
3	AQ499	2.3ML Cu+ 1.8ML Pd	N	5	CO_2	48	250	1.0%	0.04	0.04	0	0
4	AQ499	2.3ML Cu+ 1.8ML Pd	N	3	CO_2	48	250	1.6%	0.07	0.02	0.04	0.010
5	AQ499	2.3ML Cu+ 1.8ML Pd	N	3	CO	48	250	99.2%	3.98	0	3.98	0
6	AQ499	2.3ML Cu+ 1.8ML Pd	N	3	CO_2	15	250	2.7%	0.11	0.02	0.08	0.012
7	AQ499	2.3ML Cu+ 1.8ML Pd	N	No UV	CO_2	48	250	2.1%	0.08	0.05	0.03	0.004
8	CL487	5.6ML Cu+ 5.0ML Pd	N	No UV	CO	15	250	99.3%	3.98	0	3.97	0.010
9	CL487	5.6ML Cu+ 5.0ML Pd	N	3	CO_2	15	250	1.6%	0.07	0.04	0.03	0.007

10	CL487	5.6ML Cu+ 5.0ML Pd	N	3	CO_2	15	300	2.9%	0.12	0.02	0.08	0.011
11	CL487	5.6ML Cu+ 5.0ML Pd	N	3	CO	15	300	99.2%	3.98	3.94	0.02	0.012
12	AQ500	2.5ML Cu	Y	3	CO_2	15	250	2.1%	0.08	0.04	0.03	0.004
13	AQ500	2.5ML Cu	Y	3	CO_2	15	300	2.3%	0.09	0.02	0.06	0.006
14	CL490	3.2ML Pd	Y	3	CO_2	15	250	2.5%	0.10	0.04	0.06	0
15	CL490	3.2ML Pd	Y	3	CO	15	250	99.2%	3.98	0	3.98	0
16	CL490	3.2ML Pd	Y	3	CO	48	250	99.2%	3.98	0	3.98	0
17	CL490	3.2ML Pd	Y	No UV	CO	103	250	99.1%	3.98	0	3.98	0

***Note:** For all reactions with He / CO_2 (or CO) / H_2 = 1 /1 / 3, the number of μmoles of CO_2 (or CO) = 4

CHAPTER 6

CONCLUSIONS

This dissertation studies the synthesis of (1) monometallic Pt and Ag catalysts with different sizes, (2) optimal composition of Pt-Ru bimetallic electro-catalysts supported on multi-well nanotubes and (3) predictable Cu and Pd composition on Ag plasmonic by co-continuous ED. XRD, selective chemisorption and electron microscopy are applied to determine the metal particle size. Additionally, XPS and EDX analysis distinguish catalyst composition and electron information.

Firstly, $PtCl_6^{2-}$ was used as Pt source to deposit additional Pt layers on the Pt core supported on a carbon blank (VXC72 with high surface area of 250 m^2/g) to make large particle. It was found that Pt particle size distribution gets narrower with longer deposition time, resulting in a smaller average size. We then extended our study on the synthesis of different Ag particles by ED to investigate the effect Ag particle size on ethylene epoxidation. Due to the low surface area of the α-Al_2O_3 support which greatly limits the application of SEA to prepare base Ag catalyst, impregnation was used instead to prepare the 0.1 wt% Ag core for the ED process. Various sizes of Ag particle catalysts are synthesized by continuous ED through different deposition time while keeping the same HCOH and Ag^+ pumping speed. On the prepared Ag catalysts, TOF of EO formation exhibits an apparent dependence on Ag size, and the TOF was found to increases with Ag particle size determined by chemisorption. Also, Ag particle size affects the EO selectivity.

MWCNTs supported Pt and Pt-Ru electro-catalysts are also synthesized by SEA and ED. From the STEM and chemisorption estimations, the Pt particle on non-functionalized MWCNTs have a bigger size than that on the oxygen functionalized MWCNTs. XPS analysis of different carbons demonstrates that oxygen functionality is necessary for inert MWCNTs to adsorb highly dispersed Pt particles. Pt/MWCNTs-COOH and Pt/MWCNTs-

OH catalysts exhibit higher mass activity towards methanol oxidation than Pt/MWCNTs, Pt/XC72 and Pt/XC72 (commercial). due to the more positive shift of Pt binding energy caused by stronger Pt-support interaction on the functionalized support. Pt-Ru bimetallic catalysts was found to have higher mass activity than pure Pt catalysts due to the promotion of Ru in oxidating the strongly bonded CO to form CO_2 which are ready for desorption. These preliminary findings suggest that functionalized MWCNTs could be a good catalyst support and that the combination of SEA and ED can be a very useful synthesis method in preparing various functionalized MWCNTs supported metal catalysts for potential applications in fuel cells.

Finally, continuous co-ED has been used to deposit bimetallic Cu-Pd layers on silver nanorods. According to STEM EDX characterization analysis, the prepared catalyst shows a homogenous bimetal coating with uniform Pd covering over Ag surface and Cu enrichment towards the nanorod tip. This co-ED coating adheres evenly to all exposed metallic surfaces and may be applied in a consistent thickness. Furthermore, the thickness and content of the bimetal layer may be adjusted with sub-monolayer precision as demonstrated experimentally. In a customized optical flow-reactor system, the activity of the bimetallic catalysts towards the formation of CH_3OH from CO_2 reduction is evaluated. There is no obvious discernable light enhancement observed on CH_3OH formation at 250 ˚C while the CH_3OH production was increased by four times at 300°C when the UV light is on.

In summary, the ED method can be extended to many catalyst preparation on various support, such as carbon, silica, titania, and alumina. Chapter 2 and 3 investigated the dependence of the size of Pt and Ag particles generated by ED on the deposition time. By

controlling the amount of the salt being added to the ED bath, the composition of the bimetallic Pt_Ru catalyst can be precisely controlled which helps the study of the enhancement of the bimetal catalytic performance as discussed on chapter 4. Most importantly, co-ED provides the possibility to simultaneously deposit more metals and produces uniformly distributed bimetallic or even tri-metallic catalysts. Thus, ED has emerged as a noble synthesis method with a high level of versatility and usefulness in synthesizing catalysts for a wide range of applications in heterogeneous catalysis.

REFERENCES

1. Armor J., What is catalysis? The north America Catalysis Society (NACS) **2008**

2. Ma Z.; Zaera F., Encyclopedia of Inorganic Chemistry, 2nd ed. Wiley, New York **2005**.

3. Thomas J. M.; Thomas W. J., Introduction to the principles of heterogeneous catalysis. *Journal of Chemical Education* **1968**, 45, A843.

4. Somorjai G. A., Introduction to surface chemistry and catalysis. *Physics Today* 1995, 48, 58.

5. Taylor H. S., A theory of the catalytic surface, *Proceedings of the Royal Society A* **1925**, 108, 105.

6. Boudart M., catalysis by supported metal, *Advanced in Catalysis* **1969**, 20, 153.

7. Spencer N. D.; Schoonmaker R. C.; Somorjai G. A., Iron single crystals as ammonia synthesis catalysts: effect of surface structure on catalyst activity. *Journal of Catalysis* **1982**, 74, 129.

8. Bamwenda G. R.; Tsubota S.; Nakamura T.; Hartua M., The influence of the preparation methods on the catalytic activity of platinum and gold supported on TiO2 for CO oxidation. *Catalysis Letters* **1997**, 44, 83.

9. Overbury, S.; Schwartz, V.; Mullins, D.; Yan, W.; Dai, S., Evaluation of the Au size effect: CO oxidation catalyzed by Au/TiO_2.*Journal of Catalysis* **2006,** *241* (1), 56.

10. Hartua M.; Tsubota S.; Kobayashi T.; Kageyama H.; Genet M.; Delmon B., Low temperature oxidation of CO cover gold supported on TiO_2, α-Fe_2O_3 and Co_3O_4. *Journal of Catalysis* **1993**, 144, 175.

11. Bezemer G. L.; Bitter J. H.; Kuipers C. E.; Oosterbeek H.; Holewijn J. E.; Xu X.; Kaptejin F.; Dillen A. J.; de Jong K. P., Cobalt particle size effect in Fischer-Tropsch reaction studied with carbon nanofiber supported catalysis. *Journal of the American Chemical Society* **2006**, 128, 3956.

12. Grabill, C. N.; Freppon, D.; Hettinger, M.; Kuebler, S. M., Nanoscale morphology of electrolessly deposited silver metal. *Applied Surface Science* **2019,** *466*, 230.

13. Bartholomew C. H.; Farrauto R. J., Fundamentals of industrial catalytic processes, 2nd edition. *The Canadian Journal of Chemical Engineering* **2007**, 85,127.

14. Regalbuto J. R., Catalyst preparation science and engineer. CRC press: Boca Raton, FL **2007**.

15. de Jong K. P., Synthesis of solid catalysts. Whiley **2009**.

16. Seo, M. H.; Choi, S. M.; Kim, H. J.; Kim, W. B., The graphene supported Pd and Pt catalysts for highly active oxygen reduction reaction in an alkaline condition. *Electrochemistry Communications* **2011,** *13* (2), 182.

17. Mehrabadi B. A. T.; Eskandari S.; Khan U.; White R. D.; Regalbuto J. R., A review of preparation methods for supported metal catalysts. *Advances in Catalysis*, **2017**, 61, 1.

18. Hao, X.; Spieker, W. A.; Regalbuto, J. R., A further simplification of the revised physical adsorption (RPA) model. *Journal of Colloid and Interface Science* **2003,** *267* (2), 259.

19. Zhong C. J.; Regalbuto J. R., Metal nanoparticle synthesis. *Comprehensive Inorganic Chemistry II***2013**, 7, 75.

20. Hao, X.; Quach, L.; Korah, J.; Spieker, W. A.; Regalbuto, J. R., The control of platinum impregnation by PZC alteration of oxides and carbon. *Journal of Molecular Catalysis A: Chemical* **2004** *219* (1), 97.

21. Hao X.; Barnes S.; Regalbuto J.R., A fundamental study of Pt Impregnation of carbon: adsorption equilibrium and particle synthesis. *Journal of Catalysis* **2011**, 279, 48.

22. Wong A.; Liu Q.; Griffin S.; Nicholls A.; Regalbuto J. R., Synthesis of ultrasmall, homogeneously alloyed, bimetallic nanoparticles on silica supports. *Science* **2017**, 358, 1427.

23. Mehrabadi, B. A. T.; White, R.; Shakouri, A.; Regalbuto, J. R.; Weidner, J. W.; Monnier, J. R., Ruthenium–platinum bimetallic catalysts with controlled surface compositions and enhanced performance for methanol oxidation. *Catalysis Today* **2019,***334*, 156.

24. Djokic S. S.; Electroless deposition of metals and alloys. *Modern Aspects of Electrochemistry* **1982**, 35.

25. Brenner A.; Riddell G. E., Nickel plating on steel by chemical reduction. *Journal of Research of the National Bureau of Standards* **1946**, 37, 31.

26. Ohno I.; Wakababyashi O.; Haruyama S., Anodic oxidation of reductants in eletroless plating. *Journal of the Electrochemical Society* **1985**, 132, 2323.

27. Ohno I., Electrochemistry of electroless plating, *Materials Science and Engineering* **1991**, A146, 33.

28. Paunovic M.; Arndt R., The effect of some additives on electroless copper deposition. *Journal of the Electrochemical Society* **1983**, 130, 794.

29. Ting C. H.; Paunovic M., Selective electroless metal deposition in integrated circuit fabrication, *Journal of the Electrochemical Society* **1989**, 136, 456.

30. Wei, H.; Gomez, C.; Liu, J.; Guo, N.; Wu, T.; Lobo-Lapidus, R.; Marshall, C. L.; Miller, J. T.; Meyer, R. J., Selective hydrogenation of acrolein on supported silver catalysts: A kinetics study of particle size effects. *Journal of Catalysis* **2013,** *298*, 18.

31. Mallory G. O.; Haidu J. B., Electroless Plating: Fundamentals and Applications. *American Electroplaters and Surface Finishers Society* **1990**.

32. Beard, K. D.; Schaal, M. T.; Van Zee, J. W.; Monnier, J. R., Preparation of highly dispersed PEM fuel cell catalysts using electroless deposition methods. *Applied Catalysis B: Environmental* **2007,** *72* (3-4), 262.

33. Schaal, M. T.; Metcalf, A. Y.; Montoya, J. H.; Wilkinson, J. P.; Stork, C. C.; Williams, C. T.; Monnier, J. R., Hydrogenation of 3,4-epoxy-1-butene over Cu–Pd/SiO2 catalysts prepared by electroless deposition. *Catalysis Today* **2007,** *123* (1-4), 142.

34. Schaal, M.; Pickerell, A.; Williams, C.; Monnier, J., Characterization and evaluation of Ag–Pt/SiO2 catalysts prepared by electroless deposition. *Journal of Catalysis* **2008,** *254* (1), 131.

35. Rebellic J.; Detwiler M.; Ma S.; Williams C. T.; Monnier, J. R., Synthesis and characterization of Au-Pd/SiO_2 bimetallic catalysts prepared by electroless deposition. *Journal of Catalysis* **2010**, 270, 224.

36. Diao, W.; Tengco, J. M. M.; Regalbuto, J. R.; Monnier, J. R., Preparation and Characterization of Pt–Ru Bimetallic Catalysts Synthesized by Electroless Deposition Methods. *ACS Catalysis* **2015,** *5* (9), 5123.

37. Wongkaew, A.; Zhang, Y.; Tengco, J. M. M.; Blom, D. A.; Sivasubramanian, P.; Fanson, P. T.; Regalbuto, J. R.; Monnier, J. R., Characterization and evaluation of Pt-Pd electrocatalysts prepared by electroless deposition. *Applied Catalysis B: Environmental* **2016,** *188*, 367.

38. Tate, G.; Kenvin, A.; Diao, W.; Monnier, J. R., Preparation of Pt-containing bimetallic and trimetallic catalysts using continuous electroless deposition methods. *Catalysis Today* **2019,** *334*, 113.

39. Tate, G. L.; Mehrabadi, B. A. T.; Xiong, W.; Kenvin, A.; Monnier, J. R., Synthesis of Highly Active Pd@Cu-Pt/C Methanol Oxidation Electrocatalysts via Continuous, Co-Electroless Deposition. *Nanomaterials (Basel)* **2021,** *11* (3).

40. Isaifan, R. J.; Ntais, S.; Baranova, E. A., Particle size effect on catalytic activity of carbon-supported Pt nanoparticles for complete ethylene oxidation. *Applied Catalysis A: General* **2013,** *464-465*, 87.

41. Somorjai G. A.; Carrazza J., Structure sensitivity of catalytic reactions. *Journal of Industrial and Engineering Chemistry* **1986**, 25, 63.

42. Schlogl, R.; Abd Hamid, S. B., Nanocatalysis: mature science revisited or something really new? *Angew Chem Int Ed Engl* **2004,** *43* (13), 1628.

43. Bell A. T., The impact of nanoscience on heterogeneous catalysis. *Science* **2003**, 299, 1688.

44. Boudart M.; Aldag a.; Benson J. E.; Dougharty N. A.; Harkins C. G., On the specific activity of platinum catalysts. *Journal of Catalysis* **1966**, 6, 92

45. Boubnov, A.; Dahl, S.; Johnson, E.; Molina, A. P.; Simonsen, S. B.; Cano, F. M.; Helveg, S.; Lemus-Yegres, L. J.; Grunwaldt, J.-D., Structure–activity relationships of

Pt/Al2O3 catalysts for CO and NO oxidation at diesel exhaust conditions. *Applied Catalysis B: Environmental* **2012,** *126*, 315.

46. Hansen, T. K.; Høj, M.; Hansen, B. B.; Janssens, T. V. W.; Jensen, A. D., The Effect of Pt Particle Size on the Oxidation of CO, C3H6, and NO Over Pt/Al2O3 for Diesel Exhaust Aftertreatment. *Topics in Catalysis* **2017,** *60* (17-18), 1333.

47. Casapu, M.; Fischer, A.; Gänzler, A. M.; Popescu, R.; Crone, M.; Gerthsen, D.; Türk, M.; Grunwaldt, J.-D., Origin of the Normal and Inverse Hysteresis Behavior during CO Oxidation over Pt/Al2O3. *ACS Catalysis* **2016,** *7* (1), 343.

48. Zhang, W.; Wang, H.; Jiang, J.; Sui, Z.; Zhu, Y.; Chen, D.; Zhou, X., Size Dependence of Pt Catalysts for Propane Dehydrogenation: from Atomically Dispersed to Nanoparticles. *ACS Catalysis* **2020,** *10* (21), 12932.

49. Santhosh Kumar, M.; Chen, D.; Walmsley, J. C.; Holmen, A., Dehydrogenation of propane over Pt-SBA-15: Effect of Pt particle size. *Catalysis Communications* **2008,** *9* (5), 747.

50. Zhu, J.; Yang, M.-L.; Yu, Y.; Zhu, Y.-A.; Sui, Z.-J.; Zhou, X.-G.; Holmen, A.; Chen, D., Size-Dependent Reaction Mechanism and Kinetics for Propane Dehydrogenation over Pt Catalysts. *ACS Catalysis* **2015,** *5* (11), 6310.

51. Valant A. L.; Drault F.; Maleix C.; Comminges C.; Beauchet R.; Batonneau Y.; Epron F., Effect of the metallic particle size of supported Pt catalysts on methylcyclopentane hydrogenolysis: understanding of the ring opening products distribution by a geometric approach. *Journal of Catalysis* **2018**, 367, 234.

52. Sui, S.; Wang, X.; Zhou, X.; Su, Y.; Riffat, S.; Liu, C.-j., A comprehensive review of Pt electrocatalysts for the oxygen reduction reaction: Nanostructure, activity, mechanism and carbon support in PEM fuel cells. *Journal of Materials Chemistry A* **2017,** *5* (5), 1808.

53. Gasteiger, H. A.; Kocha, S. S.; Sompalli, B.; Wagner, F. T., Activity benchmarks and requirements for Pt, Pt-alloy, and non-Pt oxygen reduction catalysts for PEMFCs. *Applied Catalysis B: Environmental* **2005,** *56* (1-2), 9.

54. Gan, J.; Luo, W.; Chen, W.; Guo, J.; Xiang, Z.; Chen, B.; Yang, F.; Cao, Y.; Song, F.; Duan, X.; Zhou, X., Mechanistic Understanding of Size-Dependent Oxygen Reduction Activity and Selectivity over Pt/CNT Nanocatalysts. *European Journal of Inorganic Chemistry* **2019,** *2019* (27), 3210.

55. Ladas S.; Poppa H.; Boudart M., The adsorption and catalytic oxidation of carbon monoxide on evaporated palladium particles, *Surface Science* **1981**, 102, 151.

56. Spieker W. A.; Regalbuto J. R., A fundamental model of platinum impregnation onto alumina. *Chemical Engineering Science* **2001**, 56, 3491.

57. Fernández, P. S.; Ferreira, D. S.; Martins, C. A.; Troiani, H. E.; Camara, G. A.; Martins, M. E., Platinum nanoparticles produced by EG/PVP method: The effect of cleaning on the electro-oxidation of glycerol. *Electrochimica Acta* **2013,** *98*, 25.

58. Auer, F.; Hupfer, A.; Bösmann, A.; Szesni, N.; Wasserscheidpeter, P., Influence of the nanoparticle size on hydrogen release and side product formation in liquid organic

hydrogen carrier systems with supported platinum catalysts. *Catalysis Science & Technology* **2020,** *10* (19), 6669.

59. Ogel, E.; Casapu, M.; Doronkin, D. E.; Popescu, R.; Störmer, H.; Mechler, C.; Marzun, G.; Barcikowski, S.; Türk, M.; Grunwaldt, J. D., Impact of Preparation Method and Hydrothermal Aging on Particle Size Distribution of Pt/γ-Al2O3and Its Performance in CO and NO Oxidation. *The Journal of Physical Chemistry C* **2019,** *123* (9), 5433.

60. Li, Y.; Zaera, F., Sensitivity of the glycerol oxidation reaction to the size and shape of the platinum nanoparticles in Pt/SiO2 catalysts. *Journal of Catalysis* **2015,** *326*, 116.

61. Riyapan, S.; Zhang, Y.; Wongkaew, A.; Pongthawornsakun, B.; Monnier, J. R.; Panpranot, J., Preparation of improved Ag–Pd/TiO_2 catalysts using the combined strong electrostatic adsorption and electroless deposition methods for the selective hydrogenation of acetylene. *Catalysis Science & Technology* **2016,** *6* (14), 5608.

62. Monnier J. R.; Tate G. L.; Xiong W.; Meekins B. H., Co-electroless depostion methods for formation of methanol fuel cell catalysts. *US Patent* 2020/0313214, **2020**.

63. Datye, A. K.; Xu, Q.; Kharas, K. C.; McCarty, J. M., Particle size distributions in heterogeneous catalysts: What do they tell us about the sintering mechanism? *Catalysis Today* **2006,** *111* (1-2), 59.

64. Banerjee, R.; Liu, Q.; Tengco, J. M. M.; Regalbuto, J. R., Detection of Ambient Oxidation of Ultrasmall Supported Platinum Nanoparticles with Benchtop Powder X-Ray Diffraction. *Catalysis Letters* **2017,** *147* (7), 1754.

65. Geyer, R.; Hunold, J.; Keck, M.; Kraak, P.; Pachulski, A.; Schödel, R., Methods for Determining the Metal Crystallite Size of Ni Supported Catalysts. *Chemie Ingenieur Technik* **2012,** *84* (1-2), 160.

66. Global ehtylene oxide and ethylene gycol market 2016-2020, *TechNavio* **2016**.

67. Anderson A.; Motloung M.;Sasol achieves beneficial operation of second lake charles chemicals Project production facility, **2019**.

68. Lefort T. E., Process for the production of ethylene oxide, *US Patent* 1998878, **1931**.

69. Milligen H. V.; Vanderwilp B.; Wells G. J., Enhancemnets in the ethylene oxide / ethylene glycol manufacturing technology, White Paper, Shell Global Solutions **2016**.

70. Lauritzen A. M., Ethylene oxide catalyst and process for preparing the catalyst. *US Patent* 4761394, **1988**.

71. Punyawudho, K.; Blom, D. A.; Van Zee, J. W.; Monnier, J. R., Comparison of different methods for determination of Pt surface site concentrations for supported Pt electrocatalysts. *Electrochimica Acta* **2010,** *55* (19), 5349.

72. Strohmayer, D. E.; Geoffroy, G. L.; Vannice, M. A., Measurement of silver surface area by the H2 trtration of chemisorbed oxygen. *Appiled Catalysis* **1983,** *7*, 189.

73. Verykios X. E.; Stein F. P.; Coughlin R. W., Influence of metal crystallite size and morphology on selectivity and activity of ethylene oxidation catalyzed by supported silver, *Journal of Catalysis*, **1980**, 66, 368.

74. Lee J. K.; Verykios X. E.; Pitchai R., Support and crystallite size effects in ethylene oxidation catalysis, *Applied Catalysis* **1989**, 50, 171.
75. Goncharova S. N.; Balzhinimaev B. S.; Tsybulya S. V.; Zaikovskii V. I.; Danilyuk A. F., Synthesis of silver supported catalysts with narrow particle size distribution, *Studies in Surface Science and Catalysis* **1995**, 91, 915.
76. van den Reijen, J. E.; Kanungo, S.; Welling, T. A. J.; Versluijs-Helder, M.; Nijhuis, T. A.; de Jong, K. P.; de Jongh, P. E., Preparation and particle size effects of $Ag/\alpha\text{-}Al_2O_3$ catalysts for ethylene epoxidation. *Journal of Catalysis* **2017,** *356*, 65.
77. van Hoof, A. J. F.; Hermans, E. A. R.; van Bavel, A. P.; Friedrich, H.; Hensen, E. J. M., Structure Sensitivity of Silver-Catalyzed Ethylene Epoxidation. *ACS Catalysis* **2019,** *9* (11), 9829.
78. Diao W.; Tengco J. M. M.; Gaffeny A. M.; Regalbuto J. R.; Monnier J. R., Rational synthesis of bimetallic catalysts using electroless deposition methods, *Catalysis* **2020**, 32.
79. Monnier J. R.; Keulks G. W., The catalytic oxidation of propylene, *Journal of Catalysis*, **1981**, 68, 51.
80. Diao, W.; DiGiulio, C. D.; Schaal, M. T.; Ma, S.; Monnier, J. R., An investigation on the role of Re as a promoter in Ag Cs $Re/\alpha\text{-}Al_2O_3$ high-selectivity, ethylene epoxidation catalysts. *Journal of Catalysis* **2015,** *322*, 14.
81. Ploehn H. J.; Monnier J. R.; Chen X., Systems and methods for measuremenr of gas permeation through polymer films, *US Patent* 8424367, **2013**.

82. Jha, N.; Leelamohanareddy, A.; Shaijumon, M.; Rajalakshmi, N.; Ramaprabhu, S., Pt–Ru/multi-walled carbon nanotubes as electrocatalysts for direct methanol fuel cell. *International Journal of Hydrogen Energy* **2008,** *33* (1), 427.
83. Li L.; Xing Y., Pt-Ru nanoparticles supported on carbon nanotubes as methanol fuel cell catalysts, *The Journal of Physical Chemistry C* **2007**, 111, 2803.
84. Li W.; Wang X.; Chen Z.; Waje M.; Yan Y., Pt-Ru supported on double-walled carbon nanotubes as high-performance anode catalysts for direct methanol fuel cells, *The Journal of Physical Chemistry B* **2006**, 110, 15353.
85. Frelink T.; Visscher W.; van Veen J. A. R., On the role of Ru and Sn as promotors of methanol electro-oxidation over Pt, *Surface Science* **1995**, 335, 353.
86. Bello, M.; Zaidi, S. M. J.; Al-Ahmed, A.; Basu, S.; Park, D.-H.; Lakhi, K. S.; Vinu, A., Pt-Ru nanoparticles functionalized mesoporous carbon nitride with tunable pore diameters for DMFC applications. *Microporous and Mesoporous Materials* **2017,** *252*, 50-58.
87. Chiang, Y.-C.; Hsieh, M.-K.; Hsu, H.-H., The effect of carbon supports on the performance of platinum/carbon nanotubes for proton exchange membrane fuel cells. *Thin Solid Films* **2014,** *570*, 221-229.
88. Alegre, C.; Gálvez, M.; Moliner, R.; Lázaro, M., Influence of the Synthesis Method for Pt Catalysts Supported on Highly Mesoporous Carbon Xerogel and Vulcan Carbon Black on the Electro-Oxidation of Methanol. *Catalysts* **2015,** *5* (1), 392-405.
89. Tian, Z.; Liu, C.; Li, Q.; Hou, J.; Li, Y.; Ai, S., Nitrogen- and oxygen-functionalized carbon nanotubes supported Pt-based catalyst for the selective hydrogenation of cinnamaldehyde. *Applied Catalysis A: General* **2015,** *506*, 134-142.
90. Wu, G.; Chen, Y.-S.; Xu, B.-Q., Remarkable support effect of SWNTs in Pt catalyst for methanol electrooxidation. *Electrochemistry Communications* **2005,** *7* (12), 1237-1243.

91. Garrick, T. R.; Diao, W.; Tengco, J. M.; Stach, E. A.; Senanayake, S. D.; Chen, D. A.; Monnier, J. R.; Weidner, J. W., The Effect of the Surface Composition of Ru-Pt Bimetallic Catalysts for Methanol Oxidation. *Electrochimica Acta* **2016,** *195*, 106-111.
92. Park J.; Regalbuto J. R., A simple, accurate determination of oxide PZC and the strong buffering effect of oxide surfaces at incipient wetness, *Journal of Colloid and Interface Science*, **1995**, 175, 239.
93. O'Connell, K.; Regalbuto, J. R., High Sensitivity Silicon Slit Detectors for 1 nm Powder XRD Size Detection Limit. *Catalysis Letters* **2015,** *145* (3), 777.
94. Punyawudho, K.; Vorayos, N.; Zhang, Y.; Shimpalee, S.; Monnier, J. R., Identification and quantification of performance losses for PEM fuel cells as determined by selective chemisorption and ESA measurements. *International Journal of Hydrogen Energy* **2014,** *39* (21), 11110.
95. Banerjee, R.; Chen, D. A.; Karakalos, S.; Piedboeuf, M.-L. C.; Job, N.; Regalbuto, J. R., Ambient Oxidation of Ultrasmall Platinum Nanoparticles on Microporous Carbon Catalyst Supports. *ACS Applied Nano Materials* **2018,** *1* (10), 5876.
96. Lamber R., Electron microscopy study of the interaction of Ni, Pd and Pt with carbon, *Surface Science* **1988**, 197, 402.
97. Hu, Z.P.; Chen, C.; Ren, J.-T.; Yuan, Z.-Y., Direct dehydrogenation of propane to propylene on surface-oxidized multiwall carbon nanotubes. *Applied Catalysis A: General* **2018,** *559*, 85.
98. Mazov, I.; Kuznetsov, V. L.; Simonova, I. A.; Stadnichenko, A. I.; Ishchenko, A. V.; Romanenko, A. I.; Tkachev, E. N.; Anikeeva, O. B., Oxidation behavior of multiwall carbon nanotubes with different diameters and morphology. *Applied Surface Science* **2012,** *258* (17), 6272-.
99. Antolini, E., Carbon supports for low-temperature fuel cell catalysts. *Applied Catalysis B: Environmental* **2009,** *88*, 1.
100. Hernandez-Fernandez, P.; Baranton, S.; Rojas, S.; Ocon, P.; Leger, J. M.; Fierro, J. L., Insights into the effects of functional groups on carbon nanotubes for the electrooxidation of methanol. *Langmuir* **2011,** *27*, 9621.
101. Hull R. V.; Li L.; Xing Y.; Chusuei C. C., Pt nanoparticle binding on funtionalized multiwalled carbon nanotubes, *Chemistry of Materials*, **2006**, 18, 1780.
102. Hernández-Fernández, P.; Nuño, R.; Fatás, E.; Fierro, J. L. G.; Ocón, P., MWCNT-supported PtRu catalysts for the electrooxidation of methanol: Effect of the functionalized support. *International Journal of Hydrogen Energy* **2011,** *36* (14), 8267.
103. Li, C.; Shao, Z.; Pang, M.; Williams, C. T.; Liang, C., Carbon nanotubes supported Pt catalysts for phenylacetylene hydrogenation: effects of oxygen containing surface groups on Pt dispersion and catalytic performance. *Catalysis Today* **2012,** *186* (1), 69.
104. Wang, H.; Wang, R.; Li, H.; Wang, Q.; Kang, J.; Lei, Z., Facile synthesis of carbon-supported pseudo-core@shell PdCu@Pt nanoparticles for direct methanol fuel cells. *International Journal of Hydrogen Energy* **2011,** *36* (1), 839.
105. Maya-Cornejo, J.; Garcia-Bernabé, A.; Compañ, V., Bimetallic Pt-M electrocatalysts supported on single-wall carbon nanotubes for hydrogen and methanol electrooxidation in fuel cells applications. *International Journal of Hydrogen Energy* **2018,** *43* (2), 872.

106. Chen, Y.; Zhong, Q.; Li, G.; Tian, T.; Tan, J.; Pan, M., Electrochemical study of temperature and Nafion effects on interface property for oxygen reduction reaction. *Ionics* **2018,** *24* (12), 3905.
107. Gómez de la Fuente, J. L.; Martínez-Huerta, M. V.; Rojas, S.; Hernández-Fernández, P.; Terreros, P.; Fierro, J. L. G.; Peña, M. A., Tailoring and structure of PtRu nanoparticles supported on functionalized carbon for DMFC applications: New evidence of the hydrous ruthenium oxide phase. *Applied Catalysis B: Environmental* **2009,** *88* (3-4), 505.
108. Hsieh, C.; Lin, J.; Wei, J., Deposition and electrochemical activity of Pt-based bimetallic nanocatalysts on carbon nanotube electrodes. *International Journal of Hydrogen Energy* **2009,** *34* (2), 685.
109. Alberico, E.; Nielsen, M., Towards a methanol economy based on homogeneous catalysis: methanol to H2 and CO2 to methanol. *Chem Commun (Camb)* **2015,** *51* (31), 6714.
110. Kar, S.; Kothandaraman, J.; Goeppert, A.; Prakash, G. K. S., Advances in catalytic homogeneous hydrogenation of carbon dioxide to methanol. *Journal of CO2 Utilization* **2018,** *23*, 212.
111. Govorov, A. O.; Zhang, H.; Gun'ko, Y. K., Theory of Photoinjection of Hot Plasmonic Carriers from Metal Nanostructures into Semiconductors and Surface Molecules. *The Journal of Physical Chemistry C* **2013,** *117* (32), 16616.
112. Mukherjee, S.; Libisch, F.; Large, N.; Neumann, O.; Brown, L. V.; Cheng, J.; Lassiter, J. B.; Carter, E. A.; Nordlander, P.; Halas, N. J., Hot electrons do the impossible: plasmon-induced dissociation of H2 on Au. *Nano Lett* **2013,** *13* (1), 240.
113. Robatjazi, H.; Zhao, H.; Swearer, D. F.; Hogan, N. J.; Zhou, L.; Alabastri, A.; McClain, M. J.; Nordlander, P.; Halas, N. J., Plasmon-induced selective carbon dioxide conversion on earth-abundant aluminum-cuprous oxide antenna-reactor nanoparticles. *Nat Commun* **2017,** *8* (1), 27.
114. Nie, X.; Jiang, X.; Wang, H.; Luo, W.; Janik, M. J.; Chen, Y.; Guo, X.; Song, C., Mechanistic Understanding of Alloy Effect and Water Promotion for Pd-Cu Bimetallic Catalysts in CO2 Hydrogenation to Methanol. *ACS Catalysis* **2018,** *8* (6), 4873.

APPENDIX A

LIST OF PUBLICATIONS

1. **Wen Xiong**, **Benjamin Egelske**, Haiying and John R. Monnier, Structure sensitivity of electroless deposition driven Ag catalysis on ethylene epoxidation. to be submitted to *Journal of Catalysis*.
2. **Wen Xiong**, Bahareh A. T. Mehrabadi, Stavros G. Karakolos, Rembert D. White, Abolfazl Shakouri, Peter Kasak, Syed J. Zaidi, John W. Weidner, John R. Regalbuto, Hector Colon-Mercado and John R. Monnier, Enhanced performance of multi-walled carbon nanotubes as support for Pt and Pt-Ru bimetallic catalysts for methanol electrooxidation, *ACS Applied Energy Materials*, **3** (2020) 5487.
3. John R. Monnier, Gregory L. Tate, **Wen Xiong** and Benjamin H. Meekins, *United States Patent.*, 20200313214, 2020-10-01.
4. John R. Monnier, Gregory L. Tate, **Wen Xiong** and Benjamin H. Meekins. *Chemical Engineering Progress* April 2019.
5. Gregory L. Tate, Bahareh A.T. Mehrabadi, **Wen Xiong**, Adam Kenvin and John R. Monnier, Synthesis of highly active Pd@Cu-Pt/C methanol oxidation, *Nanomaterials*, **11** (2021) 793.

APPENDIX B

PERMISSION TO REPRINT

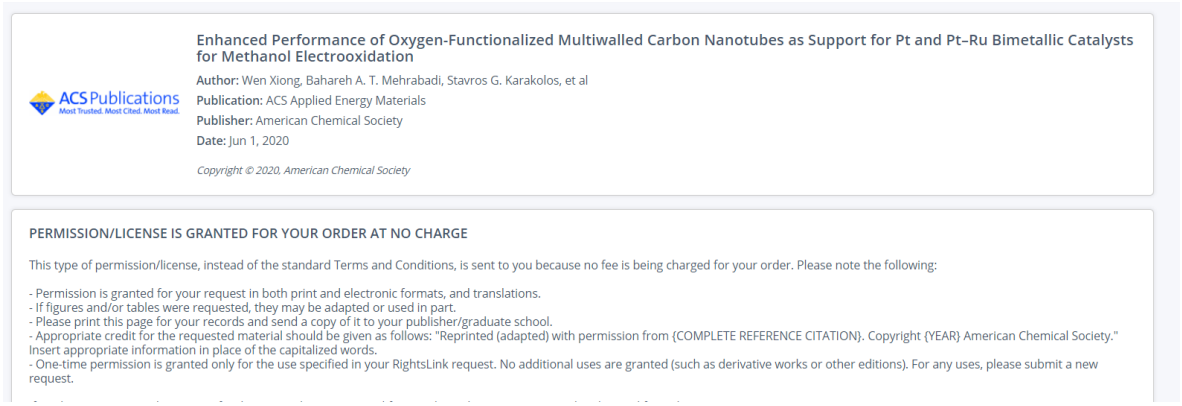

Enhanced Performance of Oxygen-Functionalized Multiwalled Carbon Nanotubes as Support for Pt and Pt–Ru Bimetallic Catalysts for Methanol Electrooxidation

Author: Wen Xiong, Bahareh A. T. Mehrabadi, Stavros G. Karakolos, et al
Publication: ACS Applied Energy Materials
Publisher: American Chemical Society
Date: Jun 1, 2020

PERMISSION/LICENSE IS GRANTED FOR YOUR ORDER AT NO CHARGE

This type of permission/license, instead of the standard Terms and Conditions, is sent to you because no fee is being charged for your order. Please note the following:

- Permission is granted for your request in both print and electronic formats, and translations.
- If figures and/or tables were requested, they may be adapted or used in part.
- Please print this page for your records and send a copy of it to your publisher/graduate school.
- Appropriate credit for the requested material should be given as follows: "Reprinted (adapted) with permission from {COMPLETE REFERENCE CITATION}. Copyright {YEAR} American Chemical Society." Insert appropriate information in place of the capitalized words.
- One-time permission is granted only for the use specified in your RightsLink request. No additional uses are granted (such as derivative works or other editions). For any uses, please submit a new request.